POLITECNICO DI TORINO

Corso di Laurea Magistrale
in
Ingegneria Aerospaziale

Tesi di Laurea Magistrale

Exploration of trans-Neptunian objects using the Direct Fusion Drive

Relatori:
Prof.ssa Sabrina Corpino
Prof. Roman Ya. Kezerashvili

Candidato:
Paolo Aime

Aprile 2020

POLITECNICO DI TORINO

New York City College of Technology

Master Degree

in

Aerospace Engineering

Master Thesis

Exploration of trans-Neptunian objects using the Direct Fusion Drive

Supervisors:
Prof.ssa Sabrina Corpino
Prof. Roman Ya. Kezerashvili

Candidate:
Paolo Aime

April 2020

A Mamma e Papà.

Abstract

The Direct Fusion Drive (DFD) is a nuclear fusion engine that will produce thrust and electrical power for any spacecraft. It is a compact engine, based on the D-^{3}He aneutronic fusion reaction that uses the Princeton field reversed configuration for the plasma confinement and an odd parity rotating magnetic field as heating method to achieve the fusion. The propellant is deuterium, which is heated by the fusion products and then expanded into a magnetic nozzle, generating an exhaust velocity and thrust. A single engine, based on the mission requirements, can be in the range of power between 1 - 10 MW and it will be able to achieve thrusts from 4 N to 55 N, depending on the chosen power, with a specific impulse of about 10^4 s.

In this work we present possibilities to reach and study the outer border of the solar system using such an engine. The objective is to travel to some trans-Neptunian object (TNO) in the Kuiper belt and beyond, such as the dwarf planets Makemake, Eris and Haumea in less than 10 years with a payload mass of at least of 1000 kg, so that it would enable all kind of missions, from scientific observation, to in-situ operations. Each mission profile chosen is the simplest possible, which is the so-called thrust-coast-thrust profile and for this reason each mission is divided into 3 phases: i. the spiral trajectory to escape Earth gravity from low earth orbit; ii. the interplanetary travel, since the exit from sphere of influence to the end of the coasting phase; iii. maneuvers to rendezvous with the dwarf planet. Propellant mass consumption, initial and final masses, velocities and ΔV for each maneuver are presented. The analyses of trajectories are performed for two cases: the simplified scenario, in which the TNOs have no inclination on the ecliptic plane and the real scenario, where the real angle of inclination is considered. After that, multiple scenarios have been studied to reach 125 AU in order to enable the study of the external border of the Sun magnetosphere.

Our calculations show that a spacecraft propelled by DFD will open unprecedented possibilities to explore the external border of the solar system, in a limited amount of time and with a very high payload to propellant mass ratio.

Contents

List of Figures

List of Tables

1 Introduction

1.1 New means of space exploration

Since the first space approach via chemical propulsion, it was clear that it could not bring the human being further than the closest planets in our Solar System, and it was also unsuitable for robotic exploration for great distances. The main reasons were its costs and its mass at launch. Furthermore, the human race has hardly reached all main celestial bodies in our Solar System, and now tends to the interstellar space. Interplanetary travel is expensive and it requires long time frames, and with present technology reaching outer space would take much longer than we expect. Next interesting objects in the open space are exoplanets, which until know we only discovered because of transit signatures detected by missions of the Kepler Space Telescope and its successor, the Transiting Exoplanets Survey Satellite, already known as TESS. Even just for study them in detail we will need to exploit some power source with greater capabilities than chemical reactions.

By looking at our solar system, instead, we can state that we reached all main celestial bodies, but not that we know them. Pluto, for instance, has been only photographed during a flyby of New Horizons mission or by Hubble Space Telescope. Both Uranus and Neptune remain unexplored, except for the flyby of Voyager 2 in 1986 and 1989, respectively [1, 2].

In addition to Pluto and its moons, in the Kuiper belt, the region which spans from 30 AU to 50 AU, there are many dwarf planets, such as Pluto itself and others like Makemake, Haumea, Quaoar, Ixion, Varuna and a great number of smaller asteroids. All of those bodies could give important information about the origin of the universe, of our solar system and maybe of life itself.

Modern means of interplanetary travels, which are mainly composed by chemical propulsion and low power electric thrust are not convenient because of the travel time. Shorter the time, higher the mass at launch, and so the cost.

1.1.1 The Solar Sail approach

Amongst all possible propulsive systems, solar sailing is one of the most studied concept. Unfortunately, since in the most primitive configuration they are based on the Solar Radiation Pressure, the propulsive capability decreases with $1/r^2$, where r is the distance from the Sun. This makes them unsuitable to be used further than Jupiter using only the Sun as propulsive source. Further information can be found in Refs. [3, 4]. By increasing the technological level in terms of sails material density and foldability, we can radically increase their capabilities, but we will always be limited by the sunlight intensity. Because of this limitation, new solution for Sail-type propulsion have been proposed, such as:

- Magnetic Sail: In this case, thanks to electromagnets, the spacecraft produces a magnetosphere which interacts with the solar (or stellar) wind or plasma flux, by generating drag and so, thrust. The amount of drag produced goes with the number and density of charged particles and the magnetic field produced by the spacecraft. Though, the amount of magnetic field required for an acceptable thrust would need a power of, in a optimistic view, in the order of 10^6 W as seen in Ref. [5].

- Electric Sail: This kind of Sail exploits the deflection of trajectories of protons with an electrical field to produce drag. The fact is that in order to obtain the same amount of thrust, we would require about 10^{12} W [5].

In Sec. 1.1.3 we will see how it is possible to reach about 20% of the speed of light with a solar sail.

1.1.2 The electric propulsion approach

It is very well know that one of the limits of electric propulsion, in the form of electrothermal, ion, grid, Hall, magneto plasma dynamic thrusters is the power source, which directly limits the total thrust obtainable and also increases the specific impulse. Given the power directed to the propulsion system P_E, it is in general valid the expression

$$\begin{aligned} \eta P_E &= \dot{m}c^2/2 \\ &= Tc/2, \end{aligned} \tag{1.1}$$

where η is the overall efficiency, $\dot{m}$ is defined as $\dot{m} = \frac{\mathrm{d}m}{\mathrm{d}t}$ and it is the rate of change of mass, c is the exhaust velocity and T is the thrust, as explained in Ref. [6]. From the previous equation, the exhaust velocity of the engine can be expressed as

$$c = \sqrt{\frac{2\eta P_E}{\dot{m}}}. \tag{1.2}$$

One limitation, though, is that in general $\eta = \frac{1}{P_E}$, so the increase in power could lead to many losses, if not mitigated, especially in the form of thermal, electric or propulsive. Many thrusters only work with power of the order of MW, or at least hundreds of kW , but only some are suited for high power systems: those are the magneto plasma dynamic (MPD) thrusters. Basically, there are two different types of MPDs, depending on the nature of the magnetic field. This could be externally applied, and in this case the thruster will be an applied field MPD (AF-MPD), or it could be self generated, thus it will be called self field MPD (SF-MPD).

These kind of thrusters would be great for interplanetary manned mission or even for some interstellar mission trajectories, but they are limited by the power sources available at the present. This, indeed, is the main issue for all the electric propulsion: the high mass-to-power ratio limits the total power available for each power system. Nowadays, conventional systems have $\alpha = 3 - 15$ kg/kW as seen in Ref. [6], but we require one or more orders of magnitude less than that in order to enable fast, safe and affordable interplanetary travels with electric propulsion.

Table 1.1: MPDs I_{sp}, η, P_E and ΔV characteristics [6]

Type	AF-MPD	SF-MPD
I_{sp}, [s]	2000-5000	2000-5000
P_E, [W]	1k-100k	200k-4M
η	0.5	0.3
Missions	High ΔV	High ΔV

The parameter α is defined as the opposite of specific power, which is measured as kW/kg. A radioisothope thermoelectric generator could reach $2.5 - 3$ kg/kW and could last for decades, while solar panels typically are around 10 kg/kW, but once they are further than Jupiter they become pointless.

Fission generators could be a powerful method of high power generation, but they presents multiple problems such as safety, reliability and miniaturization, as is explained in Section 1.2.2. Moreover, the radioactivity could be a constraint if manned mission are considered.

1.1.3 Prospective for interstellar missions

The main feature of conventional solar sails is that they have near-infinity autonomy, because the "propellant" is the radiation pressure. This makes them ideal for extremely-long-term mission, such as those looking at the interstellar space. The only limit is the distance from the star if we rely on sunlight only, but what if we could rely on a different power source, which is dedicated only to our spacecraft, such as a laser, a millimeter wave or a microwave beam?

The most ambitious mission proposed until now is the Project Starshot (see Ref.[7]), which aims to accelerate a nano-spacecraft of about 1 g for more than 10^5 g, where $g = 9.806$ m/s^2 is the gravity acceleration on Earth. The beam could originate on the Earth from a huge station where the power is gathered and then beamed.

Such a system will enable the human race to approach the closest Star System, which is Alpha/Proxima Centaury in a time period which is comparable to the human life. Though, it will require a huge exploitation of resources on Earth for the so called "Beamer" station, and a not indifferent technological improvement in terms of density and operability of sails in terms of temperatures. This is because the sail will be subject to power densities between $1 - 10^3$ MW/m^2 which will translate, with extremely low absorbivity, to temperatures in the range of $1000 - 6000$ K. All of the previous data change with the technology chosen for the beamer as seen in Ref. [8].

However, it should be also considered the technology to provide the spacecraft-Earth communication, which is extremely challenging, considering both the distance of about 4.3 light years at the arrival, the kind of payload which weights way less than 1 g and the pointing requirements for the antenna. By only taking into account these features, it results that with these technology the payload fraction will only be some point in percentage, and increasing the payload mass will mean that the sail area will grow exponentially.

The main advantage for this means of propulsion is the near-infinite specific impulse, which is ideal for extremely-long missions. It presents many cons, first of all the low thrust. This means that they are unsuitable for any kind of manned or massive missions. For those, only something that is really revolutionary will take the role of a game-changer. That is, with a good chance, a nuclear energy source, in particular, nuclear fusion.

1.2 Nuclear source of power

1.2.1 Nuclear fission and nuclear fusion

The starting point for nuclear studies has to be traced back to A. Einstein's work "*Zur Elektrodynamik bewegter Körper, in Annalen der Physik 17*", which is well explained in Ref. [9]. In fact, with the easiest and well known equation

$$E = mc^2, \tag{1.3}$$

we finally knew that mass and energy are so closely related that they should be considered as a one. Note that in this section c will be the speed of light.

It is also very well know that, while in chemical reaction the total mass is conserved, since only electrons and electromagnetic forces are involved, in nuclear reactions this is no longer true. This is because in this kind of reactions strong nuclear forces are involved, because now main players are protons and neutrons. Those are kept together by the nuclear force, a short range attractive force which overcomes the repulsive electromagnetic one between protons.

In general, three laws are always respected in a nuclear reaction, and those are:

- Conservation of mass number (A): the total number of nucleons is the same before and after the reaction.
- Conservation of charge (q): the number of total charged particles will remain the same before and after the reaction.
- Conservation of energy, linear momentum and angular momentum (only internal forces are involved in these kind of reactions).

If we were to measure masses of reactants and products of a nuclear reaction, we would find that they are slightly different. Thus, a large amount of energy would be released. This is because a small fraction of mass has been transformed to energy from Einstein's result (1.3). So (1.3) in this case has been re-arranged into

$$E = \Delta mc^2. \tag{1.4}$$

By looking at Eqs. (1.3) and (1.4), it is clear that even if a small mass is considered, this could lead to a enormous energy, since it is multiplied by the second power of the speed of light.

This defect of mass equals the binding energy. The higher the mass defect, the more energy is released. We know from literature that the most stable elements of them all is Iron, in particular its isotope ^{56}Fe, and all the other binding energies are lower, as can be seen in Fig. 1.1.

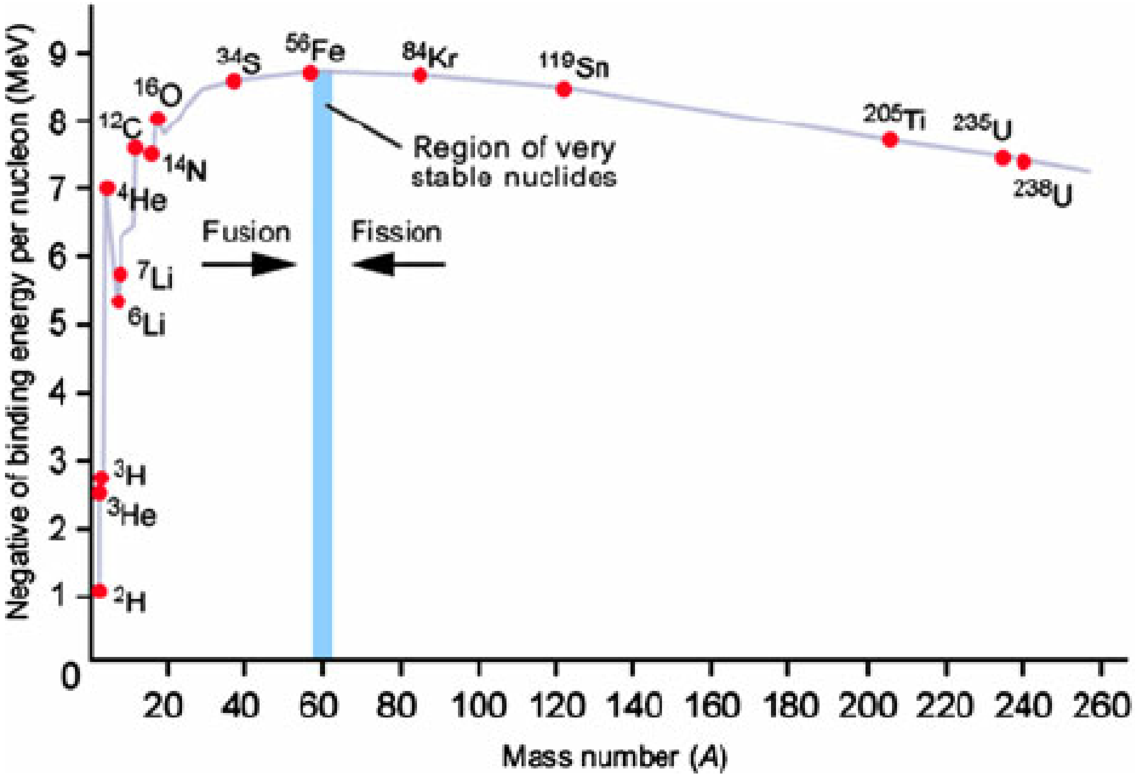

Figure 1.1: Binding energies for each nucleus divided by nucleon number

If you climb the curve from a lower energy to a higher, so that products have higher energy than reactants, it means that some energy has been released: this is equal to the mass defect multiplied by c squared, as seen in Eq. (1.4). Depending on how the curve is climbed, one can have fusion or fission reactions.

- **Fission reaction:** it is obtained by starting from heaviest elements and going left towards lower mass numbers A, meaning that the atomic nucleus is been split. There is a certain gap between the starting element, lets say ^{235}U and the product, that could be ^{84}Kr and ^{141}Ba plus neutrons.

- **Fusion Reaction:** in this case the lightest elements are taken into account, such as protons, hydrogen or some of its isotopes such as deuterium or tritium. By considering a reaction between the last two, the product would be $^{4}_{2}$He plus a neutron: in this way, the curve is climbed from left to right, with a greater gap than in nuclear fission. (Note that in Fig. 1.1, ${}^4_2$He corresponds to a peak of binding energy)

In truth, a third reaction could be achieved in the future. This is the so-called annihilation or, in other words, the matter-antimatter reaction. This consist in the reaction between antimatter and matter. In this case, the 100% of all reacting mass would be converted to elementary particles and energy, and if a proton-antiproton or hydrogen-antihydrogen reaction is considered, the only products of the reaction would be charged particles known as pions, which travels at about 94% of the speed of light as explained in Ref. [10]. This kind of reaction has been theorized for years, but at the present the problem is to actually produce antimatter and how to manage the enormous amount of energy that would be produced.

To compare the energy amount between different reactions, one has to consider the figure from before, which is the binding energy of nucleus divided by nucleon number and then compare it with the equivalent atomic mass unit of other reactions. For example, if one has to consider the energy released with a reaction of ^{235}U , which has a mass of 235.0439299u, it has to compare it with the same mass of hydrogen in order to compare energies (in this case u is the atomic mass unit, $1\ \mathrm{u} = 1.66054 \times 10^{-27}$ kg).

As it is very well known, the main problem with nuclear energy exploitation is the radioactive waste. In particular, with fission there is no way to avoid nuclear slag, while in fusion there are some particular reactions, as we will see in Sec. 1.3.2, that have such a low probability to generate neutrons that only few centimeters of insulation should be enough.

Another issue is how to harness this kind of energy and to use it for space exploration.

1.2.2 Fission Historical Background

Throughout the years since the Space Era has begun, many solutions have been proposed that included nuclear solutions. First of all, fission approach was tried in terms of a nuclear thermal propulsive system (NTP), with the nuclear engine for rocket vehicle application (NERVA) development program in the 60s, as is explained in Ref. [11]. It was a promising program, where the engine could reach an I_{sp} of about 800 s. Its working principle was a small controlled fission reaction, which was used to heat the propulsive fluid, which was hydrogen, that expanded in the nozzle: in this way, the I_{sp} doubled with respect to the more common $O_2 - H_2$ chemical reaction.

The same fission reaction could have been used in a slightly different way in nuclear electric propulsion (NEP), where the energy from fission is converted to electrical power, stored and then converted to propulsive power via conventional or unconventional electrostatic/electromagnetic/hybrid propulsion.

As far as the generation of energy is considered, as explained in Ref. [12] we have different very well known and demonstrated fission reactors. Once the energy has been harnessed via some kind of liquid and transferred to the conversion section, we need to actually converted it. Throughout the years, many solutions have been proposed to convert energy from fission in space systems as well explained in Ref. [12]

- Static nuclear converters: those in which there are not moving parts, and so the energy from nuclear fission is converted directly to electrical energy. In this case the available technologies are mainly heat pipes with liquid metal, thermoelectric converters (TE) and alkali-metal thermal-to-electric conversion (AMTEC). Efficiency are quite low, and strongly depends on the temperature. In the case of TE operating at 300 K, we could achieve efficiency of about 13%, but usually they operate at efficiency of $\eta = 6\%$, while and AMTEC would reach up to $\eta = 27\%$ operating at ~ 1100 K.

- Dynamic nuclear converters: those which are composed of moving parts and their basic principle is a thermodynamic cycle, such as Rankine, Stirling or Brayton cycles. Those can operate at a mean efficiency higher than a static converter, of about 20%. They are better than static converters when a complex and high power system is considered, mainly because of their low power to mass ratio.

A very well know generator already tested in space is the radioisothope thermal generators (RTG) technology, which exploits the radioactive decay of radioactive materials via thermocouples.

All of the high power fission technologies analyzed in previous chapters could be revolutionary for interplanetary exploration, even though extreme precautions should be taken for manned exploration. Though, fission reactors appears to be hardly scalable and still presents problems about failure mitigation and one point failures. Despite all of this, they are still not powerful enough for the interstellar approach. In engineering terms, their propulsive power to mass ratio α is still in the order of decimals of kW/kg. α is defined as

$$\alpha = \frac{P_E}{m_g}, \tag{1.5}$$

where m_g is the mass of the generation system and P_E is the power produced.

For this reason there is an increasing need to look upon nuclear fusion means of propulsion.

1.3 Introduction to Nuclear Fusion

In this section it will be analyzed the working principle of nuclear fusion reactions. Nuclear fusion does not happen naturally on Earth, with a difference respect to fission, which happens regularly under the form of radioactive decay. Nuclear fusion processes are only natural in the core of stars, and in next section will be explained why.

1.3.1 Basic Fusion Process

In order to fuse two nuclei, one has to bring them as close as possible, in order to overcome the repulsive barrier, known as the Coulomb barrier, and to let strong nuclear interaction to pull them together. This will result in a heavier nucleus, which has a higher binding energy, as shown in Fig. 1.1, and eventually some neutron and protons and an overall resulting kinetic energy, called Q. This energy is distributed between particles, with inverse correlation to their masses.

Equation (1.6) is the Coulomb barrier or, in other term, the electrostatic potential to overcome to get two nucleus as close as possible.

$$V_c = \frac{e^2}{4\pi\varepsilon_0}\frac{Z_1 Z_2}{R_1 + R_2}, \tag{1.6}$$

where Z_1 and Z_2 are atomic numbers of the two fusing particles and R_1 and R_2 are the radius, making $R_1 + R_2$ the distance of closest approach. In general, the mean radius follows the relation $r = r_0 A^{\frac{1}{3}}$, where r_0 is a constant and A is the mass number. For each nucleon, the amount of energy required to overcome the Coulomb barrier could seem relatively small, because is in the order of $1 - 10$ MeV, depending on particles considered. One could think that a collision between the two nucleus after an acceleration should be enough, but the elastic scatter would prevent the fusion. For this reason, the only way is to thermally overcome the substantial limitation imposed by Eq. (1.6). We can estimate the temperature needed by the relation $E = k_B T$, where $k_B = 8.6 \times 10^5$ eV/K^{-1} is the Boltzmann constant. Given the example of a Coulomb energy to overcome of 4.8 MeV, the required temperature would be 5.6×10^{10} K, which is a greater temperature than those found in the core of stars, by two orders of magnitude.

In stars fusion happens at a lower temperature for two reasons, which will not be analyzed here in detail:

- **Quantum tunnelling**: even if the particle has a lower energy than the one requested by Eq. (1.6), it can overcome Coulomb barrier anyway, since its probability to overcome it is different than zero (See Ref. [13]).
- **Maxwellian distribution**: if a distribution of energy of particles is considered, there will be some particle with enough energy to overcome Coulomb potential described by Eq.(1.6).

In both cases, the probability is extremely low, such that the fusion it is not likely at all, but an important factor is the enormous volume of stars. This plays a fundamental role in fusion: enough space means that fusion will eventually occur sometimes, and this is enough for the stars to keep on burning. These two factors could play a decisive role in fusion on Earth, but they would require an enormous volume to become significant, which is not possible. For this reason mankind has to develop new and safe ways to remedy this lack.

1.3.2 Possible reactions

In order to exploit the potential of a fusion nuclear reaction fully, we must take into account all possible reaction, so we can do a trade off between all reactions, by looking at the cost of fuel, its availability, its toxicity (if any), its efficiency, its manageability etc. In particular, if the reaction between the two reactants together does not produce neutrons, it will be called aneutronic.

What follows is a list of plausible reactions, organized from the lowest temperature of fusion to the highest, as explained in Ref. [14].

Note that deuterium and tritium will be taken into account and those are two hydrogen isotopes, namely D $= {}^2_1$H, with one proton and one neutron and T $= {}^3_1$H, with one proton and 2 neutrons. Though, in the following part atomic number and mass number will be specified per each reaction. It is also important to point out that with each product it is associated a certain energy, depending mainly on the inversely related to their mass. If a energy is written not associated with any product, it means that it is energy released under the form of radiation. Finally, if for the same reactant multiple reaction are possible, the percentage written refers to the likelihood of the reaction to occur, and those number depends on the cross section of different reactions.

1. **tritium+tritium**

$$ {}^3_1\mathrm{T} + {}^3_1\mathrm{T} \longrightarrow {}^4_2\mathrm{He} + 2n + 11.3\ \mathrm{MeV}\ . \tag{1.7} $$

   This is the easiest reaction to obtain, and mankind did master it in the form of neutron boost to nuclear fission bombs. In fact, two neutrons are produced for each fusion reaction.
   Furthermore, tritium half-life is 12 years, so it is unsuitable for long-term missions.

2. **deuterium+tritium**

$$ {}^2_1\mathrm{D} + {}^3_1\mathrm{T} \longrightarrow {}^4_2\mathrm{He}(3.5\ \mathrm{MeV}\ ) + n(14.1\ \mathrm{MeV}\ ). \tag{1.8} $$

   This kind of reaction has low efficiency and highly energetic neutrons, in addition to the problem related to the half life of tritium.

3. **helium-3+tritium**

$$ {}^3_2\mathrm{He} + {}^3_1\mathrm{T} \longrightarrow {}^4_2\mathrm{He} + p + n + 12.1\ \mathrm{MeV}\ \ |\ 57\%, \tag{1.9} $$

$$ {}^3_2\mathrm{He} + {}^3_1\mathrm{T} \longrightarrow {}^4_2\mathrm{He}(4.8\ \mathrm{MeV}\ ) + {}^2_1\mathrm{D}(9.5\ \mathrm{MeV}\ )\ |\ 43\%. \tag{1.10} $$

   The percentage shows the likelyhood of the reaction to occurr with the exact same reagents, but they both should be discarded for same reason as reactions in Eqs. (1.7) and (1.8) with tritium.

4. **deuterium+helium-3**

$$ {}_1^2\mathrm{D} +_2^3 \mathrm{He} \longrightarrow_4^2 \mathrm{He}(3.6 \text{ MeV }) + p(14.7 \text{ MeV }). \tag{1.11}$$

This is the first aneutronic encountered, in which all products are ionized particles. In this way they could be used in a reaction drive , thereby controlled by electromagnetic fields. This reaction, though, presents two main problems:

- Never achieved fusion with $\mathrm{D} - {}^3\mathrm{He}$ until now;
- ^{3}He is not abundant on Earth and a new source should be researched.

5. **helium-3 + lithium-6**

$$ {}_2^3\mathrm{He} +_3^6 \mathrm{Li} \longrightarrow 2_4^2\mathrm{He} + p + 16.9 \text{ MeV }. \tag{1.12}$$

It requires lithium, which is one of the most rare materials on earth. Moreover ^{6}Li is an isotope of Li which constitutes a 8% of all lithium. Furthermore, ^{3}He is quite rare as well.

6. **helium-3 + helium-3**

$$ {}_2^3\mathrm{He} +_2^3 \mathrm{He} \longrightarrow_4^2 \mathrm{He} + 2p + 12.9 \text{ MeV }. \tag{1.13}$$

This reaction is aneutronic and the products are easily controllable via electrostatic fields, and the mass of 1 u leads to the minimum losses for physical exhaust. Though, tritium has a high Coulomb barrier, which requires higher temperatures than those it is possible to create right now.

7. **deuterium + deuterium**

$$ {}_1^2\mathrm{D} +_1^2 \mathrm{D} \longrightarrow_1^3 \mathrm{T}(1.01 \text{ MeV }) + p(3.02 \text{ MeV }) \mid 50\%, \tag{1.14}$$

$$ {}_1^2\mathrm{D} +_1^2 \mathrm{D} \longrightarrow_2^3 \mathrm{He}(0.82 \text{ MeV }) + n \mid 50\%. \tag{1.15}$$

In this case, the reaction in Eq. (1.15) brings a neutron that dissipates around 1/3 of the energy. This kind of reaction would be ideal in terms of fuel costs, because 0.12 g of deuterium can be extracted from less than 5 liters of water at an insignificant cost, and this would be a great significant factor for fusion.

8. **deuterium + lithium-6**

$$ {}_1^2\mathrm{D} +_3^6 \mathrm{Li} \longrightarrow 2_2^4\mathrm{He} + 22.4 \text{ MeV }, \tag{1.16}$$

$$ {}_1^2\mathrm{D} +_3^6 \mathrm{Li} \longrightarrow .... \tag{1.17}$$

In this case, this reaction could lead to 4 different kind of products, of which only the first is important: since a huge amount of energy is released along with 2 alpha particles, it is ideal for a direct drive engine. The drawbacks of this reaction are those reactions which come along with the first one, because they are rich in neutrons, plus the fact that ^{6}Li is poor in nature.

9. **proton + lithium-6**

$$p +^6_3 \mathrm{Li} \longrightarrow^4_2 \mathrm{He}(1.7 \text{ MeV }) +^3_2 \mathrm{He}(2.3 \text{ MeV }) \tag{1.18}$$

The only problem with this aneutronic reaction is the cost of ^{6}Li.

10. **proton + boron-11**

$$p +^{11}_5 \mathrm{B} \longrightarrow 3^4_2\mathrm{He} + 8.7 \text{ MeV} \tag{1.19}$$

This reaction has a higher Coulomb barrier than reaction with hydrogen isotopes, but the products are again alpha particle. Same as lithium, is quite uncommon on the earth, but it is quite inexpensive as well.

Reactants in Eqs.(1.18) and (1.19) are particularly interesting because they could be stored in a solid state.

1.3.3 Advantage for an aneutronic reaction

What makes most fusion reactions extremely interesting is that they do not produce radioactive slag. The only problem with most of them is that neutrons are direct products of the reaction, and for this reason there has to be shielding, since neutrons are dangerous both for metals, materials in general and also for biological tissues. With aneutronic reactions, the only neutron output would be from side reactions such as $\mathrm{D-D}$ or $\mathrm{D-T}$, whose neutrons would be 2.45 MeV and 14.1 MeV. Those side reactions have very low probability to happen, but still they are a non-negligible issue. Still, those reactions are the most convenient in terms of radiation shielding mass. For many years of operations, the shielding required would be orders of magnitude inferior to that required for common fusion reactions, and this is a primary need for an efficient spacecraft.

1.3.4 Source of ^{3}He in the solar system

Now the attention should be focused on reaction (1.11), the $\mathrm{D} - {}^3\mathrm{He}$ reaction, of which the ^{3}He is the most critical part. In fact, as already said before, this isotope is not that abundant on Earth. In fact, at this moment, there are only ~ 30 kg available [14]. ^{3}He is naturally present on Earth in the atmosphere, in mantle gas vents, and in natural gas wells as well, but the ppm are extremely low, as explained by Ref. [15]. An important aspect is that Earth does not produce the ^{3}He itself, because it is only a product of fusion, and only the Sun in our solar system can produce it naturally. For this reason, it can be found in solar wind, in which the $\frac{^3\mathrm{He}}{^4\mathrm{He}}$ is about 500 ppm: this wind has been depositing ^{3}He throughout the solar system for billions of years, but Earth atmosphere could not keep it, if not for relatively small quantities. One other way to produce it is as a consequence of radioactive decay of tritium, which is one of the products of nuclear fission.

There are many interstellar sources of this isotope as well, first of all the Moon, because regolith, with its fine grain dimension, has collected and stored all the ^{3}He from the solar wind during its life. This makes the Moon a huge possible source of fuel for nuclear fusion. As far as other planets are considered, both Saturn and Jupiter could be considered as near-unlimited sources, such as Uranus and Neptune as explained in Ref.[15]. There may be ^{3}He on Mars, Venus and Mercury as well.

1.4 Objectives for this thesis work

The first objective for this thesis is to understand the physics behind the direct fusion drive (DFD), its strength points and its main advantages. This requires a general analysis on the basics of nuclear fusion processes, which ends up with the understanding of the thrust generation process inside the direct fusion drive. The second and main objective is to perform an analysis on trajectories that will enable a spacecraft to reach the border of the solar system, towards the Kuiper belt and even beyond that. In order to do so, characterization of the engine and of the scientific objectives in those far region is necessary. The calculations presented in this work are supposed to show what kind of missions can be achieved with an engine like the DFD and why it is so revolutionary.

This thesis work is organized as follows. First of all, a nuclear physics section explains the basics behind a fusion reactor and the possible combination of technology that will enable it. After that, the physics of the direct fusion drive is presented, along with the thrust generation process and its performances.

In the third chapter it is explained the basic approach to low thrust trajectory, and it also is presented the software used for the trajectory design. That software, Satellite Tool Kit, was necessary to calculate the possible trajectories feasible with the direct fusion drive, because it enabled us to customize the engine and the maneuvers.

In the fourth chapter calculations and results are shown for missions in which a spacecraft will rendezvous with dwarf planets after Neptune orbit and also for missions to reach the external border of the heliosphere.

2 Nuclear Fusion Drive

2.1 Main features about Fusion Reactors

2.1.1 Main criteria for Fusion Reactions

The greatest deal of effort is to develop a stable fusion reactor (or drive), in which enough energy can be provided to the nuclei in order to overcome Coulomb repulsion force and to fuse them. As already mentioned before, the only way is to heat the fuel up to a plasma state, in which all atoms are ionized. In this state, once the plasma reaches the critical ignition temperature, that is the minimum temperature where the power generation equals radiation losses, power can actually be produced. This temperature depends on the reaction considered, as said in Sec. 1.3.2.

The radiation loss is mainly as breaking radiation loss, already known as bremsstrahlung, in which energy is dissipated via radiation in the form of x-rays, due to deceleration of charged particles. Note that in the following section it will be used the ion density within the meaning of ion concentration.

There are two more factors that influence the possibility of energy generation:

- **Ion density** n: number of ions per units of volume;
- **Confinement time** τ: is the period for which the interacting ions are kept at a temperature equal or higher than the ignition temperature.

If we now consider the energy required to heat the plasma, which is $E_{heat} \propto n$ and the energy generated by the fusion process, which is $E_{gen} \propto n^2\tau$, we can compare them and the Lawson criterion can be derived. It states that there is a net energy output if $E_{generated} \geq E_{heat}$ if the product $n\tau$ has a minimum value. Further details about the Lawson Criterion can be found in Refs. [16, 17]. For basic reaction such as $\mathrm{D-D}$, $\mathrm{D-T}$ and $\mathrm{D-{}^3He}$ this value has been computed. Results are visible in Fig. 2.1.

$$\begin{aligned} n\tau &\geq 10^{14} s/cm^3 \quad \text{for D} - \text{T fusion reaction,} \\ n\tau &\geq 10^{16} s/cm^3 \quad \text{for D} - \text{D fusion reaction.} \end{aligned}$$

We can rewrite the criterion in the following equation, as explained in Ref. [19].

$$n\tau > \frac{12kT}{\langle v\sigma\rangle Q}. \tag{2.1}$$

In this terms it appears the ion kinetic temperature T in keV, the Boltzmann constant k, the $\langle v\sigma\rangle$ is the fusion reaction rate, with σ cross section, v the relative speed between incident particles and Q is the energy released from each elementary reaction. The factor $\langle v\sigma\rangle$ depends on the ion kinetic temperature, but it will not be analyzed here. Note that the product kT is an energy.

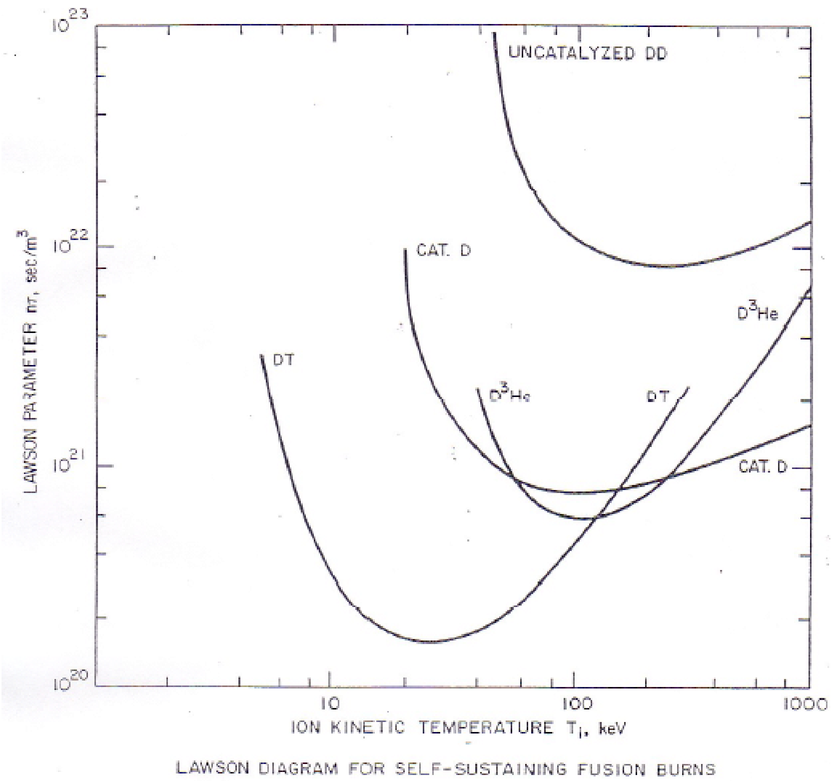

Figure 2.1: Lawson criterion for different reaction vs the temperature as in Ref. [18]. Curves show the value of $n\tau$ as a function of temperature, and for each reaction is visible a vertical asymptote for an ideal temperature, below which bremsstrahlung radiation power losses are higher than power produced by fusion. It is also present a minimum value for an optimal temperature, known as T_{opt}, for which the power gain is maximum.

This means that, in addition to enormous temperature of the plasma, this has to be extremely dense and its confinement time has to be long. The main problem with this is the confinement time, because proper conditions cannot be maintained for too long. In the next paragraph, confinement will be analyzed. Another important parameters for the reaction is the energy gain ratio Q. This is defined as

$$Q = \frac{\text{Fusion Energy}}{\text{Input Energy}}, \tag{2.2}$$

and it represents the possibility of energy generation, if $Q > 1$.

Given the pressure of a magnetic field in vacuum,

$$\text{Magnetic field pressure} = \frac{B^2}{2\mu_0},$$

where B is the magnetic field intensity in T and μ_0 is the magnetic permeability in the void, we can define the ratio of plasma pressure to magnetic field energy density

β with

$$\beta = \frac{p}{B^2/2\mu_0} = \frac{2\mu_0 p}{B^2}. \tag{2.3}$$

The magnetic field density can be interpreted as a magnetic field pressure. Therefore, Eq. (2.3) determines the ratio of the thermal pressure produced by hot energetic plasma to magnetic pressure.

Now it should be helpful to relate all the parameters of this chapter together, to estimate the specific power of the fusion system considered, as explained in Ref. [18]. In fact, one can express the electron concentration as

$$n_e = \frac{\beta B^2}{2\mu_0 f_1 T_{opt}}, \tag{2.4}$$

where T_{opt} is the optimal kinetic ion temperature which corresponds to the minimum of a Lawson Curve in Fig. 2.1. f_1 is a function of the fuel composition, and its expression is $f_1 = 1 + \sum_i n_i/n_e$, where n_i and n_e are the concentration of ions and electrons. Since the expression of the specific power produced in terms of neutrons and charged particles depends also on the ion density, one can write

$$\begin{aligned} P_{spec} &= n^2 f_2 \langle \upsilon\sigma \rangle E_{fus} \\ &= (\frac{\beta B^2}{2\mu_0 f_1 T_{opt}})^2 f_2 \langle \upsilon\sigma \rangle E_{fus}, \end{aligned} \tag{2.5}$$

where f_2 also depends on the fuel composition, and $f_2 = (n_i/n_e)/(n_j/n_e)$, where n_j depends on the type and concentration of fuel ions and E_{fus} is the energy released in a fusion reaction. It is clear at this point that in increase in B or β will eventually lead to an increase in P_{spec}.

Table 2.1: β influence on fusion specific power, with all other parameter constant and equal

	DT	D^3He
$\beta = 1\%$	1 MW/m^3	0.01 MW/m^3
$\beta = 10\%$	10^2 MW/m^3	1.2 MW/m^3
$\beta = 100\%$	10^4 MW/m^3	123 MW/m^3

From Table 2.1 it is clear that a $D-T$ reaction is way more energetic than a $D-^3He$ reaction, but the advantage of the second one is that it is aneutronic and both He and D are stable elements. Though, if $\beta > 10\%$ could be achieved, the second process could become most interesting, both in terms of power density and in the amount of radiations.

2.2 Confinement in fusion reactions

The confinement is necessary to keep the plasma in a condition in which, after a proper heating, it will be able to achieve fusion.

After a general overview on the pinch effect, which is an important and very basic phenomena in plasma physics, main means of confinement and heating will be analyzed in the following chapters. The description is a summary of what explained in Ref. [19], which analyzes the basis confinements for all reactors and drives one can imagine.

2.2.1 The pinch effect

The pinch effect is a compression of a electrically conductive mean by the action of magnetic forces. Such kind of phenomena are used to control and regulate nuclear fusion. In order to achieve them, there has to be both a magnetic and an electric field. With respect to the kind of fields taken into account, one can have different cases, but the two main pinches are the Z and θ pinches, named after the current direction. In the following section, all example will be based on plasma means.

$z-$pinch In this case, there is an axial electric field plus a azimuthal magnetic field as seen in Fig. 2.2, generated by the current itself, which compresses the plasma. We can write the volumetric magnetic force acting on the plasma as

$$f = \mathbf{j} \times \mathbf{B}, \tag{2.6}$$

where $\mathbf{J} = \int_A \mathbf{j} \mathrm{d}r \mathrm{d}\theta$. Then by considering the Ampère Law

$$\nabla \times \mathbf{B} = \mu_0 \mathbf{J}, \tag{2.7}$$

and by saying that $f_B = \nabla p$, it results that

$$\frac{d}{dr}(p + \frac{B_\theta^2}{2\mu_0}) + \frac{B_\theta^2}{\mu_0 r} = 0. \tag{2.8}$$

This kind of configuration results in a radial force that confines the plasma. In fact, while the magnetic field has to keep particles in a circle, this is a centripetal force against the plasma pressure.

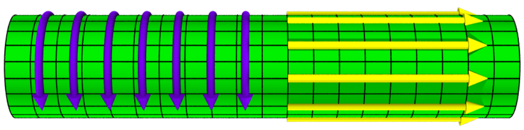

Figure 2.2: $z-$pinch, yellow arrows represents the plasma current and blu arrows the inducted magnetic field

$\theta-$pinch This kind of pinch has an azimuthal plasma current which generates an axial magnetic field. The basic equations are Eqs. (2.6) and (2.7), but the results are different. In fact, one can write that

$$\frac{d}{dr}(p + \frac{B_z^2}{2\mu_0}) = 0. \tag{2.9}$$

This means that the term $p + \frac{B_z^2}{2\mu_0}$ is constant with respect to the radius, and this provides stability to the plasma.

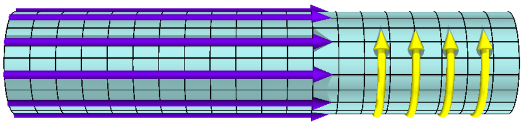

Figure 2.3: $\theta-$pinch, yellow is the electrical field and so the current, while blue is the magnetic field.

2.2.2 Magnetic Field Confinement

Basically, in a reactor a magnetic field is designed in order to keep the plasma away from walls so that enormous heating is possible. This requires a *close* magnetic field, that means field lines close in a finite space, that is the dimension of the reactor.

Its working principle is the Lorentz force: a particle with a charge q moving in a uniform magnetic field $\mathbf{B}$ experiences a force $q\mathbf{v} \times \mathbf{B}$. If the initial velocity is perpendicular to the magnetic field lines, the particle will have a circular orbit with a frequency known as cyclotron frequency. The component of velocity parallel to $\mathbf{B}$, $v_{\parallel}$, will not change, while the radius and frequency of the helical path will depend only on the perpendicular component, that is $v_{\perp}$. With this principle, we can achieve a magnetic mirror, where particle are reflected backwards on the same helical trajectory by increasing the magnetic field so that the resulting force could reverse the motion of the particle. This phenomena could be used also in a magnetic bottle, where the helical radius is changed by decreasing the magnetic field, as seen in Fig. 2.4. In this way we can confine a particle without using closed field lines.

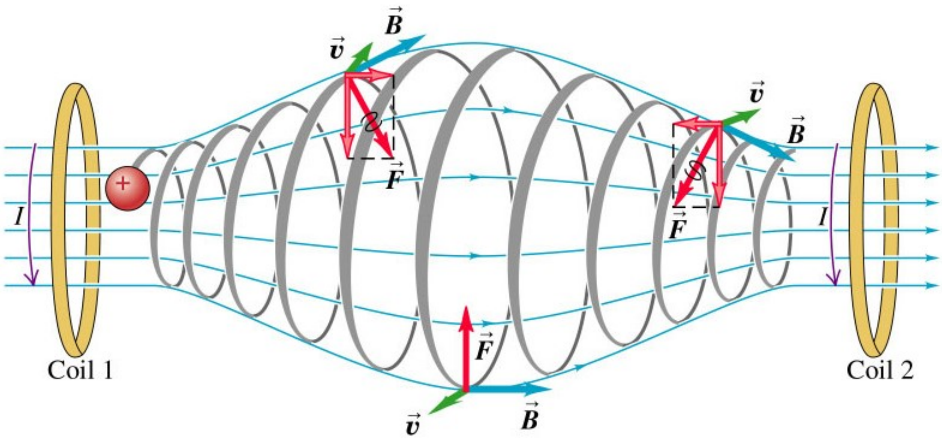

Figure 2.4: Magnetic mirror effect (in this case magnetic bottle). The ion will follow the magnetic field line and it will be subject to a force directed towards the center of the bottle. The smaller the radius, the higher the velocity.- *Photo Copyright Parsons Education Inc*

The first kind of confinement is a uniform magnetic field, which keeps charged particles to spiral around the direction of the field. In order to keep particles inside the reactor, we can act in two different ways, that are a torus shaped magnetic field that keeps particles spiraling in a ring or a magnetic mirror where high density magnetic field keeps particles from exiting the spacecraft. The peculiarity with a torus shaped magnetic field is that B is weaker at larger radii, so particles tent to approach the walls, thus dissipate energy: for this reason a poloidal component of B has to be generated. The difference between the two can be seen in Fig. 2.5. Such a configuration can be achieved in two ways:

- A set of external coils in a helical winding around the torus and by a externally induced current in the plasma, which in turn heats the plasma as well.
- A set of external windings acting as a transformer will generate the current in plasma.

The kind of reactor that uses a toroidal plus a poloidal field induced by plasma current is called Tokamak, while if external helicon winding coils are used for the poloidal field the reactor is called Stellator. In the second case, depending on the geometry of windings, it can assume different names.

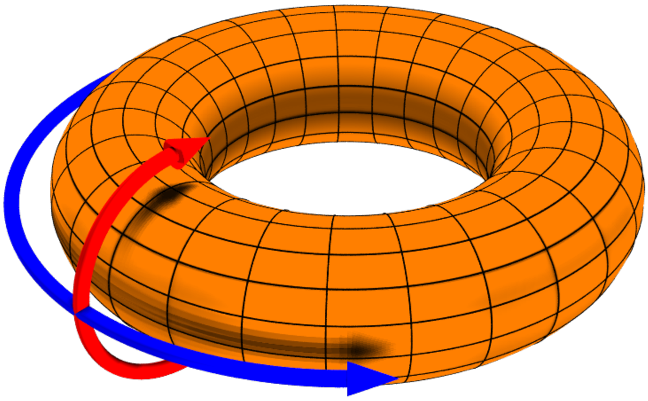

Figure 2.5: Toroidal (Blue) and Poloidal (Red) fields around a torus shape

In truth, it could also be achieved a spherical shape reactor via a spherical shaped plasma, with a hole at its center, that has the same features of a torus, but in 3 dimensions. This will enable higher plasma pressures and so smaller dimensions.

2.2.3 Inertial confinement

In this case, a solid pellet of fuel of dimensions around 1 mm is struck at the same time by many beams, that could be both photons or particles, as seen in Fig. 2.6. This is generally a laser source, but in order to satisfy the Lawson criterion enormous quantity of power are required, even if the density is considered higher that what is actually possible. This is because the pellet will collapse in about $10^{-11} - 10^{-9}$ s.

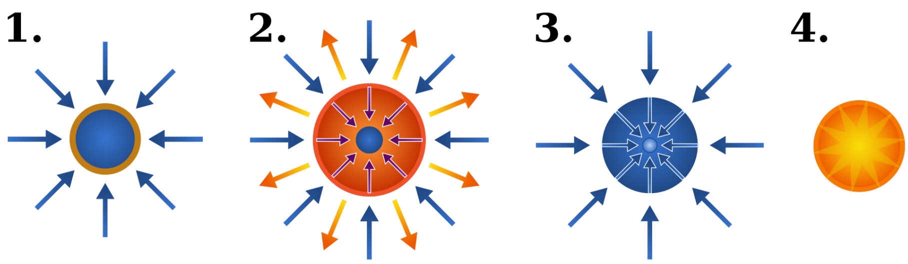

Figure 2.6: Dynamics of the inertial confinement: 1) Plasma generation due to pellet compression and heating; 2) Ablation of surface, the core is compressed; 3) At the end of compression, the fuel is hot a dense enough to ignite the fusion process; 4) The energy from fusion is released in the environment

2.2.4 Magneto-inertial confinement

Instead of a magnetic confinement fusion (MCF) or inertial confinement fusion (ICF), we can combine the two techniques in order to face the Lawson criteria not only on the density as ICF or on the confinement time as MCF, but on the two together. It is basically a ICF that operates on a magnetically confined plasma, in order to reduce heat losses and density, while more confinement time is required.

2.2.5 Heating

There are many ways to heat the plasma above the critical ignition temperature explained in section 2.1, in addition to the heat provided by plasma current, which is called ohmic heating.

- **Radio Frequency heating.** Electromagnetic waves are used to excite charged particles up to certain frequency so that they resonate and gain energy. Particles can be excited in many ways. If the applied electromagnetic wave is an applied fixed magnetic field, cyclotronic frequency of a particle has to be considered. It can be expressed as follows

$$\omega_c = qB/(m\gamma), \tag{2.10}$$
$$f_c = \omega_c/(2\pi). \tag{2.11}$$

  This particular frequency has the main feature of keeping all the particles at the same frequency, no matter their energy. Higher energy particles will have larger radius. On the other hand, if the applied field is time-varying, the system will be betatron-like, and particles will gain energy with the varying field.

  The wave could be injected in the plasma via antennas or, if microwaves are considered, via waveguides.

- **Neutral Beam Injection**. It consist in an auxiliary circuit where H or D ions are heated up to $10-100$ keV and injected into the plasma after neutralization: in this way neutral particles are still highly energetic, but not affected by the magnetic field. The heat is transferred via Coulomb scattering from plasma's ions and electrons.

Once the nuclear fusion reaction has started and it is stable, it will provide itself the energy to sustain the heat. In chapter it will be analyzed the DFD, which is the nuclear fusion drive subject of this thesis.

2.3 Nuclear Fusion for a Direct Drive

The idea behind a drive is to harness in a direct way the power from nuclear fusion, by heating a propellant and making it expand into a nozzle. In this way, it would accelerate particles of the propellant and this will produce thrust.

It will not be necessary to convert the fusion power to electrical power that will feed an electric thruster, and in this way many line losses can be avoided.

2.3.1 Open Magnetic Field Configuration

In order to use a direct propulsion system, we need to achieve the largest possible fusion extent, in order to directly convert the power to thrust, without relying on low efficiency power conversion systems to generate power for some kind of electric propulsion system. Though, a percentage of fusion power has to be converted to electrical power in order to supply auxiliary systems. A promising concept for this direct utilization is the open magnetic field (OMF) configuration, which relies on the fact that field lines escape from the plasma confinement zone, without crossing any surfaces, and this makes this kind of device suitable for direct propulsion system, still enabling some kind of power conversion system.

As stated in Ref. [18], mean features of this kind of drive are:

- Easily achievable steady-state operation;
- Natural particle exhaust;
- High β from Eq. (2.3);
- Efficient direct conversion from nuclear fusion power to thrust;

What follows is a general overview on main OMF configurations, as explained in Ref. [18].

Mirror configurations They rely on a solenoidal magnetic "bottle", which is ideal to eject plasma from one end and achieve thrust. Many configuration have been studied in order to improve stability and confinement, thus increasing mean kinetic temperatures of ions and electrons. The typical β parameter for this kind of configuration is around 20%, while it can be above this parameter for some coordinate inside the plasma.

Spheromaks The spheromak is a toroidal configuration in which there are both a poloidal and a toroidal magnetic field, of equal intensities. It can be generated in many different ways, but in general they can produce experimentally up to $\beta = 20\%$ with low confinement times, as seen in Refs. [20, 18].

Field Reversed Configuration This configuration is a compact toroid where the poloidal field is of some magnitude order higher than the toroidal one, so that the latter becomes negligible, and this is the main difference with the spheromak. Field reversed configurations (FRCs) have been discovered as a consequence of $\theta-$pinches, where the axial magnetic field induces a azimuthal electric field, hence a current is generated and so is the poloidal magnetic field. The poloidal magnetic field is, by definition, a closed field. For this reason, it has to be defined a separatrix surface between the open externally induced field and the closed one. The main advantage of such a configuration is that one can express the mean value of β via

$$\bar{\beta} = 1 - \frac{{r_s}^2}{2{r_c}^2}, \tag{2.12}$$

where r_s is the separatrix radius, and the separatrix is the zone between the close and the open magnetic field lines, where the plasma is confined. On the other hand, r_c is the flux conserver radius or, in other words, the zone in which the magnetic flux inside the conductor is conserved. Since that $r_s \leq r_c$, this means that $\bar{\beta} \geq 50\%$ [18]. This kind of confinement will be further analyzed in the following sections.

The name Field Reversed Configuration comes from the formation method, which requires to quickly revert the initial magnetic field in order to induce the toroidal current in plasma, hence the poloidal field.

2.3.2 Field Reversed Configuration in Space Propulsion

Given that the FRC-OMF plasma configuration has great β values and good confinement, the possibilities for a direct use of this technology for a space drive has been studied since 1989 as said in Ref. [21]. The possibility of a propulsion system based on these features, combined with a $\mathrm{D} - {}^3\mathrm{He}$ aneutronic reaction, could result in a compact design with high power to mass ratio.

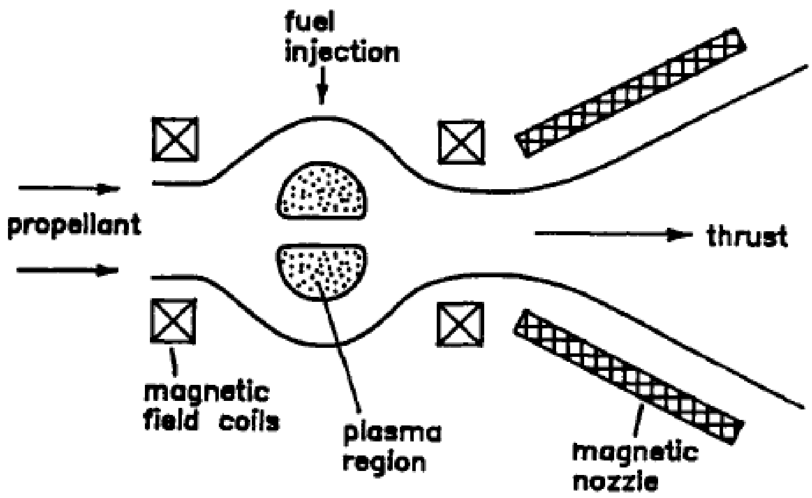

Figure 2.7: Basic of a FRC-based space drive as presented in [21]

As shown in Fig. 2.7, the drive studied by Chapman in Ref. [21] is divided into 3 main parts, that are the plasma region, when fusion happens, the magnetic bottle in which the propellant flows and gets heated by the plasma region itself and the magnetic nozzle that provides actual thrust.

As far the plasma parameters are concerned, main parameters required are a ion kinetic temperature of the magnitude of 100 keV and $\tau \approx 10$ s are taken into account. As in a common FRC, there is an azimuthal current: in this device it is controlled via both the fusion products and a controlled pellet (fuel) injection. The propellant flow flux is controlled via an unbalanced magnetic field, which keep it flowing towards the magnetic nozzle.

In the region described as magnetic bottle coexist two different kind of plasma: the one inside the separatrix surface, which is the hot one where fusion happens and an external one, between the toroidal plasma and the physical walls of the device. For this reason, the cold one gets heated from both large orbit fusion products and core radiation.

This heated plasma will expand in a magnetic nozzle, converting the thermal energy of the plasma to kinetic energy, thus providing thrust to the system. This works exactly as a physical nozzle, with the only difference that the fluid does not heat any physical wall. As can be seen in Fig. 2.8, it is the opposite of a magnetic mirror: by reducing the field lines and so the field intensity, the plasma can follow **B** and finally expand. The main feature about this reactor is that one can adjust

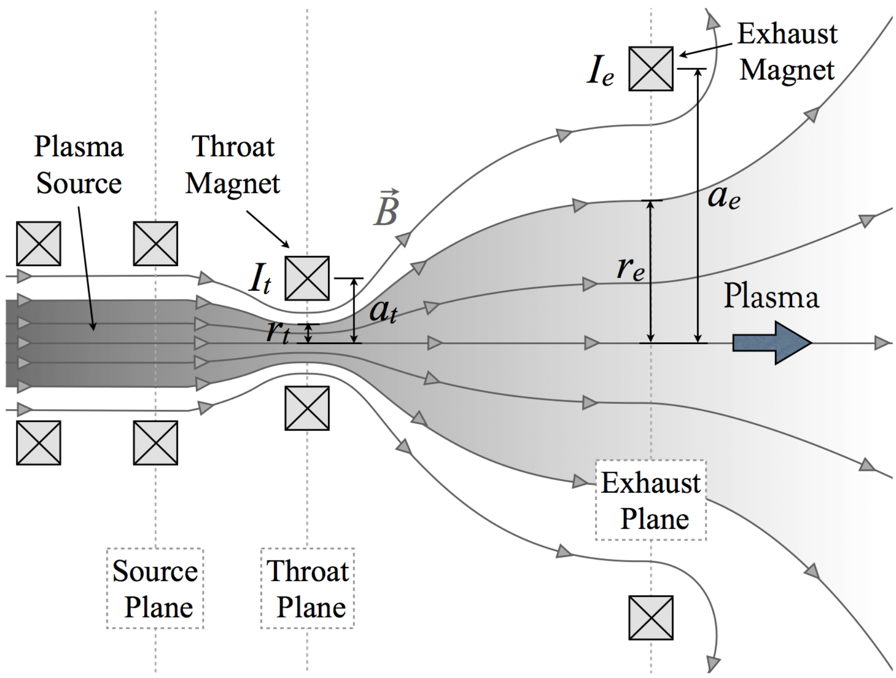

Figure 2.8: Magnetic Nozzle with field lines - in this case the plasma source is the magnetic bottle [22]

thrust and I_{sp} by changing the propellant flow. This, as expressed in Ref.[21], can lead to a thruster capable of changing its performance in the range expressed in the next table.

Table 2.2: Estimation made with the assumptions of $\beta = 50\%$ and a total power produced of about 0.5 GW

$\dot{m}$ [kg/s]	I_{sp} [s]	T [kN]
0	10^6	0.4
0.8	10^3	50

In the following chapter it will be compared with other drives.

2.4 Direct Fusion Drive

The Direct Fusion Drive (DFD) is a revolutionary steady state fusion propulsion concept, based on a compact fusion reactor. It will provide power of the order of units of MW, providing both thrust of the order of $10^0 - 10^1$ N with specific impulses between $10^3 - 10^5$ s and auxiliary power to the space system. The main feature of this drive is that it is based on the OMF FRC, so it could achieve high β with relatively low powers, thus enabling the use of advanced aneutronic fuels such as $D-^3He$. This, as already said in Sec. 1.3.3, will result in low shielding densities and acceptable specific powers.

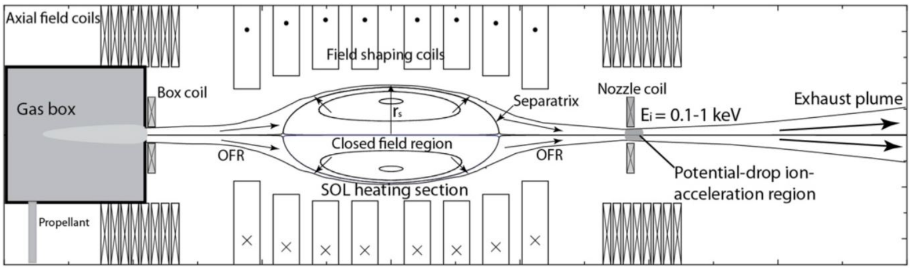

Figure 2.9: Schematics for the DFD. The gas box is where the propellant is ionized, then it will enter the zone of the open magnetic field lines, shaped by the field shaping coils, which are superconductive coils. Inside this zone, that is surrounded by the antennas that will generate the RMF_O, fusion and heat exchange with the propellant will happen. This zone ends with the nozzle coil, which will continue into a magnetic nozzle, where the heated propellant will expand, producing thrust.

2.4.1 The Princeton Field Reversed Configuration

The DFD will be based on the Princeton Field Reversed Configuration, or PFRC, which is a standard FRC where both heating and confinement is achieved with a rotating odd parity magnetic field (RMF_O). This kind of configuration generates a toroidal current powerful enough to heat the plasma to fusion-relevant temperatures. This current will in turn produce a poloidal magnetic field, which will confine the plasma into the most classical FRC configuration as in Fig. 2.10.

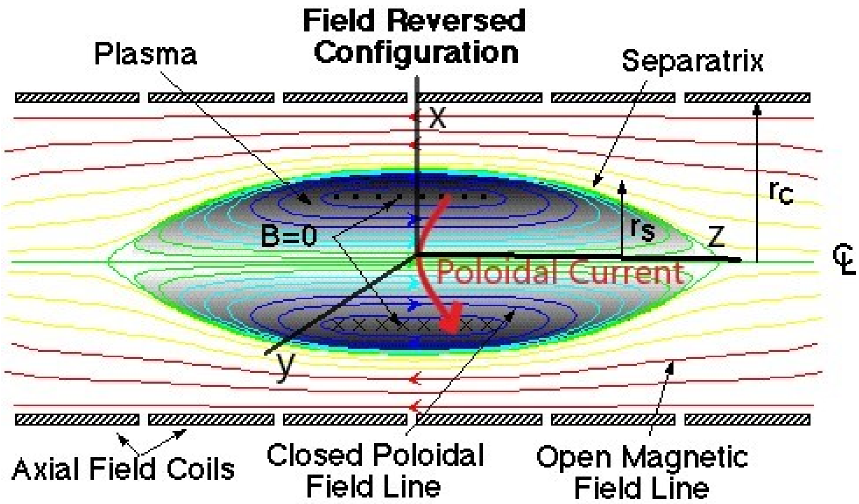

Figure 2.10: Basic FRC configuration

2.4.2 Heating Mechanism in PFRC

The peculiarity of PFRC resides into the heating mechanism, which also induces the toroidal current and so the poloidal magnetic field. The rotating magnetic field is generated by RF antennas positioned into planes parallel to $\mathbf{x}-\mathbf{z}$ and $\mathbf{y}-\mathbf{z}$ planes, with reference to Fig. 2.10. In this way, the antennas would be phased of 90° from one to the other, and by controlling the current in those antennas a transverse rotating field in the $\mathbf{x}-\mathbf{y}$ plane can be induced, as can be seen in Fig. 2.11. Note that the antenna are fixed into space, the "rotating" adjective refers to the magnetic field B_R.

As explained in Ref. [23] rotating magnetic field will generate a induced axial current. By considering a simple model based on the generalized Ohm law, we can state that

$$\mathbf{E} - \frac{1}{n_e e}(\mathbf{j} \times \mathbf{B}) = \eta \mathbf{j}, \tag{2.13}$$

where $\mathbf{E}$ is the electrical field, n_e is the electron density in plasma and η is the resistivity.

By considering only the Hall term, defined by $\mathbf{j}\times\mathbf{B}$, the Hall field product will be in the azimuthal direction θ. This means that a force that accelerates the electrons in that direction is generated, with a correlated current density that can be written as $j_\theta(r) = -n_e e v_{e\theta}(r)$. The maximum for this current is reached when $v_{e\theta}^{max} = r\omega$, where r the radius of the particle and ω is the pulsation of the rotating magnetic field. In addition to the Hall-generated current there could also be an azimuthal electrical field $\mathbf{E}$ which further accelerates the particle. The effect previously explained heats the plasma via Ohmic heating.

The other contribution comes from the frequency of the RF wave generated by antennas in the form of a electromagnetic field. In Sec. 2.2.5 it has been defined the heating mechanism via resonance, and ion-cyclotron frequency has been expressed

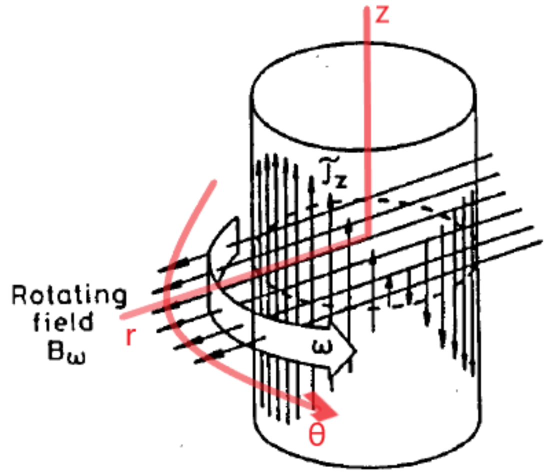

Figure 2.11: Axial current induced by the rotating field as in Ref.[23]

as $\omega_{ci} = qB/(m\gamma)$. Since both the axial externally-imposed magnetic field (B_A) and the rotating magnetic field of amplitude B_R are applied to the plasma, there are two possible characteristic frequencies, hence ω_{ciR} and ω_{ciA} . Since typically $\frac{B_R}{B_A} \approx 10^{-3}$, the first frequency would be way lower than the second. This is important because the RF in PFRC be of the same magnitude of the ion-cyclotron frequency in the axial field as explained in Ref.[24], so that $\omega_R \approx \omega_{ciA}$. In this way, if the confinement time is long enough, an appreciable heating can be observed.

Now the odd-parity nature of the RMF comes into play. First of all, the term "odd" refers to the symmetry of the field with respect to the $\mathbf{x} - \mathbf{y}$ mid-plane: at a certain coordinate $+z$, the field (in this case the rotating one) will be phased of 180° to the field at the coordinate $-z$, as can be seen in Fig. 2.12.

In practice, the antenna would be phased in a 8-shaped configuration, as can be seen in Fig. 2.13. This configuration stabilizes the FRC, because in the center of the toroidal plasma the z-negative coordinate of the torus is stabilized by the positive one, and vice versa. The result is an energy distribution along the axis that is qualitatively similar to that in Fig. 2.14. Note that higher energies corresponds to a larger radius, so Fig. 2.14 can be used to visualize particle distribution with respect to the z position, and a torus-like shape is visible.

Another plausible configuration was a even-parity RMF , but in that case the plasma will not be as stable as the odd-parity one, resulting in a lower confinement time and a very low chance of fusion happening. For further details, see Refs. [25, 26].

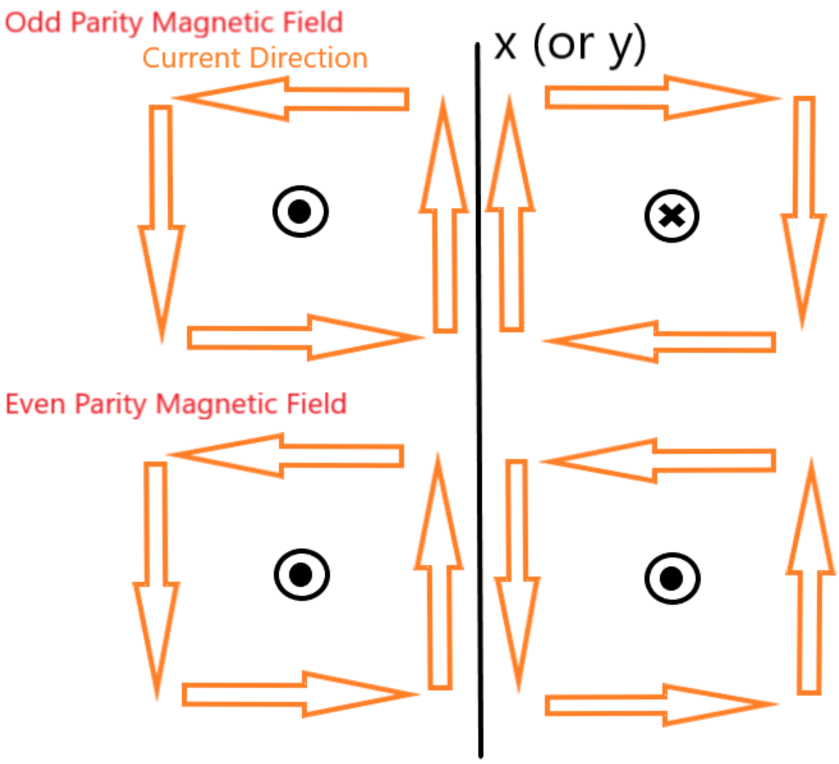

Figure 2.12: Graphical representation of the current flow in the antennas needed to generate an odd parity rotating magnetic field, compared to the equivalent magnetic field

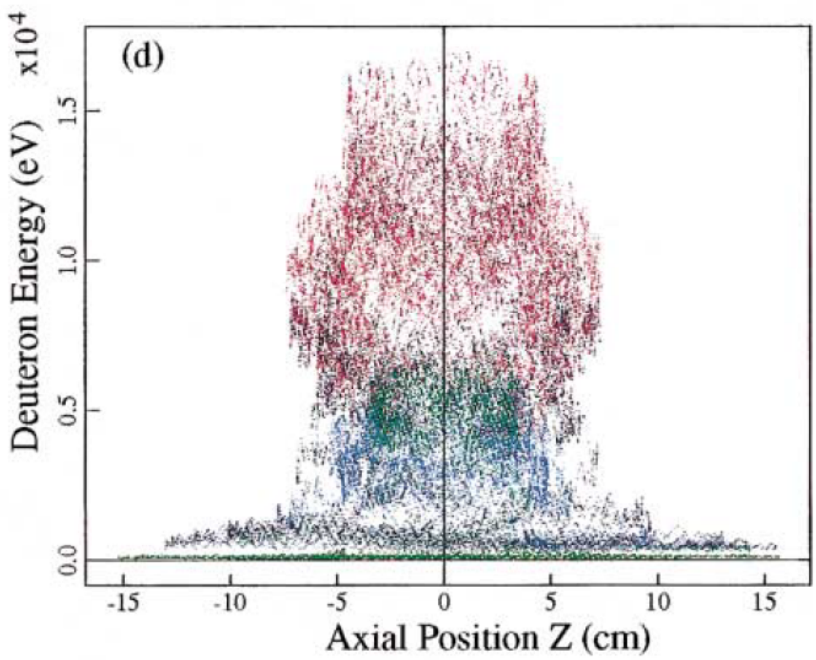

Figure 2.14: Energy distribution along the z-axis (from [24]). The colors represents the time-evolution of the energy (green-blue-red)

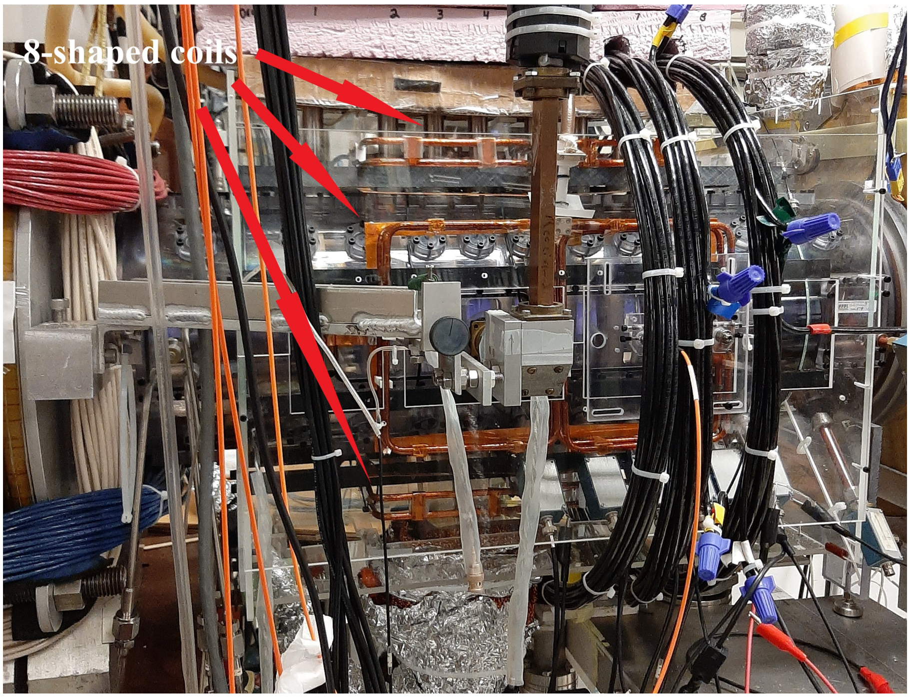

Figure 2.13: Real 8-shaped coils on the PFRC-2 reactor at Princeton Physics Plasma Laboratory - Personal Photo

In conclusion, the maximum ion energy will be proportional to ω_{RMF}, but this is dependent to the radius (r) and the plasma density (δ) in the relation $\omega_{RMF} \approx \delta r^2$. This means that to reach a certain frequency, and so the ion energy we need, both radius and density have to be limited. In this very case, the ion temperature needed is about 100 keV and the plasma radius has to be in the range of $20 - 30$ cm. This means a very diametrically small engine with a moderated plasma density configuration [27].

2.4.3 Confinement in PFRC

The confinement in this FRC is obtained as a consequence of the Odd-Parity RMF. The current, in fact, confines the plasma within the inducted poloidal field.

The odd-nature of the RF field will further increase the confinement capability, by adding odd symmetry with respect to the midplane $\mathbf{x} - \mathbf{y}$: in other words, instability phenomena linked to the axial current or magnetic field are compensated by the other half of the magnetic field. This capability will enable longer confinement time than more classical configuration, thus giving more time to plasma to heat up.

The peculiarity of this configuration is the "magnetic null" inside the torus, which means that there is a circumferential zone in which the magnetic field becomes zero and outside of it has opposite direction, depending on the radial coordinate. By looking at Fig. 2.10, given the coordinate of the magnetic null, for example, $+x$, at $x + dx$ $\mathbf{B}$ will have one direction and at $x - dx$ $\mathbf{B}$ will have another one. This will result in complex trajectories, which will vary from cyclotron to betatron motion, depending if they will cross the magnetic null or not, as seen in Ref. [27].

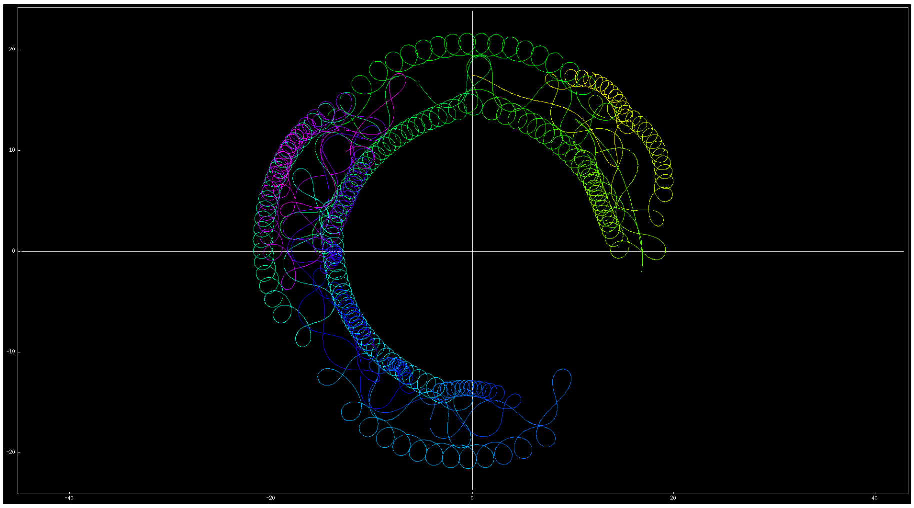

Figure 2.15: Motion of a particle which starts as a cyclotron (green end), crosses the null and reverses its trajectory, becomes betatronic (8-shaped) and back - Credits: Wikipedia Image

2.4.4 Thrust Generation

Throughout the linear dimension of this reactor, axial field coils are visible, and their role is to maintain an axial magnetic field through which the propellant will flow as in Chapman device analyzed in Sec. 2.3.2 and in Ref. [21]. This propellant is injected from the gas box at the far end of the device, then will flow axially throughout the device, receive heat from the fusion core and then expand into the magnetic flow. This process is named thrust augmentation in Ref. [27].

The heat exchange mechanism is mainly based on the Scrape Off Layer (SOL) interaction. This zone is the cold propellant plasma layer around the torus shaped hot plasma. In the DFD, the SOL is typically $5-10$ cm thick, as seen in Fig. 2.16. This zone will be reached by highly energetic fusion products (therefore with larger radius), that will exchange heat with electrons via by an electron drag energy transfer mechanism as seen in Fig. 2.17. Those will in turn transfer the heat received to ions, while the plasma exits the core and expands to the magnetic nozzle as seen in Ref. [27] and in Fig. 2.18. The other main heating mechanism of electrons is a synchrotron radiation, as explained in Ref. [28].

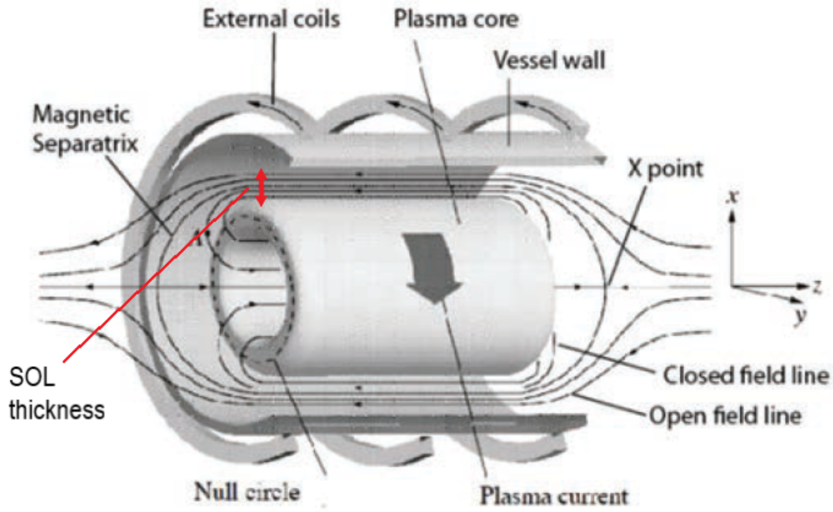

Figure 2.16: SOL thickness in a typical FRC configuration - From Ref. [29]

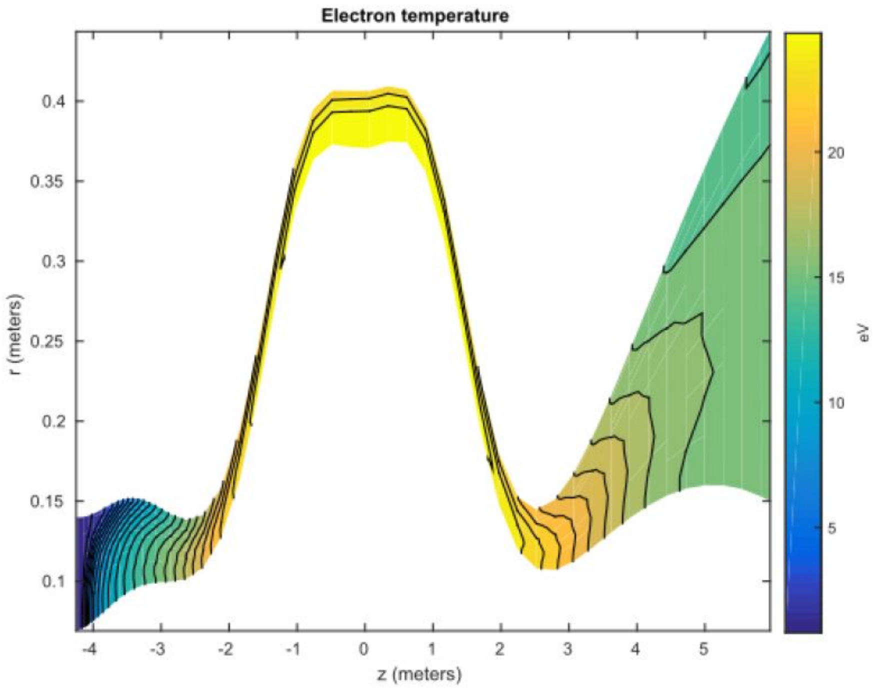

Figure 2.17: Electron temperature (energy) [eV] in the SOL for 1 MW of heating power as analyzed in Ref. [30]

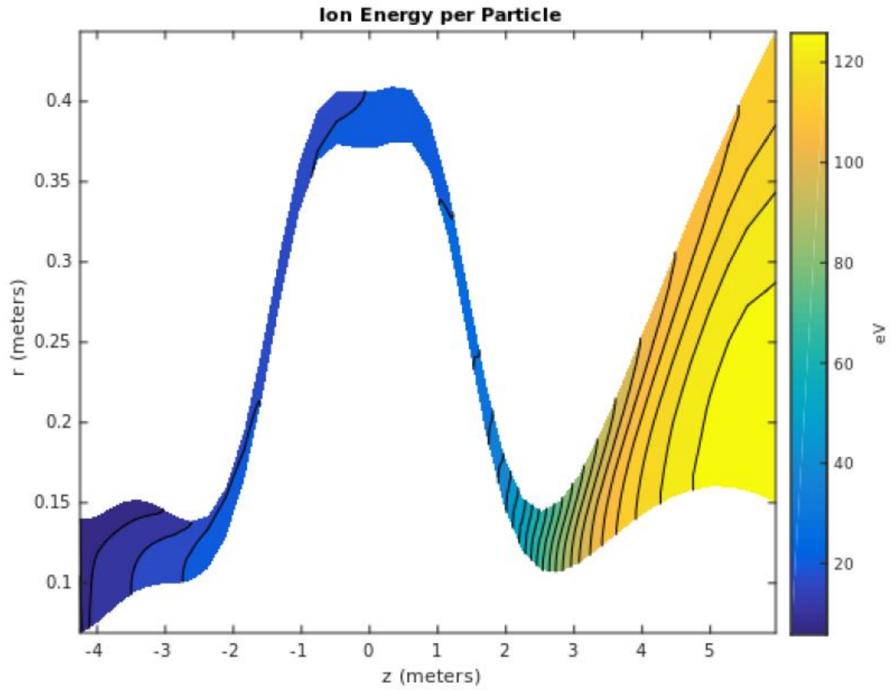

Figure 2.18: Ion temperature (energy) [eV] in the SOL for 1 MW of heating power [30]. Note that the energy from electrons in Fig. 2.17 have been transferred to the ions in the magnetic nozzle

The propellant gas would be, in most analysis, deuterium which can be synthesized easily and at a low cost. Moreover, it would be also used as one of the two components of the fusion fuel: this is the reason why it is considered as the main propellant for this engine. Theoretically, though, other low molecular weight propellant can be used, such as liquid molecular hydrogen or more complex molecules.

An ideal propellant would be Argon, that would provide, with no thermal power losses before the exhaust and in best theoretical estimations, from 700 s to 1.3×10^6 s, from Ref. [31].

2.4.5 Engine Performance

In this section thrust, specific impulse and propulsion efficiency are analyzed, with respect to the input power and the propellant feed. All the data analyzed in this section are the summary of the work made by Princeton plasma physics laboratory (PPPL) and Princeton Satellite Systems (PSS), as found in Refs. [27, 30] . All of the following data come from a state of the art estimation.

Mainly, for this kind of engine there are two inputs: the power inside the scrape off layer (the one from graphs legends) and the propellant mass flow (not the fuel mass flow responsible for the fusion itself, which is negligible). The first is of the order of $40 - 55\%$ of the total power generated by the fusion, while the latter is of the order of $0.01 - 0.1$ g/s.

The thrust and specific impulse have been estimated for a steady state via UEDGE simulations, and examples of those can be found in Ref. [30]. UEDGE is a 2D multi-species fluid code used to model the SOL region of fusion reactors, and can take into account all MHD phenomena, as well as ionization and recombination rates and it is better explained in Refs. [32, 33, 34]. Once the continuity equations of energy and momentum are solved, the exit velocity together with mass flow are used to compute the thrust and specific impulse.

$$T = \dot{m} v_{\parallel}, \tag{2.14}$$

where $v_{\parallel}$ is the velocity of particles parallel to the axis of the engine and

$$I_{sp} = \frac{T}{\dot{m} g_0}, \tag{2.15}$$

where g_0 is the acceleration of gravity on the surface of Earth, nominally $g_0 = 9.806 m/s^2$.

Finally, the propulsion efficiency, that is defined as the ratio of kinetic energy that contributes to thrust to the input power to the SOL can be written as

$$\eta = \frac{\dot{m} v_{\parallel}^2}{2P}. \tag{2.16}$$

As it is seen in Figs. 2.19 - 2.21 all the dependence of the thrust, specific impulse and efficiency rapidly falls for a particular gas input. This is because from simulations appears that increasing the propellant flow for the fixed input power leads to detachment of the plasma from outer boundary walls and this causes a drop in all values. Note that all the power reported in legends refer to the power in the SOL.

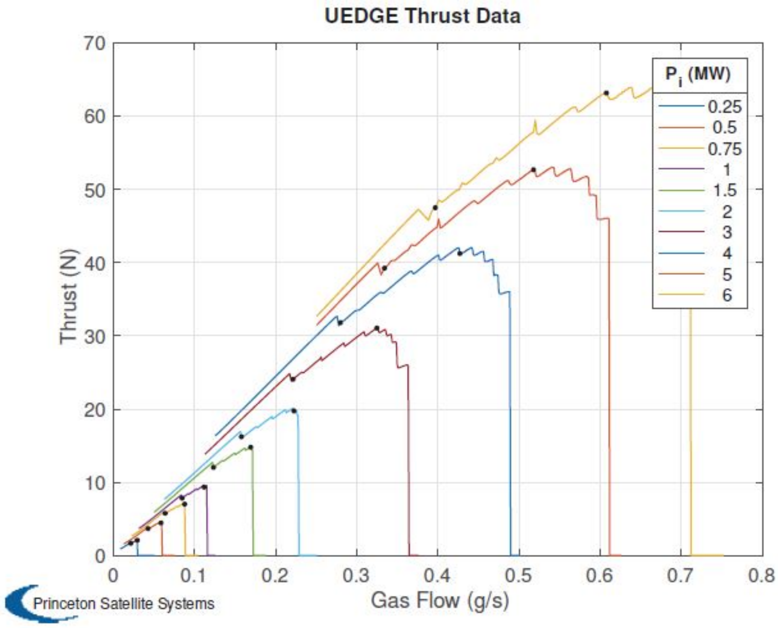

Figure 2.19: Dependence of thrust on gas input for different input powers to SOL, from Refs. [35, 36].

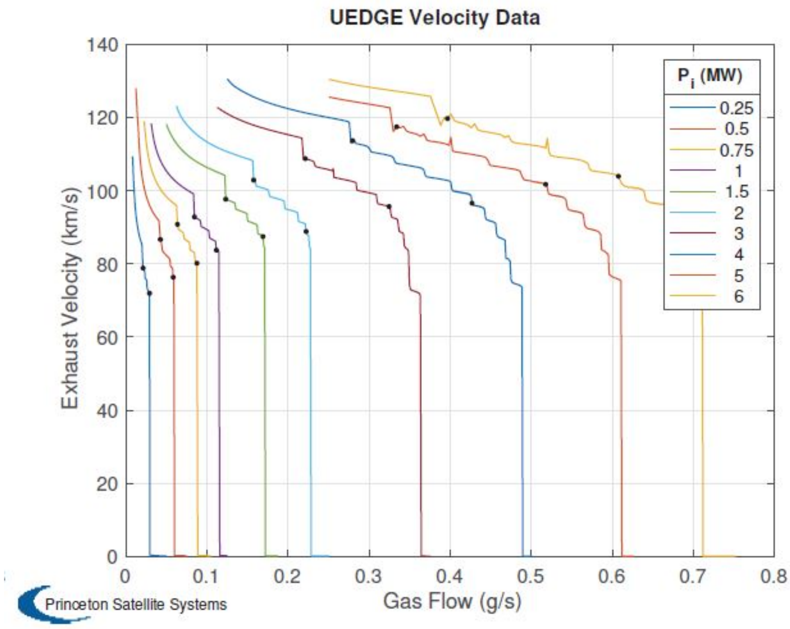

Figure 2.20: Dependence of exhaust velocity on gas input for different input powers to SOL, from Refs. [35, 36].

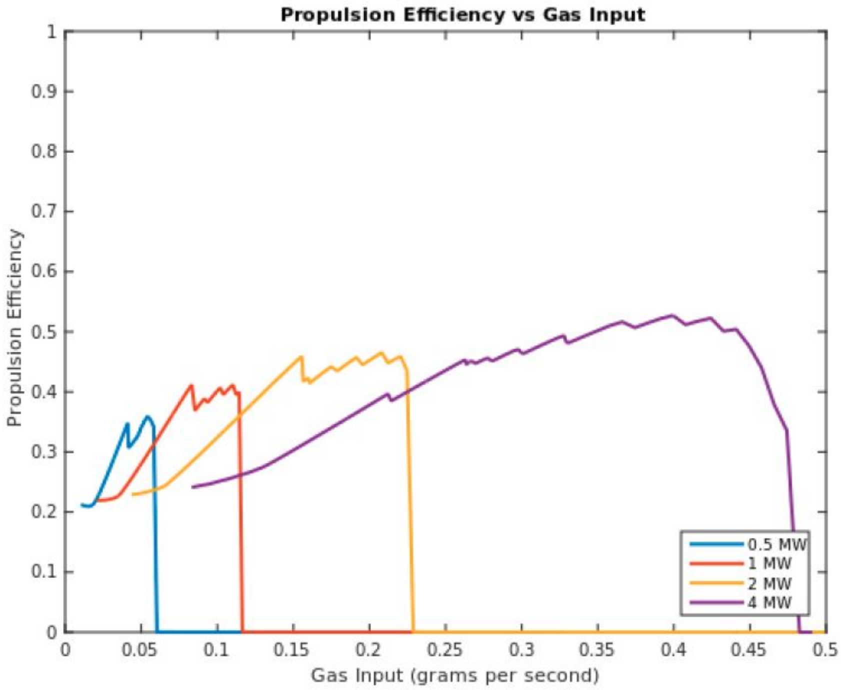

Figure 2.21: Dependence of propulsion efficiency on gas input for different input powers to SOL, from Ref. [30].

Finally, interpolating those data as seen in Ref. [35], a more complete graph is obtained, as it is shown in Fig. 2.22. The overall results are reported in Table 2.3 for the low and high power configurations. It is important to point out that the specific power is higher for the high power configuration. However, the DFD can be fully scaled in configuration for reaching the power required.

Due to the compactness of this engine, multiple modular DFDs can be combined into a cluster of many engines: it will result in a total thrust that is the sum of the thrusts from the single engines. The specific impulse, though, will remain the same, because multiple engines will not affect the propellant consumption of each DFD.

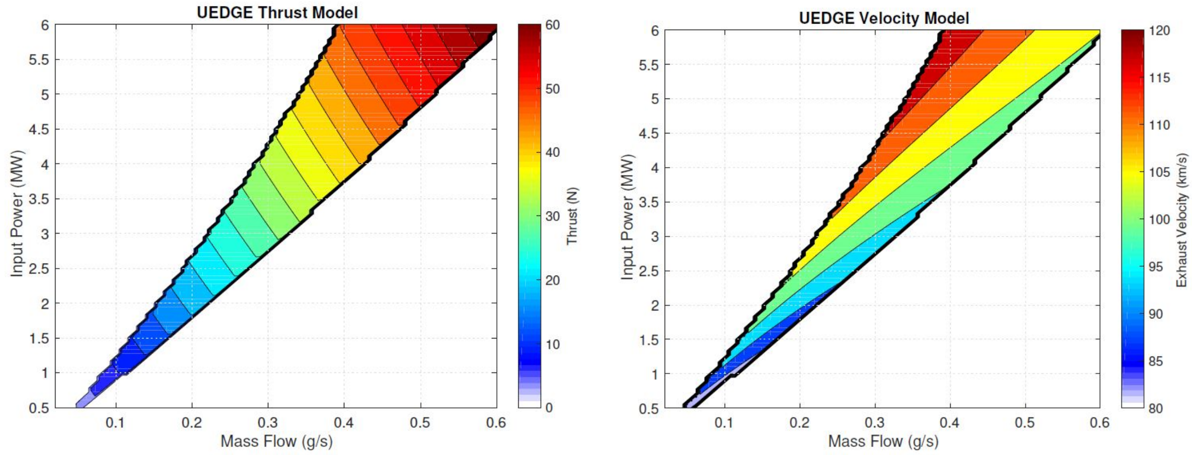

Figure 2.22: Dependence of thrust and exhaust velocity on propellant flow and SOL power. An increase of power input would require an increase of propellant mass input, but it would lead to higher thrust and I_{sp}. An increase of power input would also increase the range in which T and I_{sp} vary.

Table 2.3: DFD characteristics for low and high power configuration. Higher specific impulse will lead to lower thrust for the same configuration. [29]

	Low power configuration		High power configuration	
Fusion Power, [MW]	1		10	
I_{sp}, [s]	8500	8000	12000	9900
T, [N]	4	5	35	55
Fusion Efficiency	0.17	0.18	0.27	0.31
Thrust Power, [MW]	0.46		5.6	
Specific power, [kW/kg]	0.75		1.25	

Depending on the travel time, the payload mass and the type of mission, all the ranges between 1 and 10 MW can be selected.

Many estimations have been made about the exact specific powers for this engine, but at this point of the development only ranges can be estimated. The exact value depend on the overall mass of the engine, and it will be influenced by many factors, as it is explained in Sec. 2.4.8.

Table 2.4: Specific power estimations for the DFD as seen in Refs. [27, 29]. The thrust specific power and electric specific power refers to the power from fusion that actually goes to thrust and electric power generation.

	Highest and Lowest values achievable
Overall specific power	$0.75 - 1.25$ kW/kg
Thrust specific power	$0.45 - 0.56$ kW/kg
Electric specific power	~ 0.08 kW/kg

Table 2.5: In this table, taken from Ref. [37], the fuel consumption has been calculated by dividing the total fuel consumption by the days of mission and the fusion power. In this way it has been found a fuel consumption per day per MW of power.

Mission destination	Fusion power [MW]	Mission duration [day]	Total consumption [kg]	Fuel consumption [kg/(MW×day)]
Mars	60	110	0.98	0.000148
Pluto	0.6	1826 [5 yr]	0.16	0.000146
125 AU	0.8	3653 [10 yr]	0.43	0.000147

2.4.6 Neutron and Radiation Shielding

One of the positive aspects of the DFD is the low flux of neutrons coming from side reactions because of their low probability as discussed in Sec. 1.3.3. It is important to reduce the energy of those particles, if not to stop them. Typically, low atomic numbers materials slow down neutrons and absorbs them. Liquid water, for example, is excellent as shielding, but its liquid form is hard to handle at low temperatures and low pressures environments. The isotope ^{10}B is able to slow down and absorb neutrons and it is also stable itself. Borum carbide as a mixture of C and ^{10}B is available in nature and can also be industrially produced. We will further refer to this particular carbide with the term "enriched boron carbide".

For the DFD, simulations have been made in Ref. [27], where the conservative value of 1% of fusion power would result in neutrons from $\mathrm{D}-\mathrm{D}$ side reaction at the energy of 2.45 MeV. This would result in a shielding of 20 cm of enriched BC for 1 year of continuous operation at 1 MW/m, while 33 cm would be enough for 30 years (instead, 39 cm of not-enriched Boron Carbide can be used) as in Ref. [27].

The neutron flux can be further reduced with various techniques, decreasing the total shielding to 20 cm for a 10 years mission.

2.4.7 Fuel consumption

The fuel commonly considered for the DFD is the D-^{3}He, in a proportion of 1:3 for radiation reasons, as explained in Ref. [35]. In fact, the choice of this ratio would reduce the radiations, because the reduction of the D would avoid side reactions which are the main source of neutrons. The downside is that the power density would decrease slightly.

The ^{3}He fuel consumption, in general, is very complex to calculate and it depends on multiple factors related to the fuel reaction. In order to understand the order of magnitude of that consumption, we interpolated data from previous missions. Multiple preliminary studies have been proposed, and some of them are in a very early stage: this means that the fuel consumption is usually neglected because of its small mass, but for some of them the fuel consumption it has been simulated, based on the duration of the mission, the power and the efficiency of the fusion reaction.

As it is seen in Table 2.5, the fuel consumption is around $1.47\times10^{-4}\frac{\mathrm{kg}}{\mathrm{MWday}}$. This means that, for a 15 years mission, under the hypothesis of a 2 MW engine always on, the mass of ^{3}He required would be about 1.61 kg. This value, on a spacecraft of multiple tonnes, can be neglected in all calculations. Furthermore, even though the amount of ^{3}He is limited on Earth, as seen in Sec. 1.3.4, the value of 1.61 kg is well below the maximum availability.

2.4.8 DFD mass breakdown

Since the first studies of the DFD, it has been taken into account the mass of the various components of the engine. In this section it will be introduced the approach to the mass budget, without focusing on the details, which go beyond the purpose of this thesis.

In general, in all the mission studies performed so far of Refs. [35, 29, 36, 38], the specific power used accounts for everything linked to the engine, not only the thrust generation part. In particular, that specific power is calculated by dividing power of the engine by the total mass of the following parts:

- Shielding. It is the mass of the shielding needed to stop the neutron flux.
- Magnets. These are the superconductive coils that generates the open axial magnetic field.
- Coil cooling. It comprehends all the system that keep the requested temperature on the superconductive coils.
- RMF generation system. It is the system needed to generate the rotating magnetic field that heats the plasma.
- Electrical power generation. It is the mass of the cycle that will transform the heat from the nozzle to the electrical power for the entire spacecraft.
- Radiators. This is the subsystem that will radiate the excess power to the space.
- Structures. It is composed of all the structure that will keep the engine and all its subsystems in their places.

In Tables 2.3 and 2.4 specific power values have been reported. In the following chapter, it is always been used the value of 1 kW/kg for the 2 MW engine, and this is because no definitive value have been calculated. For this reason it has been chosen a mean value of 1 kW/kg, which is not too optimistic nor conservative.

2.4.9 DFD power breakdown

The fusion power generated by the DFD core can be further decomposed in many parts, some of which are about dissipation, while others about power conversion. The product of the fusion is decomposed in the features from Figs. 2.23 and 2.24:

- Gas box. It is the power that goes to the ionization of the propellant.
- Bremsstrahlung. This is the power dissipated because of the breaking radiation explained in Sec. 2.1.1.
- Synchrotron. This is the power radiated as a consequence of the electron heating for thrust generation.
- Neutron. This is the power lost because of the neutron emission.
- Thrust. This is the power converted to thrust power in the SOL.

Among the losses, part of that power is recovered by a cooling system that ends with a heat engine, which generates electrical power from heat. Part of that heat has to be radiated towards the space by the radiators, while the electrical power will feed the spacecraft subsystems and also the rotating magnetic field unit, that is fundamental to achieve the fusion.

In Figs. 2.23 and 2.24 it is given the power breakdown for the low and high power configuration of the DFD. Those charts are important to understand the amount of losses that undergo in a fusion reaction. The positive aspect of the DFD is that part of the power losses is recovered and converted to electrical power.

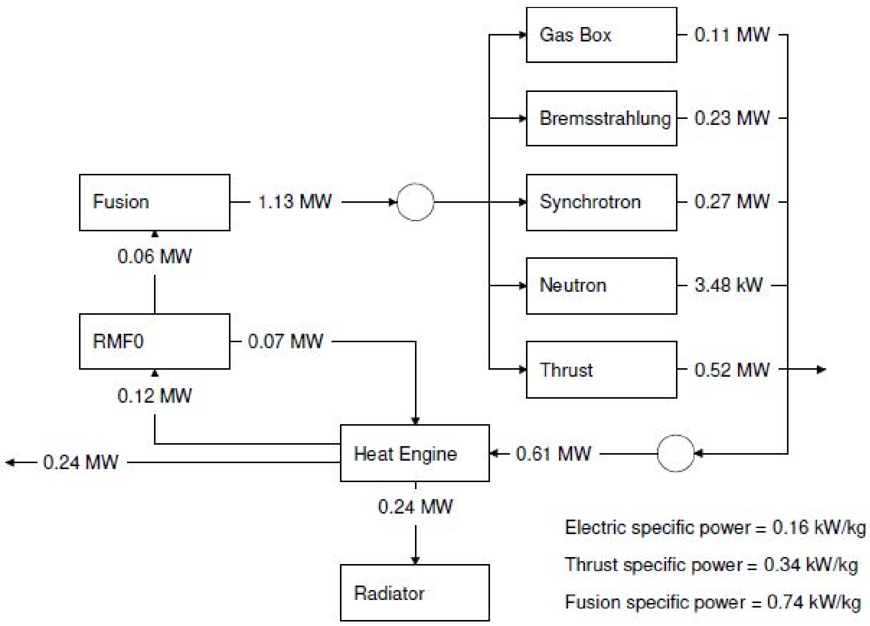

Figure 2.23: Power breakdown for the 1 MW class engine as seen in Ref. [27]

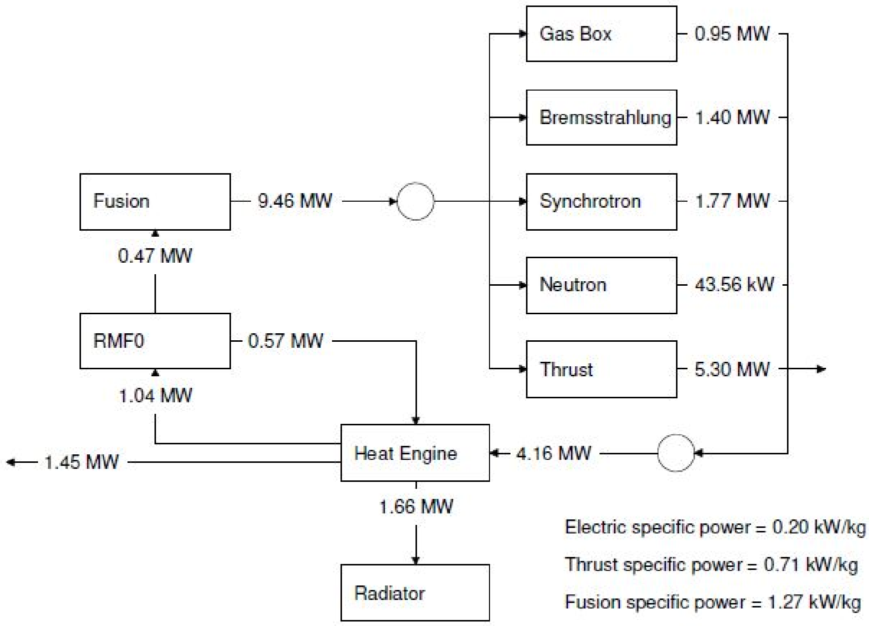

Figure 2.24: Power breakdown for the 10 MW class engine as seen in Ref. [27]

3 Low Thrust Trajectories

3.1 Finite maneuvers

Chemical rockets relies on powerful quasi-instantaneous impulses, of the order of many kN of thrust and of $10^2 - 10^3$ s of specific impulse and this means great instantaneous accelerations, but they only last minutes. On the contrary, low thrust propulsion systems provide a smaller thrust, in this case of study of the order of units of N and enormous specific impulses. Orbital maneuvers, and so, the engine burns, will last days to years, or even for the entire duration of the mission, if a variable specific impulse capability is achieved. The problem with this kind of propulsion systems is that the mathematical approach to the solution of the equation of motion is extremely complex, and an analytic optimal solution has been found only for a limited pool of cases. This requires numerical methods, which are not analyzed in this work. All the integration of motion equations is left to proven and commercials software. In this section is only analyzed the basic theory, following Ref. [39].

3.1.1 Motion equations

First of all, equations of motion have to be considered. The first one is

$$\frac{d^2\mathbf{r}}{dt^2} + \frac{\mu}{r^3}\mathbf{r} = \mathbf{F}/m, \tag{3.1}$$

and relates instantaneous acceleration to the position at time t, to gravitational constant of the central body μ and to all perturbation forces which acts of the spacecraft or our subject of analysis $\mathbf{F}$. Among all forces acting on a spacecraft, the most important are the effect of a third body, the thrust generated by the spacecraft, the effect of the atmospheric drag and the effect of the solar pressure. For our purposes, let us assume that the last two are negligible. Finally, m is the mass of the spacecraft at the instant t. The parameter μ is defined as

$$\mu = GM, \tag{3.2}$$

where G is the universal gravitational constant $G = 6.674 \cdot 10^{-11}$ Nm^{2}kg^{-2} By making the vector product of both the right and left side of Eq. (3.1) of $\mathbf{r}$ it can be obtained the angular momentum $\mathbf{H}$, as seen in

$$\frac{d\mathbf{H}}{dt} = \mathbf{r} \times \mathbf{a}. \tag{3.3}$$

On the other hand, by making the scalar product of both sides of Eq. (3.3) of $\mathbf{r}$ the following equation can be obtained, where

$$\frac{d\mathscr{E}}{dt} = \mathbf{V} \cdot \mathbf{a}, \tag{3.4}$$

where $\mathscr{E}$ is the total energy per unit mass, $\mathbf{V}$ is the velocity and $\mathbf{a}$ is defined as $\mathbf{a} = \mathbf{F}/m$. The fourth basic equation can be written as

$$\mathscr{E} = \frac{1}{2}V^2 - \frac{\mu}{r}. \tag{3.5}$$

3.1.2 Orbital Elements

Every body in space moves in a orbit, which is always contained in its orbital plane at the instant t. This very plane can be defined in a non-rotating reference frame by two angles, but when a rotating reference frame is considered more than two angles are needed. For this reason, classical orbital elements have to be considered.

First of all, the intersection between the orbital plane and the $x - y$ plane is called the line of nodes. The ascending node is the point in which the z coordinate of the body becomes positive. The opposite point is called descending node. The classical orbital elements for an osculating orbit are illustrated in Fig. 3.1 and are the following:

- The semi-major axis of the orbit (a)
- The eccentricity of the orbit (e)
- The inclination of the orbit, which is the angle between the orbital plane and the $x - y$ plane (i)
- The longitude of the ascending node, which is the angle between the x axis and the ascending node (Ω)
- The argument of periapsis, which is the angle from the line of nodes to the periapsis of the orbit (ω)
- The true anomaly, which is the angle between the periapsis and the position vector (ν or θ) .

Note that the term osculating refers to the fact that these elements are defined at a certain instant, and each perturbation modify them.

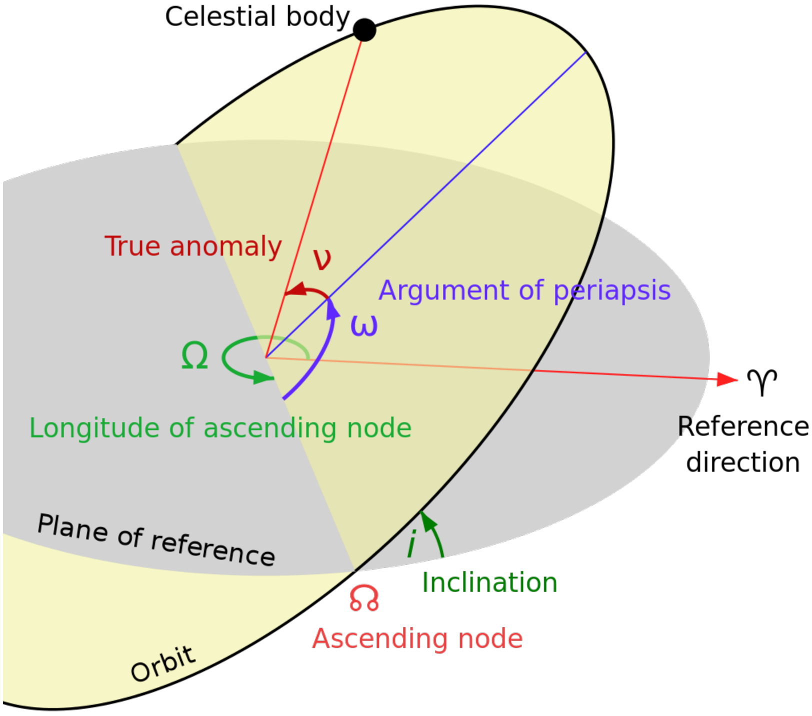

Figure 3.1: Classical osculating Orbital Elements

3.1.3 Simple solution for motion equations

If all perturbation forces acting on the spacecraft are neglected except for the gravitational influence of a central body, simple solution can be found by solving motion equation analitically (Ref. [40]). The results are conic section and the position vector can be expressed in polar coordinates, where the radius is

$$r = \frac{a(1-e^2)}{1-e\cos\nu}. \tag{3.6}$$

It is referred to this kind of orbit by the term "keplerian orbits".

This kind of approach can be used for interplanetary or interstellar calculations only if some very strict hypothesis are done, such as

- Impulsive maneuvers: the change of velocity (both direction and magnitude) of the spacecraft is considered instantaneous, and so the change in mass.
- The central body changes only when the spacecraft exits the sphere of influence, which is defined as

$$r_{SOI} \approx a(m/M)^{2/5} \tag{3.7}$$

where m is the mass of the spacecraft and M the mass of the central body, which in this work case is always the Sun.

Table 3.1: Sphere of influence, masses and semiaxis major for main planets. Mass are expressed with respect to the Earth mass, which is $m_{Earth} = 5.972 \times 10^{24}$ kg.

Planet	m [kg]	a [AU]	r_{SOI} [km]
Earth	$1.000 \times m_{Earth}$	1.000	0.929×10^6
Mars	$0.107 \times m_{Earth}$	1.524	0.578×10^6
Jupiter	$317.8 \times m_{Earth}$	5.203	48.2×10^6
Saturn	$95.16 \times m_{Earth}$	9.537	54.5×10^6
Neptune	$17.15 \times m_{Earth}$	30.069	86.8×10^6

Under previous hypothesis, some good approximations of trajectories between different planets with instantaneous maneuvers can be obtained. The most common method is the patched-conics approximation, in which the mission is divided in many segment that only consider two bodies. As long as the spacecraft remains inside the sphere of influence of a planet, the only gravitational force is that of the planet. Once it goes further than the r_{SOI}, the Sun becomes the main body and all the other gravitational forces are neglected. In this way, a multibody problem is broken down in multiple two-body problems, which are way easier to solve.

3.1.4 Gauss Planetary Equations

It is possible to express the rate of change of the orbital elements with respect to the perturbation acceleration. Those elements are constant in absence of any external perturbation.

Let us consider a cylindrical reference system for the orbit. We can still use Eq. (3.1), and now we consider that

$$\frac{\mathbf{F}}{M} = \mathbf{a} = a_r \mathbf{e_r} + a_\theta \mathbf{e}_\theta + a_z \mathbf{e_z}, \tag{3.8}$$

where $\mathbf{e_r}$,$\mathbf{e}_\theta$ and $\mathbf{e_z}$ are the unit vectors in the cylindrical reference system. We can easily express the rate of variation of $\mathscr{E}$ and H as follows

$$\dot{\mathscr{E}} = \mathbf{F} \cdot \dot{\mathbf{r}}, \tag{3.9}$$

$$\dot{\mathbf{H}} = \mathbf{r} \times \ddot{\mathbf{r}} = \mathbf{r} \times \mathbf{F} = -rF_r \mathbf{e}_\theta + rF_\theta \mathbf{e_z}. \tag{3.10}$$

Let us consider Gauss planetary equations, as are presented in Ref. [41]. They can be written as:

$$\frac{\dot{a}}{a} = \frac{2h}{\mu(1-e^2)}[e \sin\theta a_r + (1 + e\cos\theta)a_\theta], \tag{3.11}$$

$$\dot{e} = h/\mu[\sin\theta a_r + (\cos\theta + \cos E)F_\theta], \tag{3.12}$$

$$\dot{\omega} = -\frac{h}{\mu}\frac{1}{e}[\cos\theta a_r - (\frac{2 + e\cos\theta}{1 + e\cos\theta})\sin\theta a_\theta] - \frac{\cos i \sin(\omega + \theta) r a_z}{h \sin i}, \tag{3.13}$$

$$\dot{i} = \frac{\cos(\omega + \theta) r a_z}{h}, \tag{3.14}$$

$$\dot{\Omega} = \frac{sin(\omega + \theta) r a_z}{h \sin i}, \tag{3.15}$$

where E is the eccentric anomaly, that is related to the true anomaly by

$$\tan E = \frac{\sqrt{1-e^2}\sin\theta}{e + \cos\theta}. \tag{3.16}$$

The eccentric anomaly can be also used to define the mean anomaly M by

$$M = E - e\sin E. \tag{3.17}$$

Also, we define the mean motion as $n = \sqrt{\frac{\mu}{r^3}}$ and the mean motion at a certain epoch as $M_0 = M - \int_0^t n(t')\mathrm{d}t'$. At this point it can be introduced the sixth planetary equation:

$$\dot{M}_0 = \frac{h}{\mu}\frac{\sqrt{1-e^2}}{e}[(\cos\theta - \frac{2e}{1-e^2}\frac{r}{a})a_r - (1 + \frac{1}{1-e^2}\frac{r}{a})\sin\theta a_t]. \tag{3.18}$$

The problem with all of the previous equations is that, once all the initial conditions are defined, it is not possible to evaluate analytically the solution in the general case, so numerical methods have to be used.

3.1.5 Numerical methods

Let us consider the Eq. (3.1) with a perturbing acceleration different from 0. That cannot be solved in a closed form, but we can try to approach a solution in two ways: if a numeric solution is found, we talk about special perturbations techniques, while if an approximate analytic solution can be obtained, it is a general perturbation technique.

Focusing our attention on numerical methods, or special perturbation techniques, there are three main approaches.

- ***Cowell's method***. It is the easiest one, which consists in integrating the elementary form, given the initial conditions. It is not relevant the kind of conic section considered, and that is because it is the simplest method imaginable. In order to have a sufficient accuracy, the integration step should be small enough.

- ***Encke's method***. It is based on the use of reference orbit as, for example, an osculating keplerian orbit. If unperturbed, the satellite will follow $\frac{d^2\mathbf{r}'}{dt^2} - \frac{\mu}{r'^3}\mathbf{r}' = 0$, with r' radius of the osculating orbit. At each instant it can be defined a $\Delta\mathbf{r} = \mathbf{r} - \mathbf{r}'$, and then the integration is made on a motion equation obtained by deriving twice the expression of $\Delta\mathbf{r}$. This is convenient when the perturbation is strongly varying.

- ***Method of variation of orbital elements***. It is based on the variation of orbital parameters by integrating some form of variational orbital elements formulation, such as 3.1.4.

3.2 The software: Satellite Tool Kit

Analitycal Graphics Inc.'s Satellite Tool Kit is a software package that allows the user to perform analysis of air, sea and space platforms. It enables to calculate and simulate an infinite number of scenarios, but for the purpose of this thesis work only the Astrogator tool has been used.

3.2.1 Astrogator

STK-Astrogator is not the typical code to estimate duration, propellant consumption or departure plot for the mission. It is typically used as a high fidelity trajectory design tool, but for this thesis work there was the need to use it to estimate all of those data value that defines a preliminary study for any mission, which are the ΔV, fuel consumption and mission duration. In order to obtain those without an excessive level of detail, which was pointless for any early stage of design, simplified scenarios and maneuvers have been analyzed.

The philosophy of Astrogator is to work with the mission control sequence (MCS) which is a pattern of unique commands that determines what happens to the spacecraft for a certain amount of time. The command used will be explained in next sections. The initial condition for the spacecraft is defined by the initial state segment, in which the epoch and all the orbital parameters can be defined.

3.2.2 Propagation segment

The first command is the propagator segment, that numerically integrates the equation of motion of the satellite from Eq. (3.1) until a user defined condition, that could be a duration, a distance from a reference system origin or plane, a vector magnitude (for example the velocity vector of a satellite) or many others. The solution of differential equations for the calculation of the trajectory can achieved via different methods, but the most used is a Runge-Kutta-Fehlberg method of order 7, and this means that at each step there are 7 terms in the numerical expansion. For further detail on those numerical methods see Refs. [42, 43].

The great aspect about Astrogator tool is that the user can decide the propagator to use. This means that the perturbation forces that act on the spacecraft can be chosen. In fact, for the calculation in this work, two different propagators have been used:

- For the near Earth operations, a point-mass propagator has been used. This keeps into account the earth gravity as concentrated all in the center of it, and the moon and sun influence is neglected. With the term "near Earth operations" we refer to the period of time in which the spacecraft is inside the Hill sphere.

- Once the spacecraft is outside the sphere of influence of the Earth, the propagator switch to a heliocentric one, and that means that has as central body the Sun, but all the other celestial bodies act as a third body perturbation, as seen in Sec. 3.1.1. All of those bodies, though, does not influence the trajectory of the spacecraft unless the get very close to their sphere of influence.

In addition to the choice of the propagator, the propagation segment needs to have one basic input, which is the stopping condition. Given the state of the spacecraft at which the propagator starts in terms of position vector and velocity vector, the propagator will calculate and plot the solution until the stopping condition, which is a numerical value with a tolerance. The typical stopping parameter is the duration, that can range from seconds to years.

3.2.3 Maneuver segment

This segment enables the user to define a maneuver with a specific engine, that perturbs the motion of the spacecraft. Mainly, two kind of maneuvers can be used: impulsive burn and finite burn. The first case is not relevant to this study, since the subject is a low thrust engine. The finite burn, on the other hand, enables the use of the same propagators used in the propagation segment, so multiple stopping condition can be used even in this case.

The other fundamental input is the thrust vector. It is in fact user defined, and can be used as aligned with the velocity direction, opposite to it or it can have Cartesian coordinates to orient it in space or in a plane. In most complex and advanced scenarios, it can be defined as variable in time.

In most maneuvers, the most challenging part is to use the right thrust vector combined with a proper stopping condition. Moreover, the software itself does not converge very well if the thrust vector is defined in a translating and rotating reference system: for this reason, it has been mainly used inertially fixed in time. When there was the need, multiple maneuvers in a pattern with different thrust vector direction were used.

3.2.4 Target sequence

This object enables to control parameters of the propagation and maneuver segment in order to achieve a certain condition at a defined instant at the end of a specified segment. This is done automatically by the selected tool after a set of input and expected output are selected, along with tolerances and solution method. The parameters that can be defined by the user are all usable by the target sequence.

Multiple tool can be used to modify the input parameters, and in this study two of them were used, and those are:

- The differential corrector is an algorithm that changes by a user defined step a set of user specified independent variables to obtain the requested value of the dependent variable chosen as a result. This algorithm works in an optimal way when very few (1-2) independent variables are used.

- The SNOPT optimizer is a non linear optimization algorithm that enables the software to minimize a result or to keep it within certain boundaries by changing multiple variables. With this tool multiple independent variables can be modified at the same time.

With these two tools that control propagation and mission segment user defined variables, the process of obtain the desired trajectory is faster and easier than changing manually all the parameters. The con is that they need a value close to the solution to converge, otherwise the convergence is not granted.

3.2.5 Limitations of Astrogator

The biggest limitation of the software is that it requires a tremendous amount of input, with a good level of precision. Furthermore, it does not allow to study a set of possible solution in an approximate way, it can only calculate the exact trajectory given all the inputs. This means that it is not possible to study, for example, a set of solution for different departure dates or dry masses without changing all of the other parameters. A slight change of the initial mass, after a finite burn of many days at low accelerations and a propagation of months would result in thousands (or even millions) of kilometers of distance from the desired target. This means that as a first thing, fuel and dry mass have to be decided, and if changed later, that would influence all the trajectory.

4 Mission Design

4.1 Scientific objectives in the outer Solar System

4.1.1 Trans Neptunian Objects

The Kuiper belt is a disc of objects of various dimensions that extends from past the orbit of Neptune at 30 AU to approximately 50 AU [44]. It is home to many rocky asteroids and ice words, and a dozen of them have a diameter of about 1000 km or slightly more. A Kuiper belt object is considered so if his semiaxis major is bigger than 30 AU, and also its perihelia has to be further than 30 AU from the Sun. This is because the region inside Neptune orbit is dynamically unstable due to perturbations from other planets, as it is discussed in Ref. [45]. For the previous reason those object are also referred as trans Neptunian objects (TNO). The orbit of many of the objects in this far region is influenced by Neptune, in such a way that they are considered to be resonant with the eight planet. This means that depending on the type of resonance, they all have a particular semiaxis, inclination and eccentricity [45, 46]. Among TNOs, the most numerous are the classical objects, with $39.4 < a < 47.8$ AU and at the second place there are the scattered objects, that have $a > 30$ AU and usually the aphelia extend outside the Kuiper belt, sometimes up to 100 AU.

All of the objects in those far region are linked in some way to the origin of the solar system, and for this reason they are of fundamental importance to understand the evolution of the other planets. Also, many of those icy words could preserve real materials heritage of what happened in the last billions of years. Furthermore, some of the biggest TNOs could have a subsurface liquid ocean, just as that hypothesized on jovian satellites Europa, Ganimede and Callisto, as explained Ref. [47].

Many studies have been performed of missions to trans neptunian objects throughout the years, both for typical high thrust and low thrust maneuvers with gravity assists can be found in Refs. [48, 49, 50, 51, 52].

What follows is quick characterization of the dwarf planets Haumea, Makemake and Eris as explained in Refs. [45, 53, 54, 55] and are a subjects of this thesis. The main TNO objects are illustrated in Fig. 4.1.

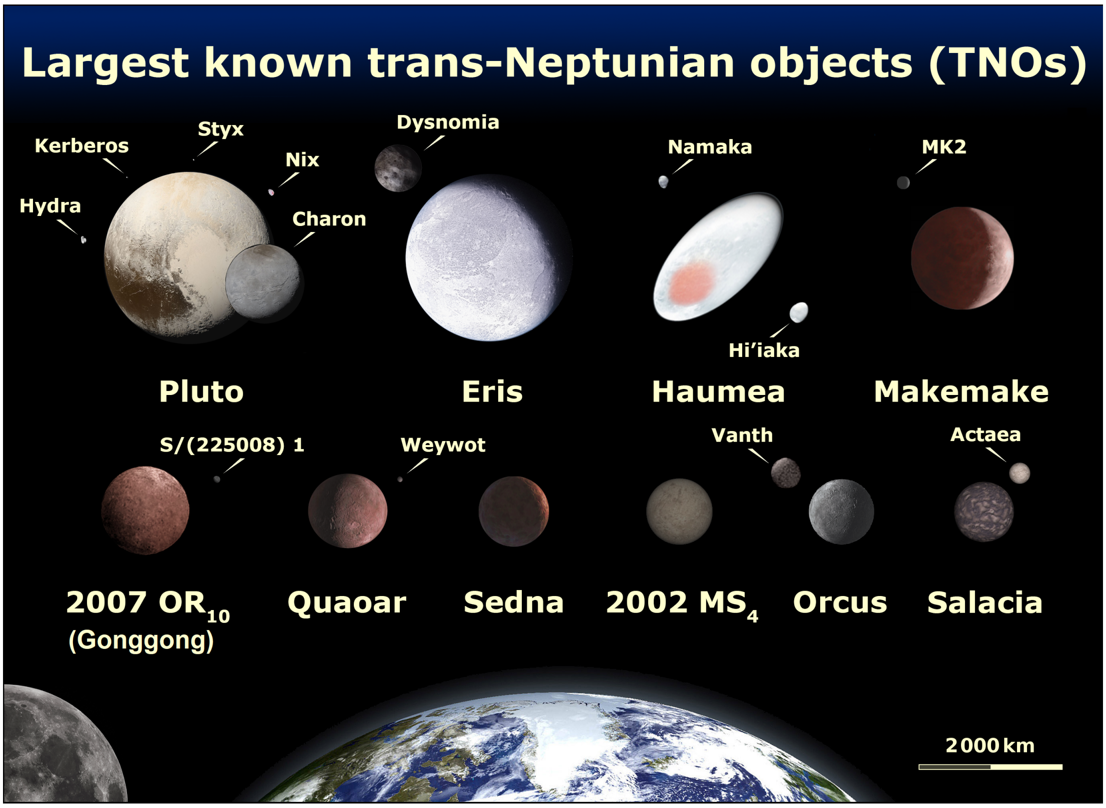

Figure 4.1: The image is a qualitative illustration of the possible appearance of the largest TNOs, based on their magnitude and observed spectrum. The image is taken from Ref. [56].

Among the objects presented in Fig. 4.1, it has been chosen to focus on the biggest three, excluding Pluto, which are Haumea, Makemake and Eris. Pluto it is not taken into account because a mission with the rendezvous with the dwarf planet that also accounts for a lander is analyzed in Ref. [35].

The following dwarf planets are presented with their provisional designation at the moment of discovery and its permanent designation. The first one starts with the year of discovery, while the letters and the numbers are associated with the day and month of discovery [57]. By glancing at the year of discovery, it is clear that all of them have been discovered after the year 2000, and this place them among the latest discovery of a celestial body in the solar system.

2003 EL$_{61}$ - Haumea This dwarf planet has a mass of 1/3 of that of Pluto and it is supposed to be a fast spinning ellipsoid [58], with two known moon, that have been given the name of Hi'iaka and Namaka. Its rotation period is supposed to be of about 4 hours, and this influences its brightness. It is supposed to be a high density - rocky planet, and its surface temperature is lower than 50 K.

2005 FY_9 - Makemake This TNO object is the second largest and brightest of the Kuiper belt after Pluto [59]. It has one satellite and a temperature on the surface of about 40 K that enables the presence of ices of methane, ethane and nitrogen.

2003 UB_{313} - Eris It is the heaviest dwarf planet with a mass of 27% more than that of Pluto. It is a scattered TNO with extremely high eccentricity, inclination and semi-major axis. It has one known moon, called Dysnomia. For further information see Ref. [60].

In the following table main parameters for the three dwarf planets are analyzed, with respect to those of Pluto.

Table 4.1: Main orbit properties for objective dwarf planets

	Pluto	Haumea	Makemake	Eris
Mass, [kg]	1.30×10^{22}	4.01×10^{21}	3.1×10^{21}	1.66×10^{22}
Semi-major axis [AU]	39.482	43.287	45.561	67.740
Aphelion, [AU]	49.305	51.600	52.761	97.468
Perihelion, [AU]	29.658	34.973	38.360	38.013
Eccentricity	0.249	0.192	0.158	0.439
Inclination, [deg]	17.16°	28.12°	28.98°	44.14°

The scientific results that could come from a long period of close-by studies of those worlds would be unprecedented. Studies about the magnetic field, the possible atmosphere, the geological activity and even the presence of liquid water can lead to formidable discovery both in astronomy and planetology.

4.1.2 Heliosphere

The heliosphere is the region of space that it is formed by the solar wind, which is formally plasma, that surrounds the Sun. This region is basically a bubble inside the interstellar medium (ISM), which is formed by the matter and the radiation that are present in the space between different star systems, as it is explained in Refs. [61, 62]. The amount of galactic cosmic rays inside the heliosphere is milder than outside, so it works as a shield from heavier radiation from distant stars.

This zone follows the Sun in its movement across the galaxy, so the shape it is not properly a sphere, it is more like a comet-like shape. We can identify three main parts that are relevant for the study of the nature of heliosphere: the termination shock, the heliosheath and the heliopause. Those are all associated with the fact that the solar wind, which is a plasma, interacts with the interstellar medium, which is also a plasma, but with smaller densities. This leads to magneto fluid dynamic phenomena such as shock waves and more. Those phenomena have been studied for years, both from earth and within its orbit, such as with the interstellar boundary explorer mission (IBEX) of Ref. [63], and also in situ by the two voyager missions.

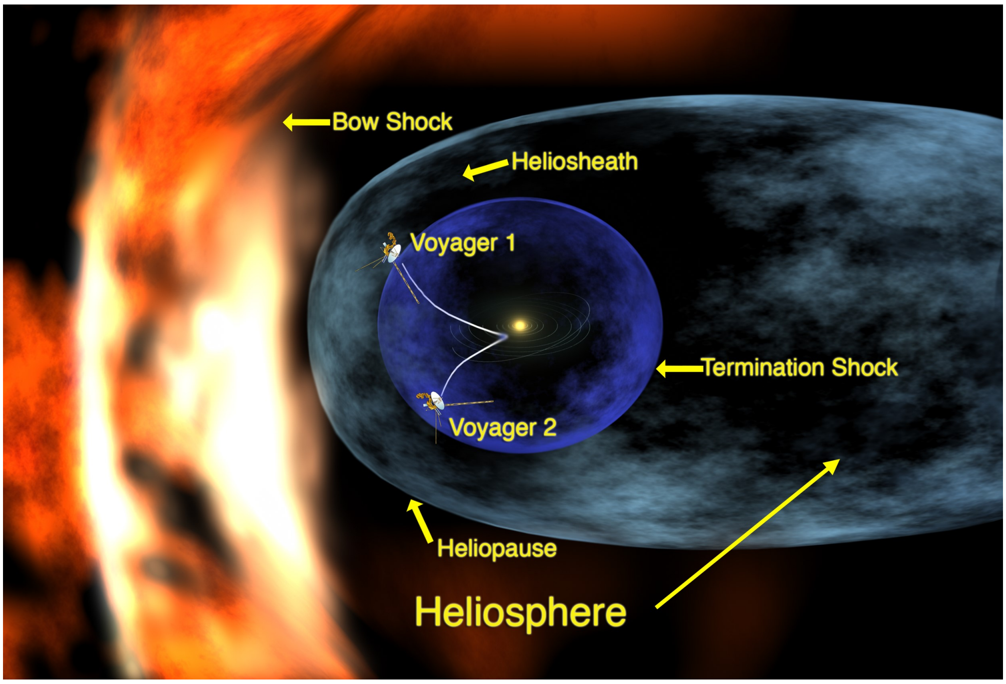

Figure 4.2: Qualitative description of the heliosphere with its main parts analyzed in this section. Credits: NASA

Those far space region will also be visited in the near term future by the New Horizons spacecraft, as explained in Ref. [64]. Further information on Voyager 1 and 2 missions are found in Refs. [1, 2].

The termination shock. The speed of sound in the ISM is lower than the speed of the solar wind, because of the low pressure and the even lower density of the ISM. The pressure inside the heliosphere decreases with the square of the distance from the Sun, and at a certain point it is not high enough to maintain the supersonic flow. For this reason the solar wind speed falls below the speed of sound, causing a shock wave which is the termination shock, as explained in Ref. [65]. This zone is expected to be from 75 to 90 AU from the Sun and at the present only Voyager 1 and Voyager 2 spacecraft reported to have crossed it [66]. Further information on those missions can be found at Refs. [67, 68, 69, 70].

The heliosheath. This is the zone beyond the termination shock, in which the wind is compressed and becomes turbulent because of the interaction with the interstellar medium. It is supposed to be formed by many bubbles of about 1 AU of width, as it is explained in Ref. [65]. These are probably caused by the fact that the Sun spins and its magnetic field rotates with it, and it becomes twisted and wrinkled at huge distances as explained in Refs. [71, 72, 73]. The heliosheath is considered to lay at 80-100 AU in the closest point.

The heliopause. As explained in Ref. [65], this is the zone where the solar wind is stopped by the ISM and the pressures become equal. After this "barrier", the amount of charged particles from the solar wind decrease very steeply and the amount of galactic cosmic rays increases. Voyager 1 seems to have crossed even this boundary in 2012 at a distance of 121 AU [74, 75].

All of the previous part are very important to study in detail and in-situ to develop a better knowledge on how the solar wind and the Sun magnetosphere behaves near the border with the ISM. After those region, the most important zone to study is the interstellar medium, just outside the heliopause. As discussed in Ref. [76], by studying the presence of ^{3}He, D, and ^{7}Li information can be obtained about the big bang, and data on general relativity and anisotropies in the structure of space can be inferred by the study of the position, trajectory and communication of the spacecraft. Further information on the local interstellar medium can be found in Refs. [61, 62].

Throughout the years, many mission to reach and explore the interstellar medium have been proposed, of which the most famous are the TAU mission (1987), the interstellar probe (1999), the realistic interstellar explorer (2002), the innovative interstellar explorer (2003), the interstellar heliopause probe (2006) and the interstellar probe (ISP, 2018). Description of those missions can be found in Refs. [77, 78, 79, 80, 81, 82, 83, 84].

4.2 Kuiper Belt Missions

4.2.1 Approach

In this section the philosophy adopted for the trajectory design for this thesis will be explained. It is necessary to point out that many decisions and approaches are a direct consequence of the limitation of the software explained in Sec. 3.2.5, and what explained in the following part is the way that was adopted to overcome them.

The objective for the rendezvous mission is to bring at least 1000 kg of payload mass to the desired target. Given a 2 MW engine, that is a specific power of 1 kW/kg, it would result in 2000 kg of engine. This means that the delivered mass should be at least 3000 kg. Because of what said in Sec. 3.2.5, the total fuel mass also needs to be fixed, and a value of 4488 kg is chosen as baseline. Of that mass which is not used, except for a system margin, could be as well considered as payload mass.

The objective is to design a mission that will last at least 15 years, where in the first part the spacecraft will reach its destination, while in the later years it will follow the path of its objective to study it from up close. The 15 years have been chosen under the hypothesis of keeping the ^{3}He fuel consumption under 2 kg, as explained in Sec. 2.4.7.

The initial orbit is chosen to be a low Earth orbit (LEO), so that the spacecraft will not need any particular launcher to be injected in an escape trajectory. It will leave Earth influence all by itself, with a spiraling phase.

In this phase, the thrust vector is supposed to be always parallel to the velocity of the spacecraft. This is an approximation of the optimal solution as seen in Ref. [85], and it also was easier to calculate. The spiral phase ends when the spacecraft exit the SOI of Earth with an hyperbolic trajectory with respect to Earth. At this moment, the velocity of the spacecraft with respect to the Sun had to be parallel to that of the Earth, so that the velocity in a Sun reference system is maximized.

Subsequent to the exit from Earth SOI, the spacecraft is in an elliptic orbit around the Sun. Many days of acceleration are needed at this point to obtain a Heliocentric hyperbolic orbit, and the thrust vector is once again aligned with the velocity of the spacecraft. If a change of inclination is required, the thrust vector will have a component outside the plane, so that the hyperbolic trajectory propagated in time will lead to the desired inclination.

After the hyperbolic injection, the spacecraft will need to face many years of coasting, given the tremendous distance of the Kuiper belt objects. This phase is very time demanding, and it will constitute the most part of the mission: for this reason, it is important to chose the duration of the acceleration phase in order to limit the duration of the coasting. The most distance is also traveled during this period. It has been decided to limit the global mission time of flight to 11 years, so that the mission will have at least 4 years for the operations once reached the destination, for a total of 15 years. Once the coast segment is defined, by changing the epoch of departure and the out of plane component of the thrust, the spacecraft position vector at the end of the coasting phase will need to be nearly parallel to that of destination.

The last part of the trajectory is the rendezvous part, in which the spacecraft is slowed down and than its velocity vector is turned. This is because changing the direction of motion during the hyperbolic trajectory is nearly unfeasible. Optimally, the thrust direction should start opposed to the velocity, and then over time it should increment is radial component. Another possible and nearly optimal solution was to have a thrust direction fixed in time with respect to an inertial frame. The former with Astrogator would have taken too long and would have required a level of detail which was pointless at this point of the study. The latter solution was adopted only for two scenarios due to numerical reasons: in fact, the SNOPT optimizer used to search for the thrust direction did not converge for the other cases, no matter how parameters were changed. In those cases, a two step maneuver was adopted: in the first half, a pure deceleration phase is adopted, and then a radial component is added, so that the trajectory begin to turn, and also it will be still slowing.

The velocity at the end of the burn needs to be as close as that of the target, and also the spacecraft will need to be inside its SOI. It appeared that even though the r_{SOI} for the dwarf planets it is of the order of 10^6 km, the spacecraft is actually captured by the planet at a distance of less than 10^5 km. The trajectory design is considered completed when the spacecraft is placed in any orbit under 10^5 km from the target.

A graphical representation of the previously explained three phases is visible in

Fig. 4.3.

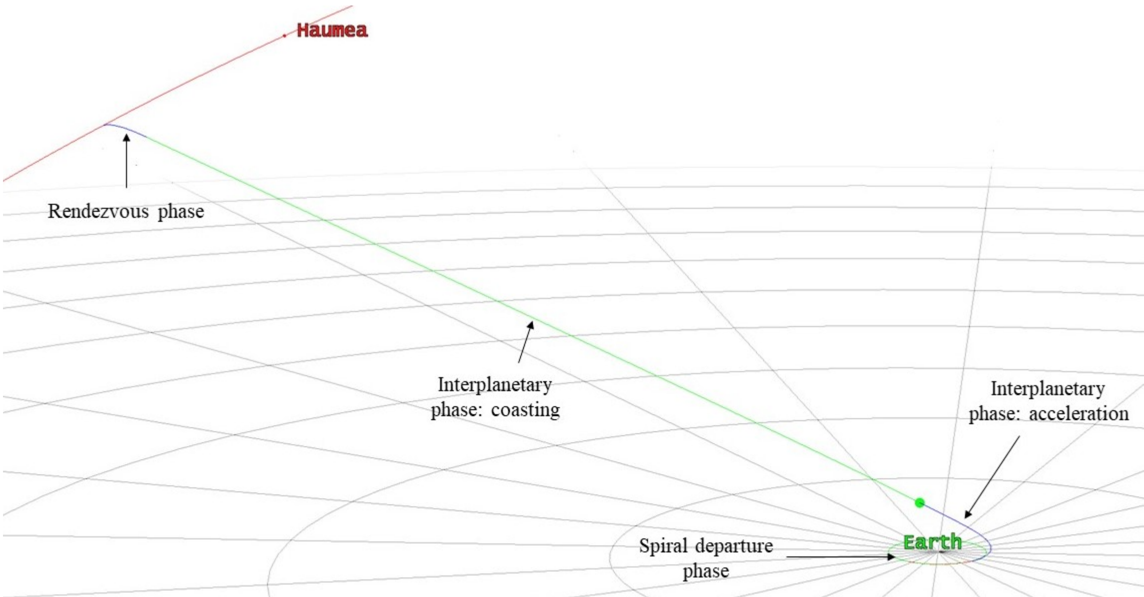

Figure 4.3: Straight line trajectory to reach Haumea. Each phase is here showed. Earth orbit and a section of Haumea orbit are visible in this figure, respectively in the bottom right and top left. The visible grid represents the ecliptic plane.

4.2.2 Dwarf Planets ephemeris

In Table 4.2 orbital elements for Haumea planet can be appreciated. Those values have been used in STK to add Haumea as an asteroid, since it was not present in the basic SPICE ephemeris database. The same thing has been done for the other dwarf planets, Makemake and Eris.

Table 4.2: Orbital parameters for Haumea dwarf planet from Ref. [86] in the Sun J2000 ICRF

	Simplified scenario	Real scenario
a, [km]	$6.48341e + 09$	$6.48341e + 09$
a, [AU]	43.15619	43.15619
Perihelion distance, [AU]	34.8401	34.8401
Aphelion distance, [AU]	51.4723	51.4723
Orbit period, [yr]	283.51292	283.51292
e	0.192697	0.192697
i, [deg]	0	28.1913
ω, [deg]	240.453	240.453
$RAAN$, [deg]	121.788	121.788

If we consider Haumea and we plot the 0° degrees inclined orbit and the real one we obtain what is shown in Fig. 4.4. Haumea is moving towards the descending node (180° from the ascending node), which will reach around the year 2072. This means that for the real scenario, the later the mission will depart, the easiest will be to reach the dwarf planet.

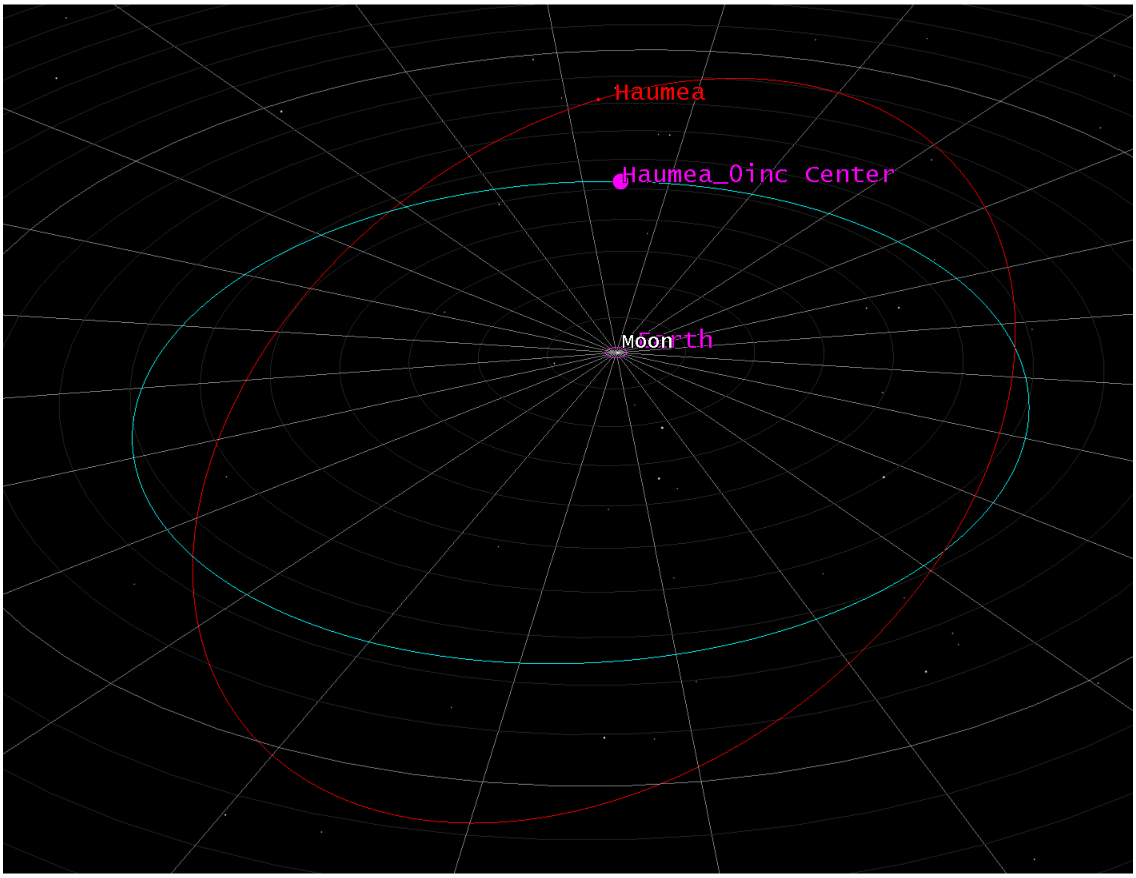

Figure 4.4: Orbit plot for Haumea with real inclination and Haumea with 0° inclination for the year 2050. The grid is the ecliptic plane.

The same analysis has been done for dwarf planets Makemake and Eris, and in Table 4.3 main parameters are reported. In the following section, the term "simplified scenario" will always refer to a planet with a 0° orbit inclination, with all the other parameters constant.

In Fig. 4.5 orbits for the three subject of this study are plotted.

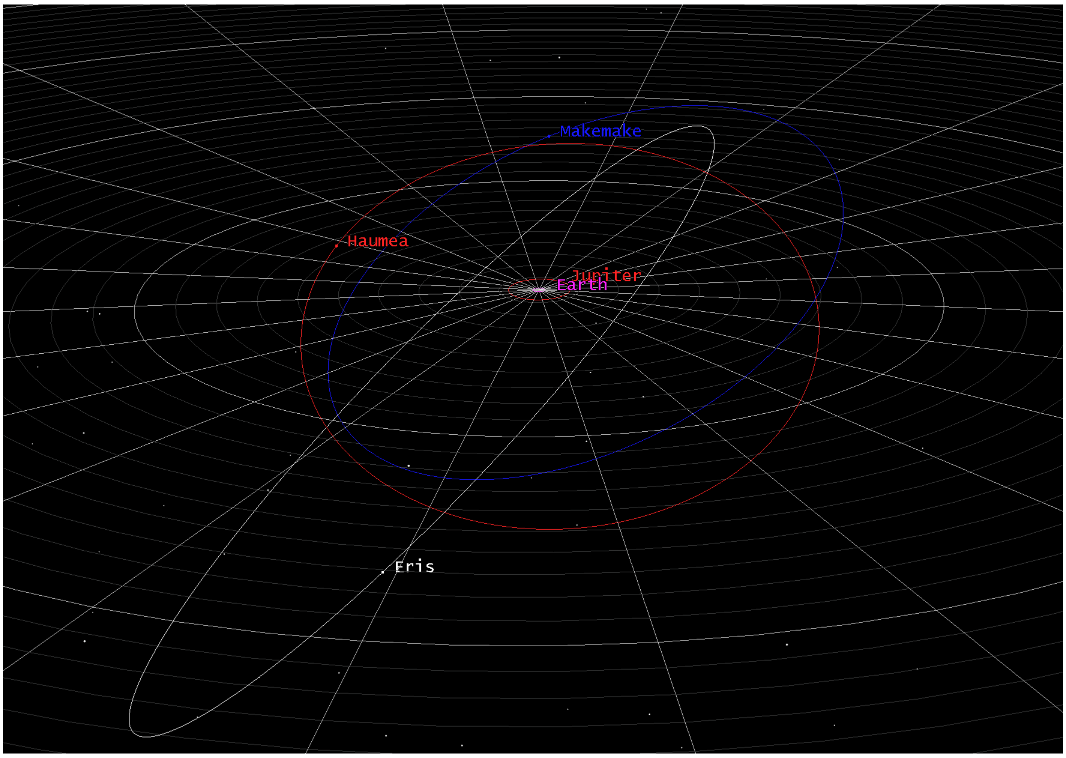

Figure 4.5: Orbit plot for Haumea, Makemake and Eris dwarf planets. Jupiter and Earth orbits are also visible in the figure, so the real distance of those celestial bodies can be appreciated.

Table 4.3: Orbital Parameters for Makemake and Eris dwarf planets from Ref. [86] in the Sun J2000 ICRF

	Makemake	Eris
a, [km]	$6.8465e+9$	$1.0194e+10$
a, [AU]	45.6434	67.9619
Perihelion distance, [AU]	38.4409	38.2693
Aphelion distance, [AU]	52.8459	97.6545
Orbit period, [yr]	308.3726	560.2820
e	0.1578	0.4369
i, [deg]	29.0113	43.8786
ω, [deg]	240.453	150.8052
$RAAN$, [deg]	79.3101	36.0342

Once those bodies have been added to STK database, it becomes possible to plot their orbits, their orbital parameters and all of the physical characteristic of their orbit.

4.2.3 Haumea Mission - Simplified Scenario

In this first approach to the orbit design, it has been imagined a mission that will rendezvous to the dwarf planet Haumea and follow its path inside the Kuiper Belt.

The objective of this mission was to try to reach the Dwarf planet in less than 10 years with a payload mass of at least of 1000 kg, so that it would enable all kind of missions, from scientific to observation, or even in-situ operations.

In these first calculations, constant values for thrust and specific impulse are chosen, and reasonable specific power values are chosen for the mass computation. In Table 4.4 are summarized all the main spacecraft properties. Note that the thrust power corresponds to the input power of Figs. 2.19, 2.20, 2.21 and 2.22.

Before analyzing trajectories, it is important to point out that the fuel mass expressed in Table 4.4 is the initial mass allocated for the fuel. All of that mass which is not used for the maneuver, except for an amount used as a margin, will result in additional payload mass, which will be analyzed at the end of this section.

Table 4.4: First iteration spacecraft and engine properties. In this work it is referred to first iteration in terms of the first result obtained without any numerical optimization.

	Spacecraft properties
Final mass (Dry)	3000 kg
Engine mass	1500 kg - 2000 kg
Payload mass	1500 kg - 1000 kg
Fuel mass	4488 kg
Initial mass	7488 kg
Final mass to initial mass ratio	0.40
Final mass to initial fuel mass ratio	0.67
	Engine properties
Fusion power	2 MW
Power to thrust	1 MW
Specific power	1 kW/kg
Thrust	8 N
Specific impulse	10000 s
Mass flow	0.08 g/s = 6.912 kg/day

In the simplified scenario Haumea orbit lies on the ecliptic plane and because of its distance from the Sun and its orbital period of about 283 years, the opposition with Earth happens once a year. With these consideration and the fact that the planet moves very slowly (about 5.5 km/s with respect to the Sun), the year of departure is nearly irrelevant for the purposes of this scenario.

The mission can be ideally divided into 3 phases. The mission profile chosen is the simplest possible, which is the so-called Thrust-Coast-Thrust profile as can also be seen in Ref. [87]. The first phase is the spiral trajectory to escape Earth gravity, the second phase is the one relative to the interplanetary travel, since the exit from Earth sphere of influence to the end of the coasting phase, while the last phase is relative to the maneuvers to rendezvous with Haumea. A fourth phase of orbit injection is not analyzed, but it is estimated to be possible with a ΔV of about $1 - 1.5$ km/s in the worst case, that would mean less than 80 kg of propellant.

Initial condition for the spacecraft are summarized as classical orbital elements in Table 4.5. The following calculations are all done with the hypothesis of a LEO departing orbit, without taking into account a possible hyperbolic orbit injection by the launcher itself. This engine will be demonstrated to be fully capable of both the departing and the arrival phases.

Table 4.5: Orbital parameters for the spacecraft in an Earth J2000 reference frame at the departure.

Departure Date	28 Sep 2044
a, [km]	6771
e	0
i, [deg]	23
RAAN, [deg]	0
ω, [deg]	0
ν, [deg]	150

Note that all of the following maneuvers are not optimized.

Spiral trajectory This part consists in a burn of about 76 days, with the thrust direction parallel to the velocity vector. The limit of the Hill sphere is placed at 1×10^6 km from the center of the Earth. The initial spacecraft orbit is a circular LEO as can be seen in Table 4.5. Note that the inclination is chosen in order to exit from the planet on the ecliptic plane. The final velocity will be nearly parallel to that of the Earth with respect to the Sun in order to maximize the velocity gain as explained is Sec. 4.2.1.

Due to the electromagnetic nature of the engine and because of safety reasons for the spacecraft itself, is preferable to spend less time possible inside the Inner Van Allen Belt, and in particular its most dangerous part which extends from 1000 km to 6000 km of altitude, even though the peak of radiation is typically reached at about 2550 km of altitude, as explained in Ref. [88].

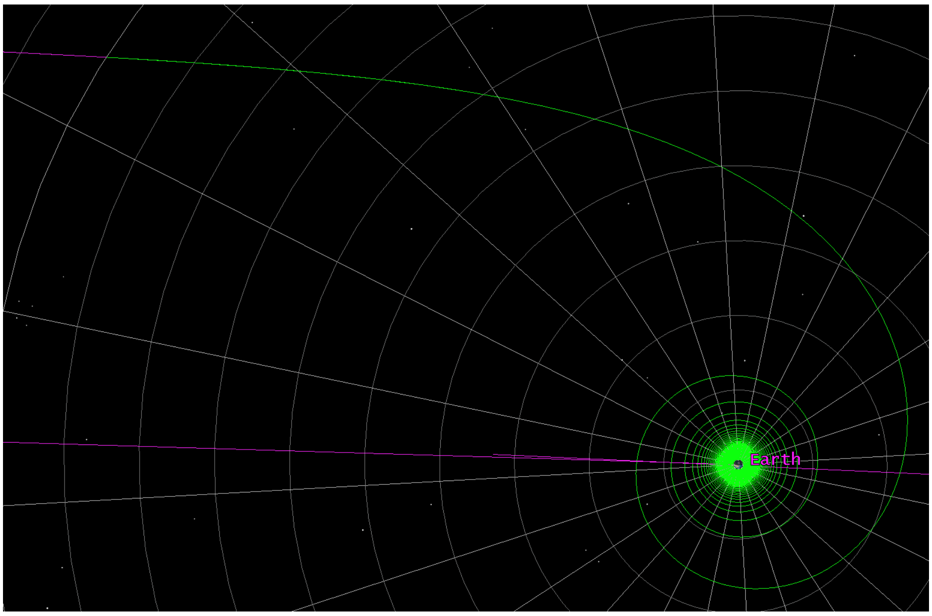

Figure 4.6: Spiral trajectory for Earth escape. The green segment ends when the spacecraft is exiting the Hill sphere, entering the interplanetary space

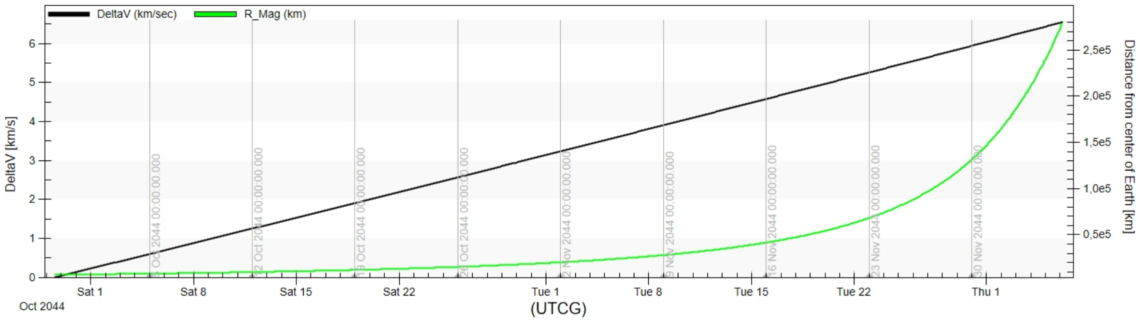

Figure 4.7: ΔV (black line) and distance (green line) for the escape spiral with respect to the Earth

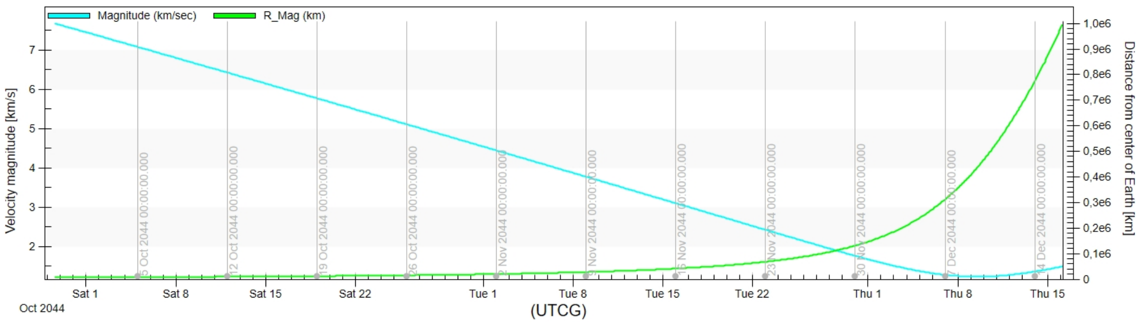

Figure 4.8: Velocity (blue line) and distance (green line) during the escape spiral vs time with respect to the Earth

A maneuver summary is reported in Table 4.6.

Table 4.6: Spiral trajectory summary. The Van Allen belt time is the time spent inside the inner belt.

Initial date	28 Sep 2044
Opposition angle	114°
Duration	79 days
ΔV	7.54 km/s
Fuel used	554 kg
Van Allen Belt time	18 days

Interplanetary phase This is composed of a first phase in which the thrust is aligned with velocity vector, so that the spacecraft will be in a hyperbolic trajectory with respect to the Sun. This burn is essentially the continuation of the burn to escape from Earth. Because of this additional thrust time, the trajectory will appear as a straight line in a heliocentric view. After the maneuver phase, there will be a 5-year-long coasting phase.

Table 4.7: Interplanetary phase summary for Haumea - simplified scenario

	Maneuver phase
Duration	200 days
ΔV gain	22.29 km/s
Fuel used	1410 kg
Initial velocity	31.77 km/s
Final velocity	37.14 km/s

	Coasting phase
Duration	5 years
Initial sun distance	2.78 au
Final sun distance	33.40 au
Initial velocity	37.14 km/s
Final velocity	28.19 km/s

Rendezvous phase The rendezvous phase is the one in which it is necessary to slow down and turn the velocity vector towards the same direction of Haumea velocity vector, so that the last burn will change the orbital parameters so that the spacecraft would follow the Dwarf planet inside the Kuiper Belt, or even get captured by the gravity of the asteroid.

In this first study, those maneuvers are not optimized, it is a first iteration needed to understand how the spacecraft velocity should be decreased and its trajectory turned into an ellipse. All the fuel usage masses can be further decreased in a second iteration.

The first part of this maneuver is a deceleration phase in which the velocity is reduced from 28.19 km/s to 13.97 km/s, in which the thrust vector direction is opposite to that of velocity. After that, it is easier to turn the velocity vector by pointing the thrust vector radially, still with component directed opposite to the velocity of the spacecraft. At the end of the maneuver, the velocity vector has been rotated of about 90°. It is important to point out that it is known that the optimal thrust direction is nearly constant in time with respect to an inertial system, but it could not be found the correct angle for numerical reasons, and because of this the presented results are the best we could obtain for this iteration.

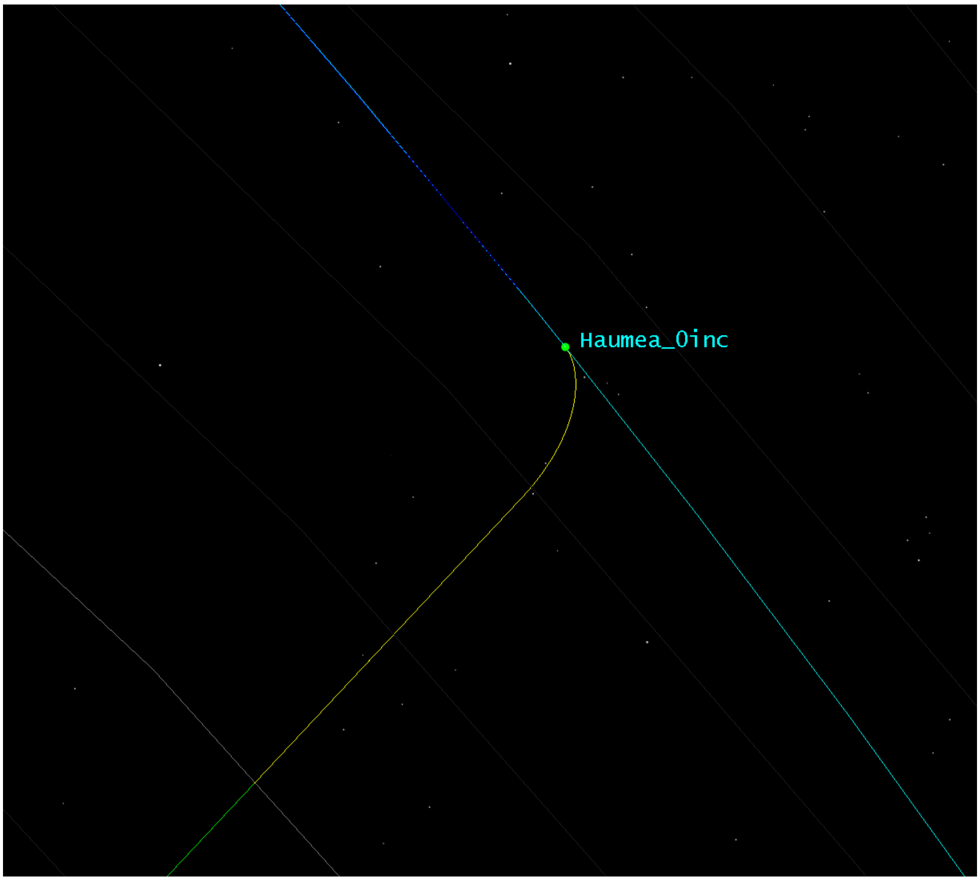

Figure 4.9: Rendezvous Phase

Table 4.8: Summary for the rendezvous phase

Duration	205 days
ΔV	29.76 km/s
Propellant mass used	1445 kg
Initial Velocity	28.19 km/s
Final Velocity	5.44 km/s
Closest pass from Haumea	60000 km

Scenario summary In this first computation, it is clear that all the maneuvers are not optimal at all. Moreover, in this scenario the engine is supposed to work at constant thrust and specific impulse, even though it is capable of increase the specific impulse and decrease the thrust by decreasing the mass flow. This capability

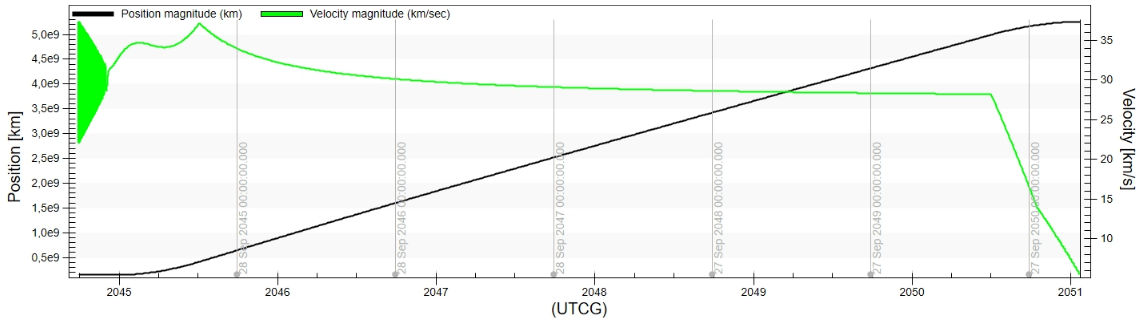

Figure 4.11: Velocity (green line) and position (black line) with respect to the Sun

would further reduce the fuel consumption. Still, the obtained results are extremely promising in terms of payload capability and time of flight, as seen in Table 4.9. In Fig. 4.10 the masses evolution during the entire mission can be appreciated, while in Fig. 4.11 position and velocity are plotted over time. Note that in the last graph, the final velocity vector is very close to that of Haumea, both in magnitude and direction.

Table 4.9: Summary for the trajectory to Haumea (with 0° inclination)

Destination	Haumea - Elliptic orbit on the ecliptic plane
Mission duration	6 years and 4 months
Final mass delivered	4077 kg
Propulsive system	DFD with Constant I_{sp} and T
Fuel mass used	3409 kg
Total ΔV	59.59 km/s
Number of burns	2: Earth escape, rendezvous
Distance at rendezvous	35.14 AU

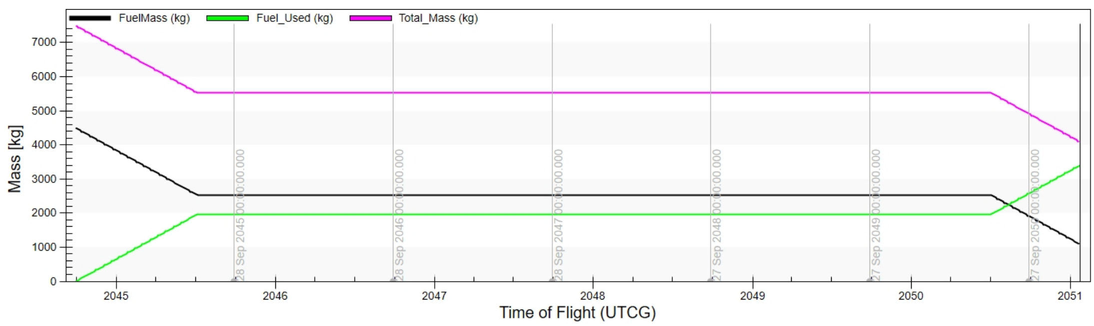

Figure 4.10: Total mass (purple line) and propellant mass consumption (green line) and remaining (black line) over time

4.2.4 Haumea Mission - Real Scenario

The spacecraft parameters in this case are the same as reported in Table 4.4. Haumea lies now on a 28.19° inclined orbital plane as seen in Table 4.2. In this scenario it has been decided to change the inclination of the spacecraft right after the escape maneuver. As seen in Sec. 4.2.2, the latter the departure, the closer will be the asteroid to the ecliptic plane, hence the plane change will be less demanding.

Because of previous considerations, trajectory analysis has been done for a departure date in the 50s, so that the plane change could have been analyzed. A departure date in the 60s, on the other hand, would provide the same results obtained in Sec. 4.2.3.
Even though, the two scenarios have very similar characteristics, the only changes are in the interplanetary phase and in the rendez-vous phase.

Spiral trajectory The burn will be about 79 days as seen in Sec. 4.2.3. Initial conditions are the same as the simplified case, except for the initial date and so the true anomaly. The direction of the thrust is considered parallel to the spacecraft velocity vector. Maneuver summary is found in Table 4.6.

Table 4.10: Orbital Parameters in Earth with respect to Earth ICRF reference system

Departure Date	24 Oct 2055
a [km]	6771
e	0
i [deg]	23.44
RAAN, [deg]	0
ω, [deg]	0
ν, [deg]	146.14

Interplanetary phase In this scenario it has been decided to aim at the planet by a burn with a thrust component in a direction normal to the ecliptic plane, so that the inclination of the hyperbolic trajectory is changed at the beginning of its path.

Table 4.11: Interplanetary maneuver summary for Haumea real scenario

	Escape
Duration	225 day
ΔV gain	25.47 km/s
Fuel Used	1586 kg
Initial velocity (VNC)	31.64 km/s
Final velocity (VNC)	38.22 km/s
	Coasting phase
Duration	4 years and 9 months
Initial sun distance	3.18 au
Final sun distance	34.57 au
Initial velocity	38.22 km/s
Final velocity	30.87 km/s

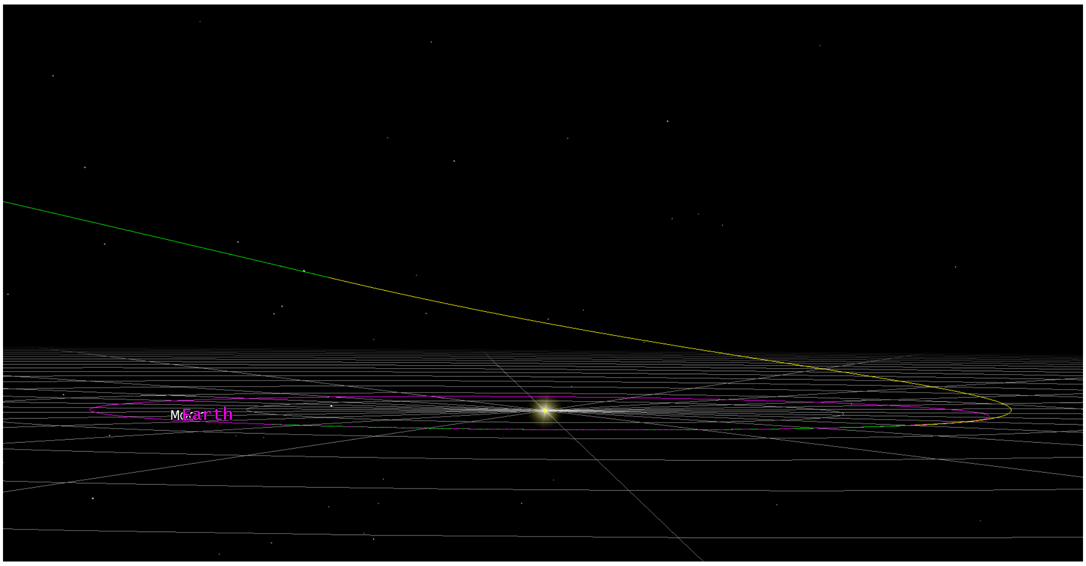

Figure 4.12: Detail of the inclination change maneuver for Haumea mission

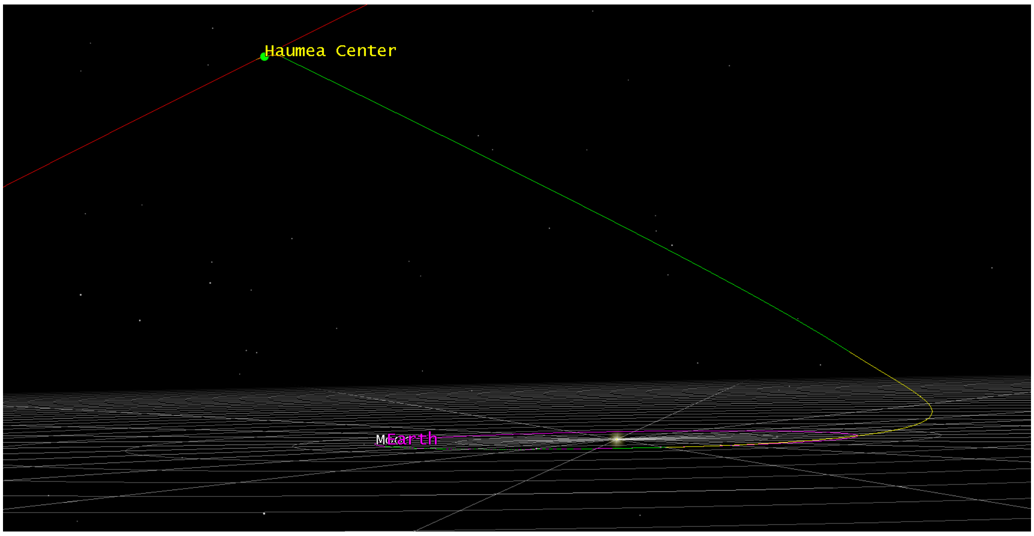

Figure 4.13: Another detail of the inclination change maneuver for Haumea mission

Rendezvous phase In this phase, besides the slow-down maneuver, it is needed to achieve at least the same RAAN and the same inclination of Haumea. This kind of maneuver requires a complex rotation of the velocity vector, and the thrust direction can be optimized for each instant of the burn, but for this scenario it has been chosen to be fixed with the VNC axis. A representation for this phase is shown in Fig. 4.14. As in the simplified scenario, the velocity vector is rotated of about 90°.

Table 4.12: Summary for the rendezvous phase for the real case scenario for Haumea with i =28°

Duration	206 days
ΔV	31.15 km/s
Propellant mass used	1455 kg
Initial Velocity	30.87 km/s
Final Velocity	5.35 km/s
Closest pass from Haumea	60000 km

Scenario summary Results from this scenario are very similar to those obtained in 4.2.3. In fact, by changing the inclination of the orbit during the acceleration phase by using a small component of the thrust direction outside the plane, the resulting propellant consumption is comparable to that of the simplified scenario.

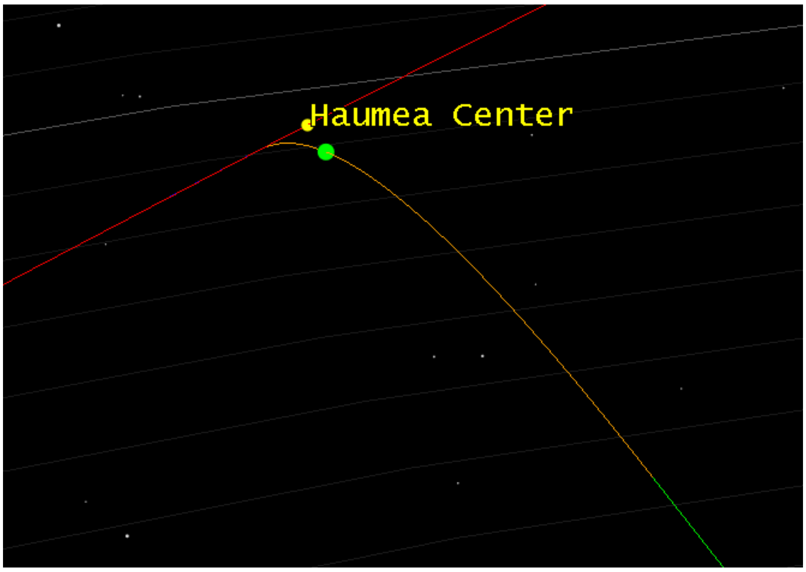

Figure 4.14: Maneuvers for rendezvous with Haumea mission in the real scenario

Table 4.13: Summary for the trajectory to Haumea (with 28.19° inclination).

Destination	Haumea - Elliptic orbit inclined of 28.19° on the ecliptic plane
Mission duration	6 years and 1 months
Final mass delivered	3892 kg
Propulsive system	DFD with constant I_{sp} and T
Fuel mass used	3595 kg
Total ΔV	64.16 km/s
Number of burns	2: Earth escape and inclination change, rendezvous
Distance at rendezvous	36.51 AU

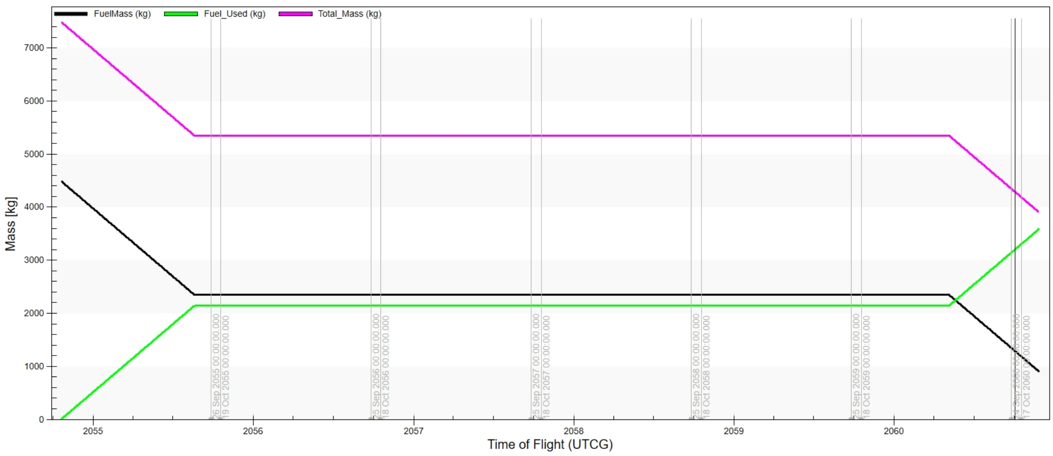

Figure 4.15: Total mass (purple line) and propellant mass consumption (green line) and remaining (black line) over time for the real case

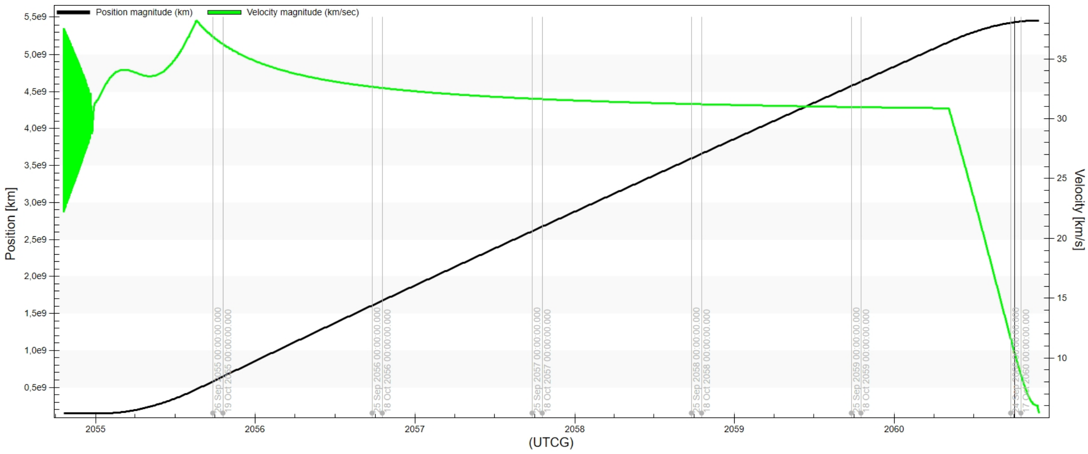

Figure 4.16: Velocity (green line) and distance (black line) with respect to the Sun for the real case

4.2.5 Comparison and comments between the two Haumea scenarios

By looking at Figs. 4.10 and 4.15, and at the summaries for the two maneuvers in Tabs. 4.9 and 4.13 it appears that propellant consumption differs only of less than 200 kg. This can sound strange, expecially because the in the real orbit scenario there is a plane change of 28 degrees done without a flyby, but all the difference is due to the initial plane change, because the rendezvous phase is very similar between the two scenarios.

Table 4.14: Duration and fuel consumption for the two Haumea scenarios for the interplanetary and rendezvous phases

	Haumea 0°	Haumea 28°
Interplanetary phase		
Duration	200 days	225 days
Propellant consumption	1410 kg	1586 kg
Rendezvous phase		
Duration	205 days	206 days
Propellant consumption	1445 kg	1455 kg

Table 4.15: Comparison between departure, time of flight, fuel consumption and ΔV for the two Haumea scenarios

	Simplified scenario	Real scenario
Departure	30 September 2044	24 Oct 2055
Duration	6 years and 4 months	6 years and 1 month
Fuel consumption	3409 kg	3595 kg
Total ΔV	59.59 km/s	64.16 km/s

4.2.6 Variation of payload mass for the Haumea mission

It soon became important to study what kind of propellant gain or loss would be obtained by changing the payload mass. This is because all the calculations done so far (and also those analyzed in next sections) refers to a defined launch mass.

In previous computations, as explained in Sec. 4.2.3, the dry mass is set to 3000 kg, of which 1000-1500 kg would be of payload, depending on the specific power of the engine. As already outlined, all the remaining mass allocated for propellant can be considered as part of the payload itself. For this scenario, the total mission time is kept constant, the propellant is again 4488 kg, but the dry mass changes: only two more simulations have been calculated in order to understand the changes in the propellant consumption. The study case is that of Haumea with $i = 28.19°$.

Table 4.16: The nominal case is the one analyzed in Sec. 4.2.4 and is here referred as Case 2, while the other two cases are the one in which the starting payload mass is changed. The starting payload mass is the first iteration mass with which we start the trajectory design, as explained in Sec. 4.2.1. The initial mass is the launch mass. The final mass is the total mass which we will have at destination, that is payload plus engine plus remaining fuel mass. The effective payload mass is the starting payload mass plus all the mass allocated for fuel that is not used. m_f is the final mass, m_i is the initial mass, m_p is the effective payload mass and m_{prop} is the propellant mass used

	Case 1	Case 2	Case 3
Starting payload mass, [kg]	500	1000	2000
Initial mass, [kg]	6988	7488	8488
Final mass, [kg]	3579	3892	4216
Effective payload mass, [kg]	1579	1892	2216
Propellant mass used, [kg]	3409	3595	4272
m_f/m_i	0.512	0.520	0.497
m_p/m_i	0.226	0.253	0.261
m_p/m_{prop}	0.463	0.526	0.519

Let us look at Table 4.16. The first thing to note is that there is only a slight difference between the three m_f/m_i ratios. The first case is expected to be higher, but it is important to consider that about 2000 kg of engine are fixed, so even though there is a launch mass lower than nominal, the propellant used is quite high anyway, as is seen in the m_p/m_{prop}. As expected, the m_f/m_i ratio is the lowest for the second case, but that is because the starting payload mass has been doubled. The m_p/m_{prop} ratio, though, is very similar to that of the payload. From these considerations, an important observation on the engine can be derived: the 2 MW DFD engine is very effective for a payload that is over 1000 kg, but if the payload mass is decreased, it becomes excessive. In that case, it could be useful to consider a lower power DFD, so that is optimized for the same mission time but lower mass constraints of the mission.

4.2.7 Makemake mission

Now let us analyze a mission to rendezvous with Makemake. The spacecraft and engine parameters at the departure are the same reported in Table 4.4, though the final mass will be slightly different. As in the previous scenario, the later will be the departure date, the closer Makemake will be to the line of nodes, hence less change of inclination will be required: for this reason the departure date is again chosen to be in the 50s. This scenario is extremely similar to that of Haumea in the real case, with small variations in the interplanetary and rendezvous phase. For this reason there was no need to analyze it in its simplified scenario. Initial condition for the spiral trajectory are the same, and the departure date is the 31st of July, 2054.

Spiral trajectory This maneuver is the same as in Sec. 4.2.3 and 4.2.4, and its analysis is omitted. The only difference is the departure date, but the ΔV and propellant used is the same, as well as the time required to reach 10^6 km from the center of the Earth.

Interplanetary phase As in the interplanetary phase for the scenario in which Haumea has 28° of inclination, the plane change is achieved thanks to a thrust component out of plane as seen in Fig. 4.17. In this case, once again, the hyperbolic trajectory will be out of the ecliptic plane, as it is shown in Fig. 4.18.

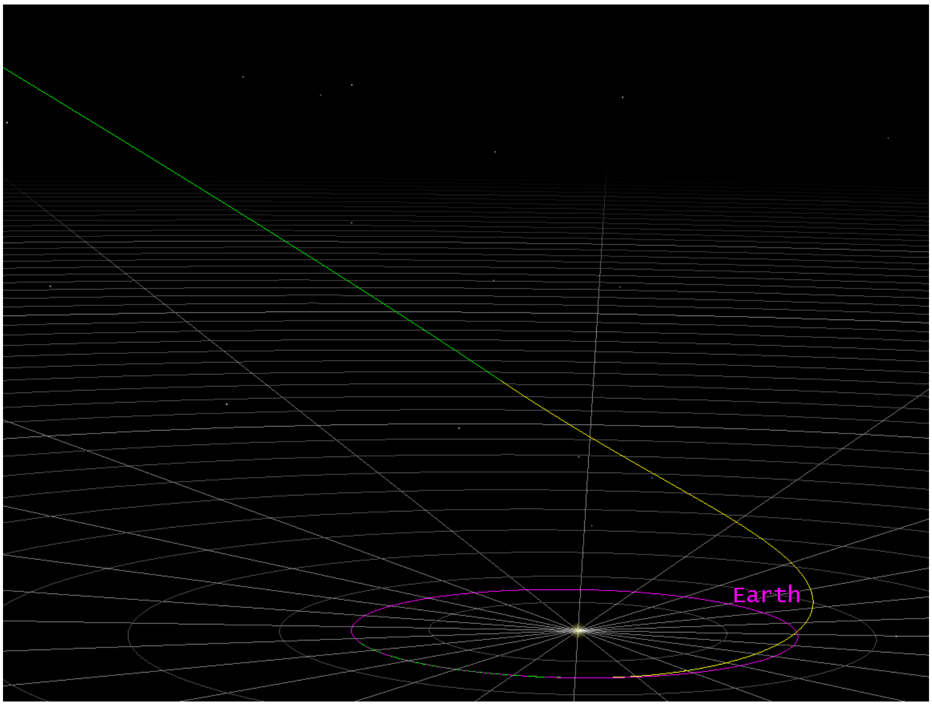

Figure 4.17: Detail of the inclination change maneuver. The yellow segment represents the propelled trajectory.

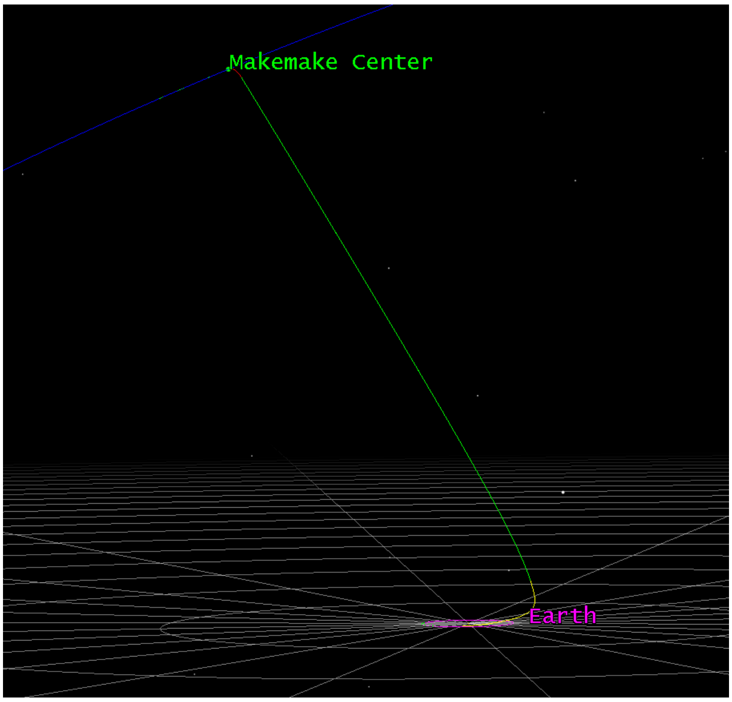

Figure 4.18: Detail of the maneuver to achieve the required hyperbolic velocity and the needed plane

Table 4.17: Interplanetary phase summary for Makemake mission

	Burn
Duration	251 day
ΔV gain	28.89 km/s
Fuel Used	1769 kg
Initial velocity (VNC)	31.37 km/s
Final velocity (VNC)	37.86 km/s

	Coasting phase
Duration	5 years and 10 months
Initial sun distance	3.44 au
Final sun distance	42.48 au
Initial velocity	37.86 km/s
Final velocity	30.99 km/s

Rendezvous phase The rendezvous with the planet is obtained as in previous cases with a continuous burn that also has a radial component, which will turn the velocity vector of about 90° as in both the Haumea scenarios. This maneuver is done once the spacecraft is slow enough after the first deceleration phase, as it is shown in Figs. 4.19 and 4.20. In Table 4.18 main parameters for this maneuver can be found.

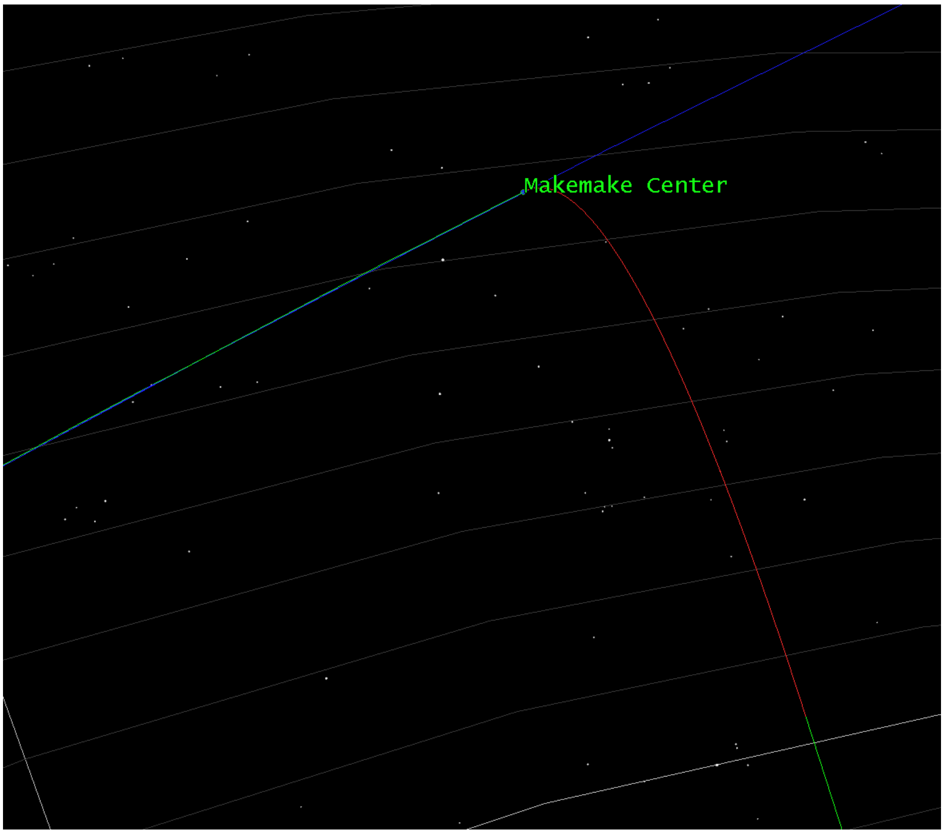

Figure 4.19: Detail of the maneuver to rendezvous with Makemake. The green segment in the bottom right side is the end of the coast segment. The red one is the deceleration burn, that at the end turns the trajectory. The blue line is the dwarf planet orbit, and the green segment that overlaps the orbit is the trajectory of the spacecraft after the rendezvous.

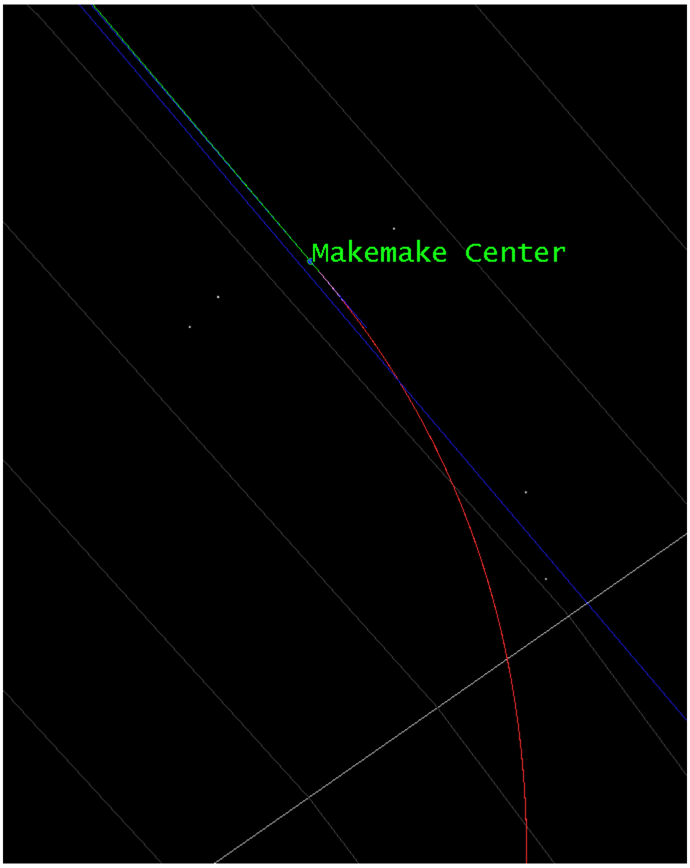

Figure 4.20: Close up of the last part of the burn

Table 4.18: Summary for the rendezvous phase for the real case scenario for Haumea with i =28°

Duration	204 days
ΔV	31.96 km/s
Propellant mass used	1436 kg
Initial Velocity	30.99 km/s
Final Velocity	4.58 km/s
Closest pass from Makemake	16000 km

Scenario summary As already said earlier in this section, the mission is very similar to the mission to Haumea in the realistic scenario. The main difference resides in the acceleration phase, because even though the two planets are at the same distance from the central body, which is in this case the Sun, Makemake is further from the line of nodes. This means that its distance from the ecliptic plane is higher, thus the component of thrust perpendicular to the plane is enhanced, and this has to be compensated by more days of thrust. This is clear in the last part of

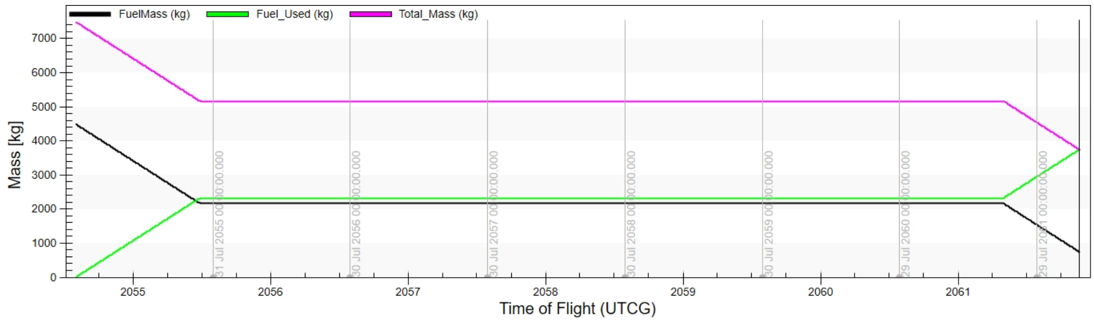

Figure 4.21: Propellant mass consumption (green line) and remaining (black line) and total spacecraft mass (purple line) evolution in time for Makemake mission.

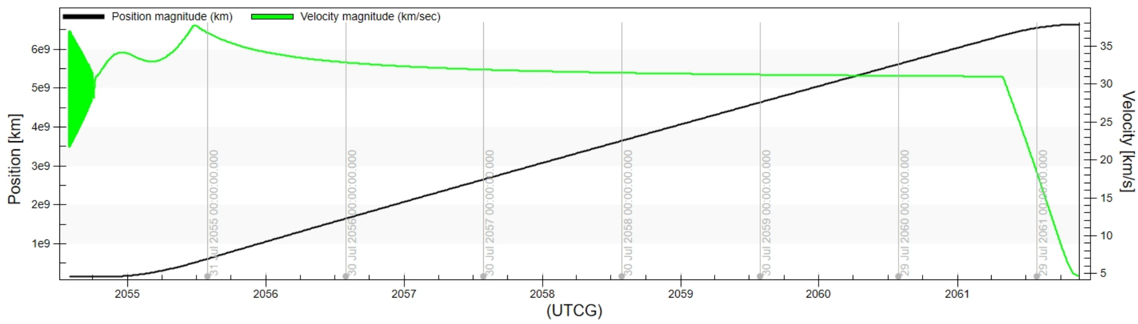

Figure 4.22: Position (black line) and velocity evolution (green line) in time for Makemake mission.

Figs. 4.22 and 4.21, in which the velocity is nearly constant, while the propellant still decreases.

Table 4.19: Summary for the trajectory to Makemake (with 28.19° inclination).

Destination	Makemake - Elliptic orbit inclined of 29.01°
Mission duration	7 years and 3 months
Final mass delivered	3733 kg
Propulsive system	DFD with constant I_{sp} and T
Fuel mass used	3754 kg
Total ΔV	68.40 km/s
Number of burns	2: Earth escape and inclination change, rendezvous
Distance at rendezvous	44.35 AU

4.2.8 Eris Mission - Simplified scenario

In this case, since the high eccentricity, inclination and distance of the dwarf planet Eris, there was the need to study it for a scenario with 0° inclination, in order to understand the type of maneuvers required and estimate the overall fuel consumption.

First iteration spacecraft parameters are very close to those of the other cases.

Again, the mission is divided into three phases: spiral trajectory, interplanetary phase and rendezvous. The overall trajectory is shown in Fig. 4.23.

Spiral trajectory Formally, it is the same as in previous scenarios. The departure date from LEO is supposed to be the 22nd of January, 2056.

Interplanetary phase This phase is summarized in Table 4.20.

Table 4.20: Interplanetary phase summary for Eris with $i = 0°$ mission

	Burn
Duration	270 day
ΔV gain	31.41 km/s
Fuel Used	1900 kg
Initial velocity (VNC)	31.24 km/s
Final velocity (VNC)	43.33 km/s

	Coasting phase
Duration	8 years and 8 months
Initial sun distance	4.14 au
Final sun distance	75.44 au
Initial velocity	43.33 km/s
Final velocity	38.36 km/s

Rendezvous phase This maneuver for Eris rendezvous is the most demanding of the three missions, especially because the speed is at least 10 km/s higher than in previous case and, more importantly, the velocity vector has to be turned of about 120° within a single burn.

Table 4.21: Summary for the rendezvous phase for the simplified case scenario for Eris with i =0°

Duration	248 days
ΔV	41.70 km/s
Propellant mass used	1744 kg
Initial Velocity	38.36 km/s
Final Velocity	3.27 km/s
Closest pass from Eris	25000 km

Scenario summary In Table (4.22) main mission parameters are summarized.

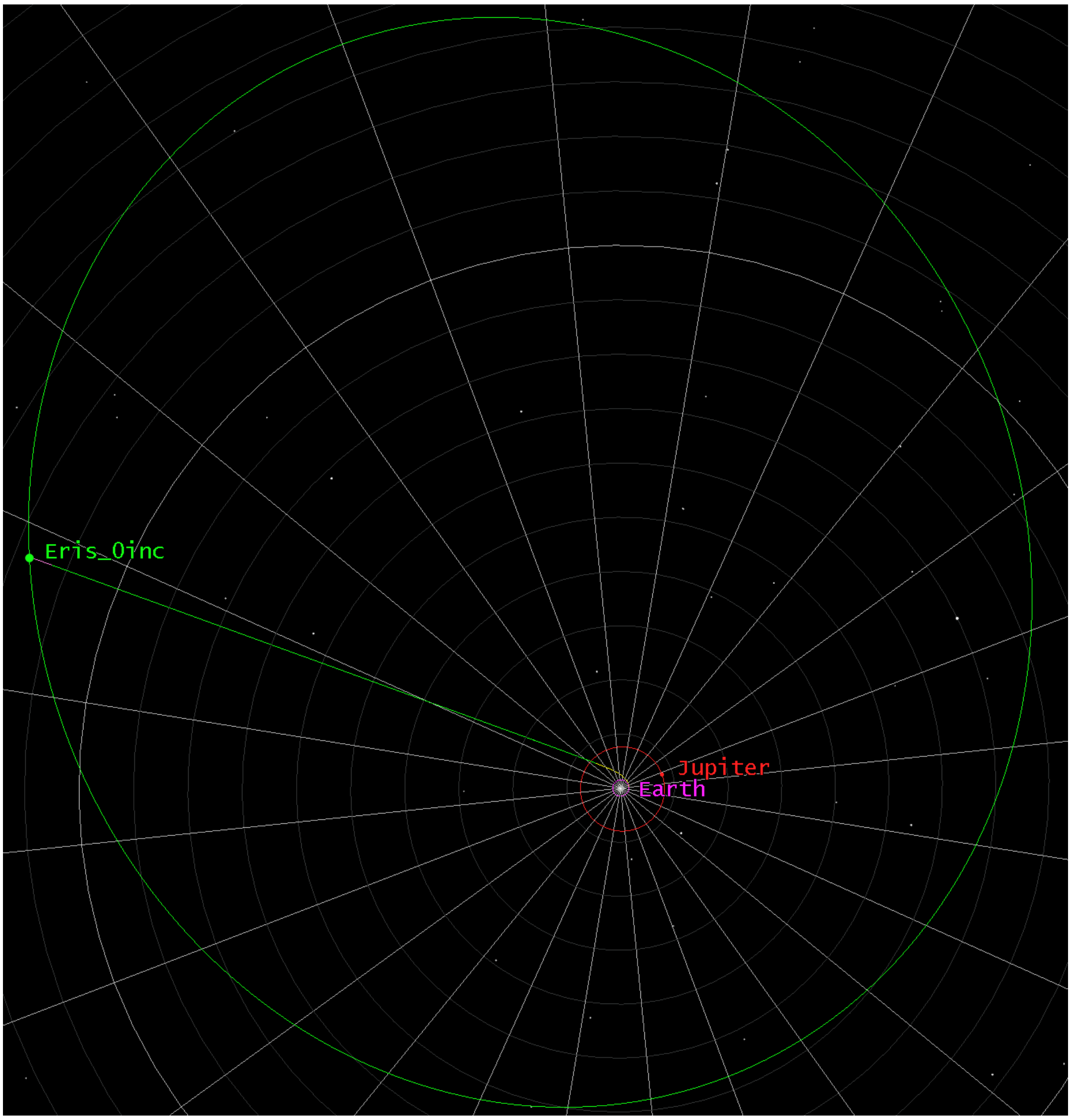

Figure 4.23: Trajectory for Eris in the simplified scenario

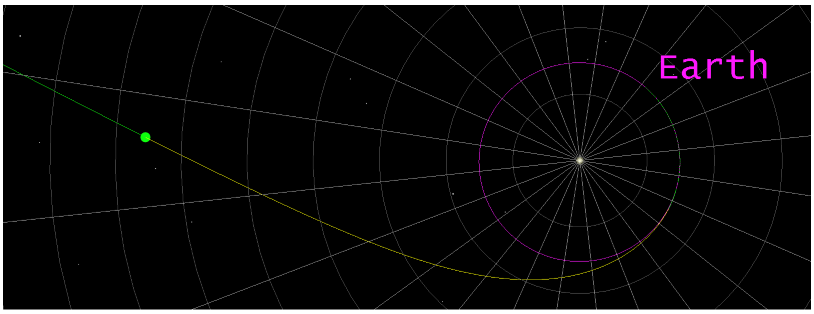

Figure 4.24: Detail for the trajectory for the acceleration phase for Eris simplified scenario

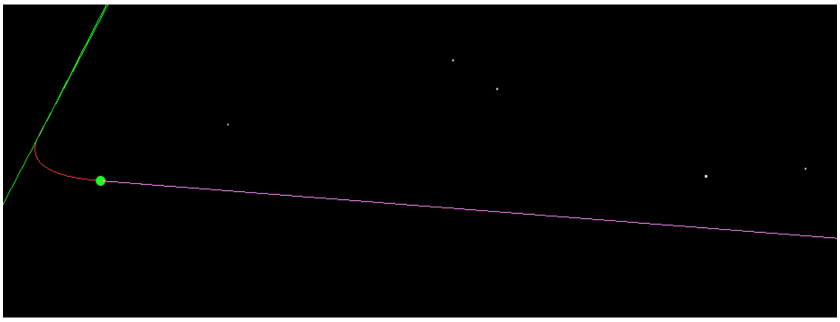

Figure 4.25: In this snapshot of the rendezvous phase of the trajectory, the pink line represents the pure deceleration phase, while the red segment is the one in which there is a component of thrust directed radially.

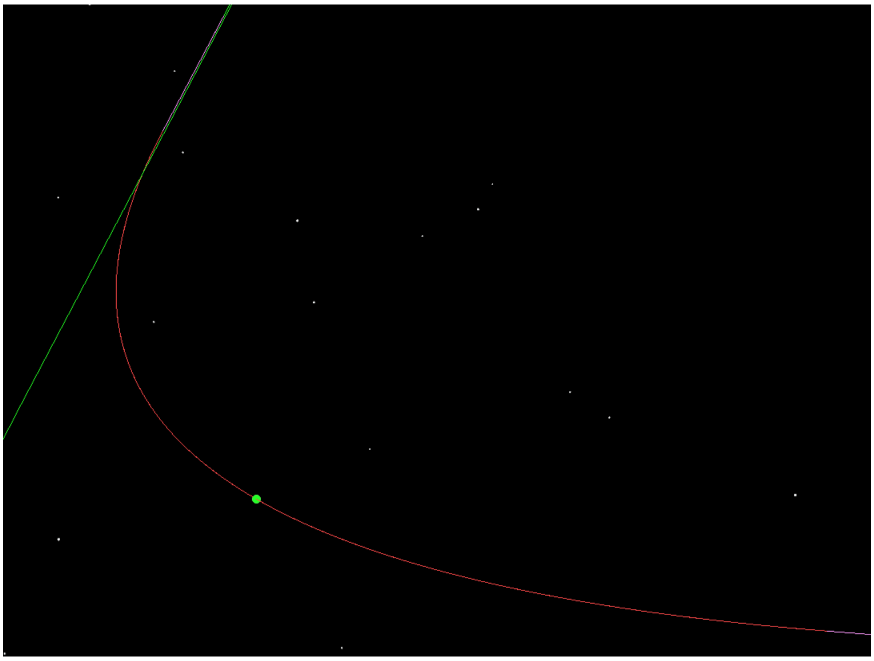

Figure 4.26: Close up on the maneuver in which the velocity vector is turned.

Table 4.22: Summary for the trajectory to Eris (with 0° inclination).

Destination	Eris - Elliptic orbit with $i = 0°$
Mission duration	10 yr and 4 months
Final mass delivered	3288 kg
Propulsive system	DFD with constant I_{sp} and T
Fuel mass used	4199 kg
Total ΔV	80.69 km/s
Number of burns	2: Earth escape and inclination change, rendezvous
Distance at rendezvous	78.19 AU

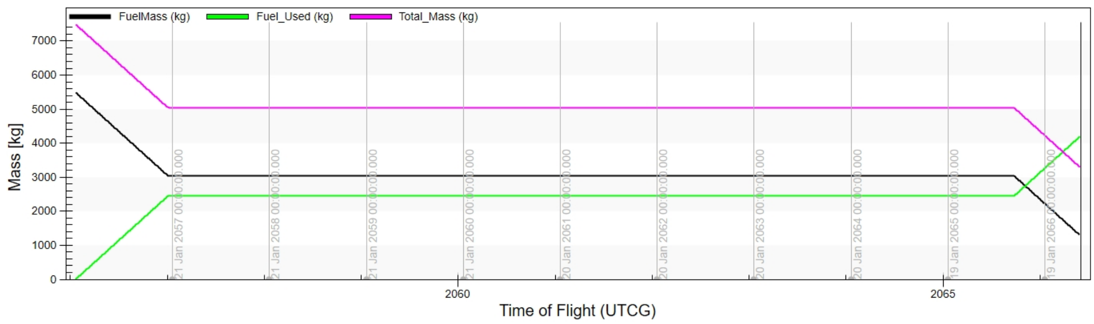

Figure 4.27: Propellant mass consumption (green line) and remaining (black line) and total spacecraft mass evolution (purple line) in time for simplified Eris mission.

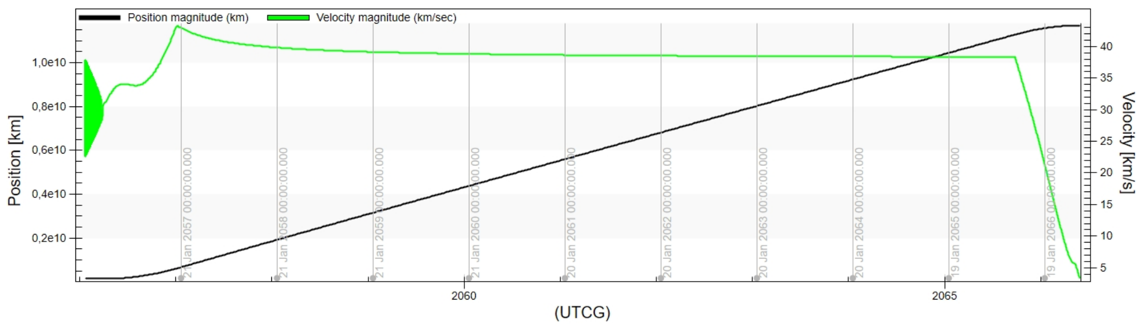

Figure 4.28: Distance (black line) and velocity evolution (green line) in time for simplified Eris mission.

4.2.9 Eris Mission - Real scenario

This mission is the most challenging of all of those analyzed so far. This is because the high inclination and eccentricity of Eris ($i = 43.88°$ and $e = 0.44$) and its distance of about 80 AU at the departure requires an hyperbolic trajectory with very high initial velocity with respect to the Sun, in order to have a good trade off between propellant consumption and flight time. Also, Eris is moving towards its lines of nodes and, after that, its perigee. This means that the later will be the departure time, the closer Eris will be to the Earth.

Spiral trajectory It is the same as in previous cases, because the initial mass is the same. The departure date is the 25th of January, 2056.

Interplanetary phase This phase is characterized by a change of inclination obtained by a thrust component directed outside the orbit plane during the acceleration phase, just like in the other scenarios explained so far. Table 4.23 summarizes main parameters for this phase.

Table 4.23: Interplanetary phase summary for Eris with i =43.88° mission

	Burn
Duration	279 day
ΔV gain	32.71 km/s
Fuel Used	1966 kg
Initial velocity (VNC)	31.21 km/s
Final velocity (VNC)	43.33 km/s

	Coasting phase
Duration	8 years and 8 months
Initial sun distance	4.27 au
Final sun distance	75.46 au
Initial velocity	43.33 km/s
Final velocity	38.52 km/s

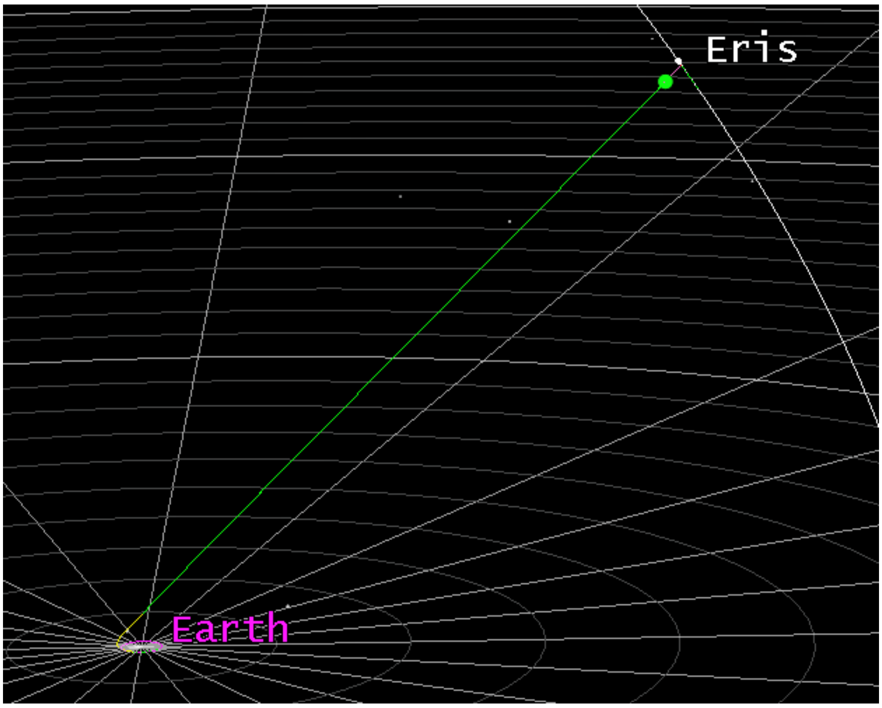

Figure 4.29: Trajectory for Eris in the real scenario

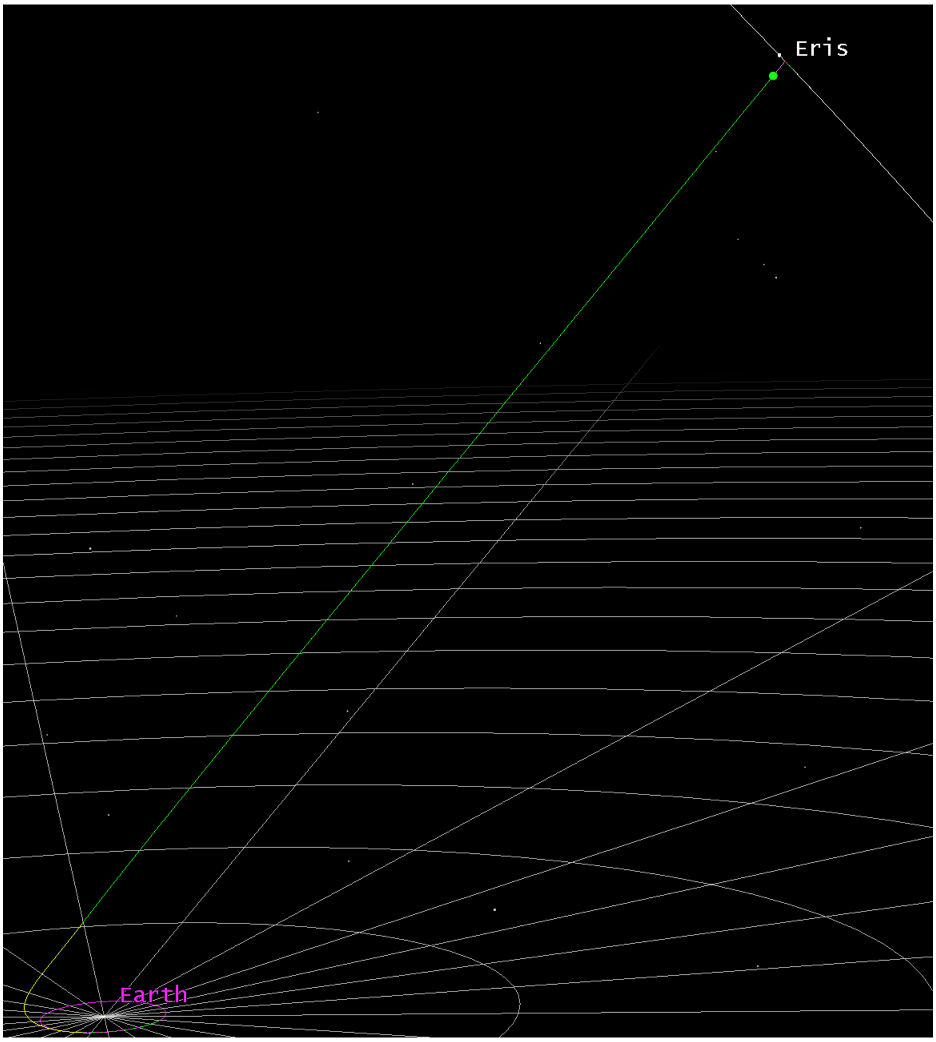

Figure 4.30: Detail for the trajectory for the acceleration phase in the real scenario

Rendezvous phase This maneuver, as in the simplified case, is extremely challenging, as it is reported in Table 4.24.

Table 4.24: Summary for the rendezvous phase for the real case scenario for Eris with i =43.88°

Duration	243 days
ΔV	41.37 km/s
Propellant mass used	1709 kg
Initial Velocity	38.52 km/s
Final Velocity	3.09 km/s
Closest pass from Eris	30000 km

Scenario summary In Table 4.25 the summary for the real case scenario can be found. Fuel evolution is analyzed in Fig. 4.31, while in Fig. 4.32 velocity and position are plotted versus the time.

Table 4.25: Summary for the trajectory to Eris (with $i = 43.88°$).

Destination	Eris - Elliptic orbit with $i = 43.88°$
Mission duration	10 yr and 4 months
Final mass delivered	3257 kg
Propulsive system	DFD with constant I_{sp} and T
Fuel mass used	4231 kg
Total ΔV	81.63 km/s
Number of burns	2: Earth escape and inclination change, rendezvous
Distance at rendezvous	78.20 AU

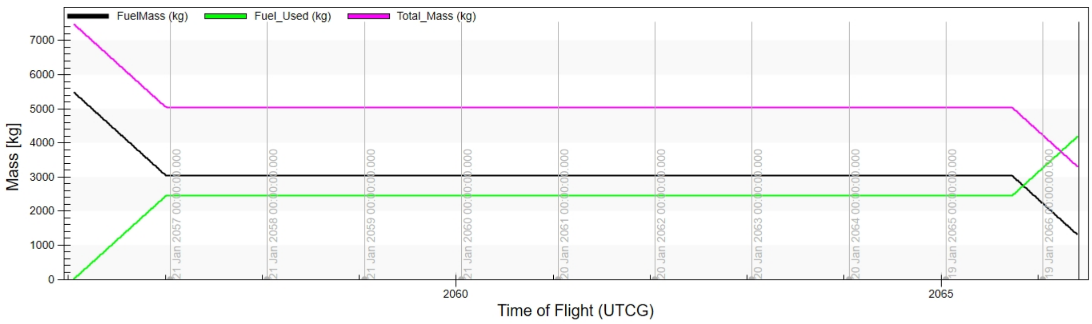

Figure 4.31: Propellant mass consumption (green line) and remaining (black line) and total spacecraft mass evolution (purple line) in time for real Eris mission.

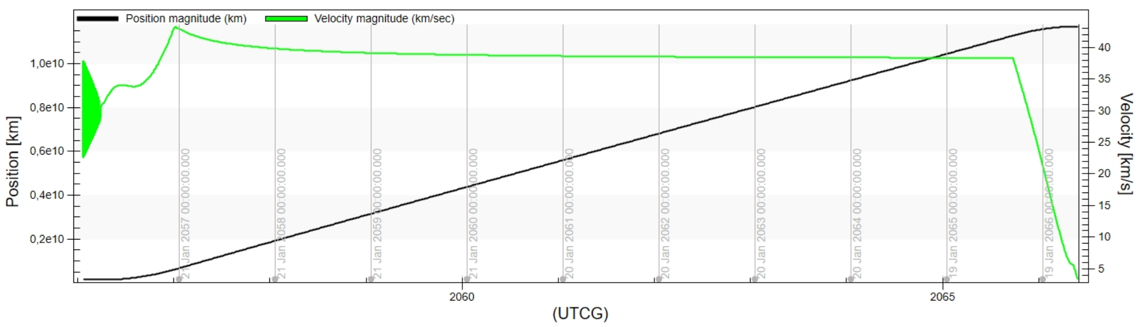

Figure 4.32: Distance (black line) and velocity (green line) evolution in time for real Eris mission.

4.2.10 Comparison between the two Eris scenarios

Results reported in Tabs. 4.26 and 4.27 clearly shows that the difference between the delivered mass of the two mission is less than 50 kg. This is due to two factors:

- The rendezvous maneuver is clearly still to optimize in both cases, but in the case with $i = 0°$ a better solution that uses at least the same amount of fuel as $i = 43.88°$ can be found. Though, due to numerical reasons, it was not possible to find that in these calculations.

- The small difference in the acceleration phase of burn days, which is of 9 days, seems not to explain the very demanding change of inclination achieved in this phase for the $i = 43.88°$ case. This, though, is explained by saying that the enormous distance traveled during the coasting phase of about 70 au, makes it possible to use only a small component of thrust in the direction normal to the plane. The spacecraft in the two cases will have the exact velocity at the end of the acceleration phase, so the results are indeed comparable.

Table 4.26: Duration and fuel consumption for the two Eris scenarios for the interplanetary and rendezvous phases

	Eris 0°	Eris 43.88°
Interplanetary phase		
Duration	270 days	279 days
Propellant consumption	1900 kg	1966 kg
Rendezvous phase		
Duration	248 days	243 days
Propellant consumption	1744 kg	1709 kg

Table 4.27: Comparison between departure, time of flight, fuel consumption and ΔV for the two Eris scenarios

	Simplified scenario	Real scenario
Departure	22 Jan 2056	25 Jan 2056
Duration	10 yr and 4 months	10 yr and 4 months
Fuel consumption	4199 kg	4231 kg
Total ΔV	80.69 km/s	81.63 km/s

4.3 Interstellar missions

The objective for this kind of mission is to compute the amount of propellant and the time of flight of some mission that will depart from a LEO and will reach an imaginary point at 125 AU from the Sun. During the flight, the spacecraft will eventually cross the boundaries of the heliosphere, which are explained in Sec. 4.1.2, and so it will be able to study them in detail. The first scenario will take into account also a flyby of Eris, while the other scenarios will show what happens if the time of acceleration is varied. The choice of Eris for the flyby is arbitrary, any other TNO could have worked, but the purpose of that calculation is to show that is possible

Table 4.28: The table shows the input parameters for the calculation. In this case, the same engine as in previous chapter is considered. The calculation are done with 3000 kg of dry mass and 7500 kg of propellant as input and all of the propellant not used is then accounted as dry mass, just as done in previous calculation and explained in Sec. 4.2.1. The dry mass reported is the initial dry mass plus the propellant not used.

	Spacecraft properties
Final mass (Dry)	3350 kg
Fuel mass	4150 kg
Initial mass	7500 kg
Final mass to initial mass ratio	0.45
Final mass to initial fuel mass ratio	0.74
	Engine properties
Fusion power	2 MW
Power to thrust	1 MW
Specific power	1 kg/kW
Thrust	8 N
Specific impulse	10000 s
Mass flow	0.08 g/s = 6.912 kg/day

to design a mission that will be able to pass extremely close to any dwarf planet as it is already been done by New Horizons mission and then will also travel towards the interstellar space. The acceleration phase study can also be easily applied to the mission with the flyby of the dwarf planet.

4.3.1 125 AU with Eris flyby

Just as it is shown in previous chapters about the dwarf planets, the trajectory start from a low Earth orbit and, thanks to a spiral trajectory, the spacecraft achieves velocity and escape the sphere of influence of the Earth. After this phase, an additional acceleration phase is used, in which the change of plane is achieved. After that, a coasting period of many years is taken into account. The destination is a point at 125 AU out of the ecliptic plane, but before that there will be a flyby at 20000 km from the surface of the furthest dwarf planet, Eris.

Note that the velocity gain of the spacecraft because of the flyby is negligible, and for this reason it is not considered.

In Table. 4.28 the main characteristic for the spacecraft and the engine are summarized.

Spiral trajectory In this section the thrust will be aligned with the velocity vector of the spacecraft. This phase will end when the spacecraft will exit the sphere of influence of the Earth, which is considered to be at about 1×10^6 km from the center.

Table 4.29: Spiral trajectory for Earth escape with main parameters. As in the previous sections, the thrust direction is aligned with the velocity direction.

Departure date	9 Jan 2050
Duration	79 days
ΔV	7.55 km/s
Propellant used	556 kg

Acceleration and propagation phase In this part it is presented the phase in which the spacecraft is further accelerated after the exit from the sphere of influence and, after that, a 7 years long coasting phase, in which the engine does not produce thrust. In this last phase, the spacecraft travels the most distance, and practically the velocity does not decrease. During the acceleration phase, the thrust has a component normal to the ecliptic plane, so that the spacecraft can achieve the inclination necessary to flyby Eris, which has an orbit inclined of $i = 43.88°$ on the ecliptic.

During the propagation phase, towards the end, the spacecraft will flyby the dwarf planet Eris at a distance of 20000 km after approximately 6 years of flight.

Table 4.30: Acceleration phase for the 125 AU mission with Eris flyby

	Acceleration phase
Duration	510 days
ΔV gain	71.50 km/s
Fuel used	3595 kg
Initial velocity	29.04 km/s (6.13 AU/yr)
Final velocity	77.41 km/s (16.33 AU/yr)

Table 4.31: Coasting phase summary for the 125 AU mission with Eris flyby

	Coasting phase
Duration	7 years
Initial sun distance	11.34 AU
Distance at flyby	80.23 AU
Final sun distance	125 AU
Initial velocity	77.14 km/s
Velocity at flyby	76.55 km/s
Final velocity	76.49 km/s

Summary The 510 days long acceleration phase brings the spacecraft to have enormous velocities and those that will enable it to travel 125 AU in under 9 years.

This, though, neglects the possibility to slow down once arrived at 125 AU, because the deceleration phase required would be of about 500 more days, but the propellant left will be not enough. The deceleration, on the other hand, it is not necessary, since this kind of mission aims at crossing the termination shock, the heliosheath and finally reach the interstellar space. For this reason, after accomplish those objectives, the spacecraft could continue its journey through the interstellar space at a very high velocity and continue its study of the interstellar medium.

Table 4.32: Summary for the trajectory to 125 AU with Eris flyby

Destination	125 AU with Eris flyby
Mission duration	8 yr and 8 months
Final mass delivered	3350 kg
Propulsive system	DFD with constant I_{sp} and T
Fuel mass used	4150 kg
Total ΔV	79.05 km/s
Number of burns	2: Earth escape and inclination change, rendezvous
Maneuver numerical optimization	No

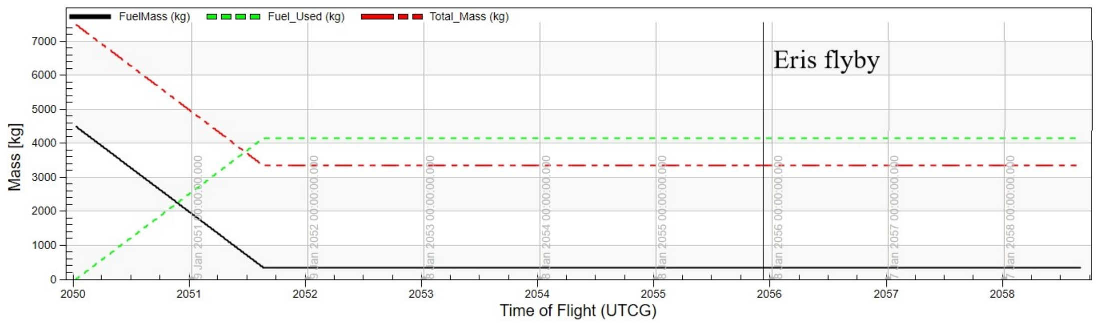

Figure 4.33: The dash-dotted line is the total mass evolution during the time of flight, the dotted line is the propellant mass consumption and the continuous line is the propellant mass in the reservoir for the mission length

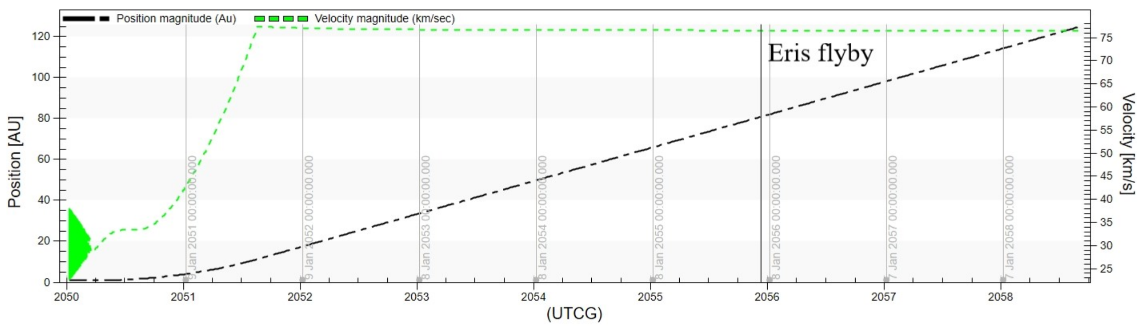

Figure 4.34: The dotted line is evolution of the velocity of the spacecraft in time, while the dash-dotted line is the distance traveled from the Sun

4.3.2 125 AU with different acceleration phases

This section presents the results obtained for the study of some scenarios in which the 125 AU destination is reached by considering different acceleration phases. The destination is considered to be on the ecliptic plane, so no change of plane is required. The calculations are done for two different initial dry mass and propellant mass with the same 2 MW engine. Mass properties are reported in Table 4.33. As in the other calculation, all the propellant mass not used will be considered as dry mass.

Table 4.33: The dry mass and the propellant mass in this table are those of first iteration, that means that they are the input used for the calculation. In the same table there are reported the characteristics for the spiral trajectory for the escape, which changes with respect to the initial masses

	Case 1	Case 2
Dry mass, [kg]	2500	3000
Propellant mass, [kg]	3488	4500
Spiral time, [day]	64	79
ΔV, [km/s]	7.65	7.55
Propellant used for escape, [kg]	450	556

For each case the spiral phase is identical, the only changes are done in the duration of the acceleration phase, in order to understand of the results are affected, and those results are shown in Tables. 4.34 and 4.35 and in Figs. 4.35 and 4.36.

Table 4.34: In this table the results for the first case are reported, in which the starting dry mass is 2500 kg and the propellant mass is 3488 kg. The different solutions are referred to different days of thrust. The acceleration days are the days in which the engine has the thrust aligned with the velocity vector, so the spacecraft is accelerated. The dry mass is the initial dry mass plus the propellant mass not used. The propellant mass is the propellant used in the acceleration phase and in the spiral phase (450 kg). The time of flight is the elapsed time from the departure date. The coasting velocity is the speed of the spacecraft with respect to the Sun at the end of the acceleration phase and it will remain constant throughout the coasting phase

Acceleration days, [day]	Dry mass at destination, [kg]	Propellant mass, [kg]	Time of flight, [yr]	Coasting velocity, [AU/yr]
340	3142	2846	9.13	13.62
360	3001	2987	8.47	14.53
380	2860	3128	7.87	15.48
400	2719	3269	7.30	16.5
420	2578	3410	6.80	17.5

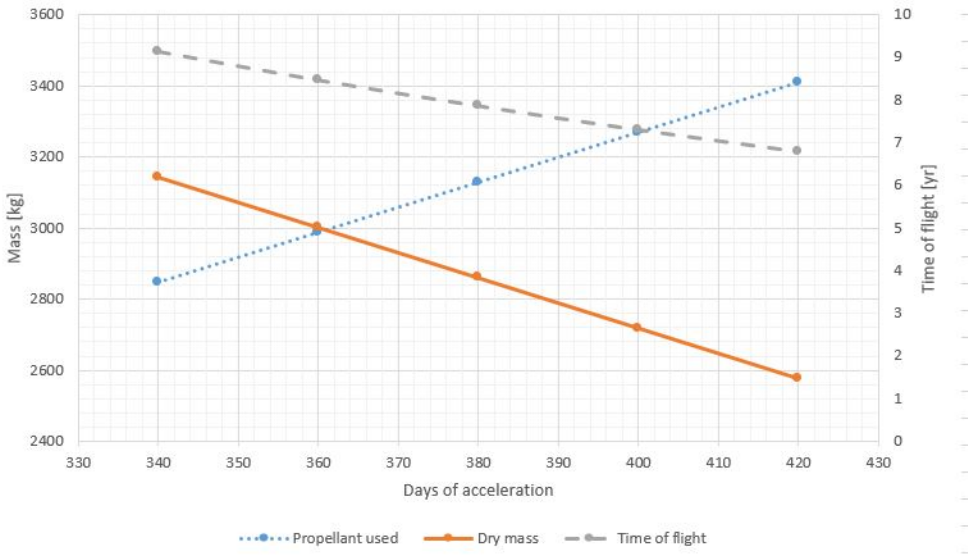

Figure 4.35: In this graphs the values from Table 4.34 are plotted against the acceleration days. In particular, the continuous line is the dry mass, composed of the the starting dry mass of 2500 kg plus the propellant mass not used. The dashed line is the time of flight of the entire mission. The dotted line is the propellant mass used.

Table 4.35: In this table the results for the second case are reported, in which the starting dry mass is 3000 kg and the propellant mass is 4500 kg. The different solutions are referred to different days of thrust. The acceleration days are the days in which the engine has the thrust aligned with the velocity vector, so the spacecraft is accelerated. The dry mass is the initial dry mass plus the propellant mass not used. The propellant mass is the propellant used in the acceleration phase and in the spiral phase (556 kg). The time of flight is the elapsed time from the departure date. The coasting velocity is the speed of the spacecraft with respect to the Sun at the end of the acceleration phase and it will remain constant throughout the coasting phase

Acceleration days, [day]	Dry mass at destination, [kg]	Propellant mass, [kg]	Time of flight, [yr]	Coasting velocity, [AU/yr]
430	3914	3586	9.10	13.46
450	3773	3727	8.56	14.19
470	3631	3869	8.05	14.95
490	3491	4009	7.58	15.75
510	3349	4151	7.14	16.58

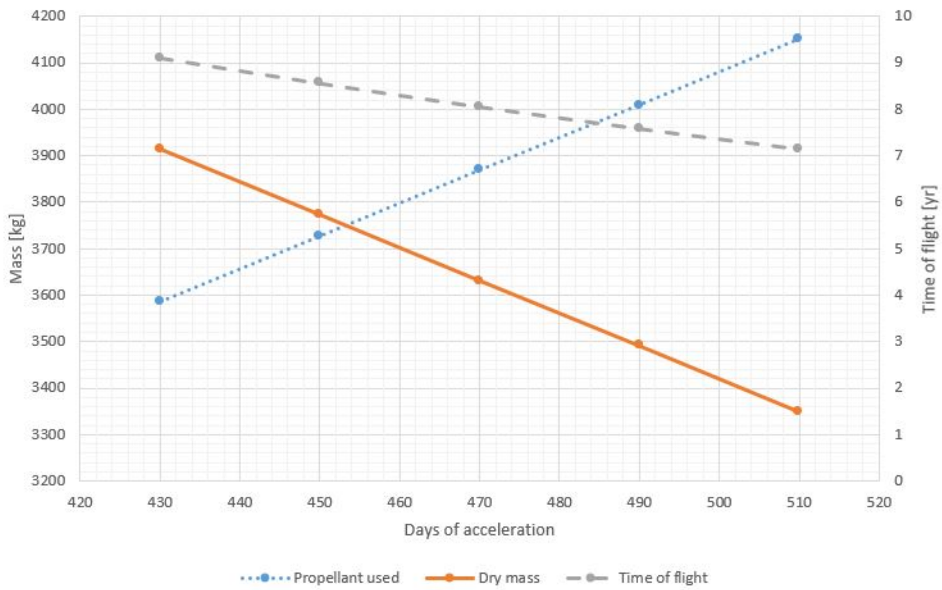

Figure 4.36: In this graphs the values from Table 4.35 are plotted against the acceleration days. In particular, the continuous line is the dry mass, composed of the the starting dry mass of 3000 kg plus the propellant mass not used. The dashed line is the time of flight of the entire mission. The dotted line is the propellant mass used.

The results shown in Tables. 4.34 and 4.35 and in Figs. 4.35 and 4.36 very interesting, because they show, first of all, the correlation between the acceleration time and the overall time of flight. A difference of 20 days during acceleration leads to half a year (about 6 months) less of mission time. Starting at 9 years, in both cases, the time of flight is reduced to about 7 years. This means that 80 days of difference of thrust will result in a 2 year gain. Those consideration will fit very well the request from the mission, making this engine quite flexible and capable of many mission scenarios, in which the masses are different.

If a higher mass will be required, both the time of flight and the propellant mass can be increased, depending on the time and launch limitations of the mission.

5 Conclusions

In this work it has been demonstrated that a spacecraft propelled by the direct fusion drive will enable a entire new class of missions and will pave the way to a first practical approach to the interstellar travel.

For a matter of time, for this work it has been decided to fix the engine, which is a 2 MW class DFD, the launch masses and also the maximum mission time. This enabled us to perform multiple simulations in order to get an idea of the order of magnitude of the propellant mass required, the flight time as well as the type of maneuver. All of those results are the outcome of multiple assumptions. First of them, the decision to use a thrust-coast-thrust profile, that is a huge hypothesis which requires that the engine will not produce thrust for many years, which is in theory possible, but not certain. This means that it would be off for multiple years and turned on again when needed or that it would operate without the propellant. Secondly, a very basic numeric optimization process was performed. That was because the convergence was very hard to achieve, given the enormous distances, where a slight change in a value would result in billions of km of difference at the destination. Though, a basic optimization has proven to be useful to approximate the thrust direction and to minimize the duration of burns, hence the propellant used. Even considering all of these approximations, the obtained results are extremely promising.

What is shown in Table 5.1 is a summary for the three main missions to trans-Neptunian objects. Those are very representative because they show that even though the objectives are $10-40$ AU apart, the propellant required is of the same order of magnitude. This is linked to the fact that a change in the acceleration period of some days will result in higher or lower velocities that, if propagated for many years, will highly affect the time of flight. On the other hand, higher velocities will require longer deceleration periods and this will mean more days of burn. The interesting fact is that, for example, 10 more days of acceleration will require approximately 10 more days of deceleration, with an overall decrease of the flight time.

One of the main results for the calculations is that we demonstrated that it will be possible to reach those dwarf planets and even to rendezvous with them to perform detailed studies in less than 10 years. So far, very few mission have been presented to study those worlds, and even fewer will be able to orbit the dwarf planets, because such a deceleration with the technology available at the moment will be in impossible in most cases, or at least too demanding. The DFD, though, will be so powerful that will be capable of accelerating the spacecraft to extremely high velocities and then to decelerate it to the required speed, reducing of many years the time of flight. This deceleration capability is the real game changer: in fact, so far, all the outer planets such as Neptune and Uranus and the dwarf planet Pluto have only been flied by the Voyager 2 mission and by New Horizons, but actually no mission has ever performed a rendezvous or orbit injection. Such kind of maneuver would have been too demanding and also would have kept the spacecraft in the same orbit until the end of the mission, while the objective of both the Voyager missions and of New Horizons has always been to travel towards as many objects as possible, and then towards the interstellar space. A mission purposely thought to visit a trans-Neptunian object, though, would be easier than ever with this kind of engine.

Table 5.1: In this table the main results for the calculations performed for real scenarios are presented. The distance at rendezvous and the inclination defines the arrival orbit and the ΔV is an index of the complexity of the mission. The higher is the ΔV, the higher will be the propellant consumption. An optimization would reduce the propellant consumption, but it will inevitably increase with the ΔV.

	Haumea	Makemake	Eris
Inclination	28.19°	29.01°	43.87°
Distance at rendezvous	36.51 AU	44.35 AU	78.20 AU
Time of flight	6 yr and 1 month	7 yr and 3 months	10 yr and 4 months
Total ΔV	64.16 km/s	68.40 km/s	81.63 km/s
Dry mass at destination	3892 kg	3733 kg	3257 kg
Propellant mass	3595 kg	3754 kg	4231 kg

What is important to point out, as it is already introduced in this chapter, is that the DFD would be very versatile, both in terms of power class and also in term of mission itself. In fact, as it is seen for the 125 AU missions, with a slight increase of the acceleration days the gain in flight time will be not negligible. By changing of 80 days the acceleration period, the mission flight time can be decreased of two years in the best case. This feature is what makes the trajectory design with the DFD so interesting: each mission can be tailored on the needs of the design team, depending on the flight time desired and mass budget. Furthermore, it demonstrated that it will be possible to flyby Eris and reach the 125 AU destination within the same mission, which is something that will enable a study of both the dwarf planet and the magnetosphere. The same kind of calculations can be done for any other TNO: a flyby of any of those objects with final destination 125 AU will be possible mainly because no slingshot will be needed to achieve enough velocity, and the reason is that the DFD will enable those kind of mission all by itself. Moreover, the possible trajectories to any other TNOs will not differ very much for the presented Eris flyby, both in terms of duration and propellant mass. Obviously, the flyby of the desired TNO will happen at different time of the mission, but it all depends on the initial conditions of the hyperbolic orbit.

The only huge constraint is relative to the fuel mass that will be needed to power the fusion reaction. As analyzed in Sections 1.3.4 and 2.4.7, the mass of fuel needs to be kept as low as possible because at the present date the availability of ^{3}He is extremely limited.

All the mission scenarios analyzed so far fit really well in to the pool of missions already analyzed, both robotic and human, such as those presented in Refs. [29, 27, 28, 38, 89]. The engine will be very versatile, because it can be combined, when needed, in a cluster of multiple engine, thus achieving up to many hundreds of N of thrust. In its smaller configuration, that is the 1 MW class, the thrust would comparable to that of the most promising electromagnetic thrusters, but the specific impulse would be higher. An engine like this one, if successfully developed, will take over a huge share of market of thrusters. In fact, it will be able to compete with the chemical thrusters for fast missions to inner planets and also will enable rapid missions to the outer planets and the border of the solar system, without the need of complex flybys, as it is presented in this work.

References

[1] NASA, Solar System Exploration: Voyager 1 (2019).
URL https://solarsystem.nasa.gov/missions/voyager-1/in-depth/

[2] NASA, Solar System Exploration: Voyager 2 (2019).
URL https://solarsystem.nasa.gov/missions/voyager-2/in-depth/

[3] C. R. McInnes, Solar Sailing - Technology, Dynamics and Mission Applications, Praxis Publishing, 1999.

[4] G. M. G. Vulpetti, L. Johnson, Solar Sails - A Novel Approach to Interplanetary Travel, 2008.

[5] A. Jackson IV, Gram-scale Nano-spacecraft Entry into Star Systems, Journal of the British Interplanetary Society 71 (2018) 294–297.

[6] L. Casalino, Space propulsion, appunti di lezione (2019).

[7] P. Daukantas, Breakthrough starshot, Optics and Photonics News 28 (5) (2017) 26–33.

[8] J. Benford, G. Matloff, Intermediate beamers for starshot-Probes to the Sun's Inner Gravity Focus, Journal of the British Interplanetary Society 72 (2019) 51 – 55.

[9] R. Kezerashvili, The hundredth anniversary of Einstein's Annus Mirabilis, arXiv preprint physics (2005).

[10] R. L. Forward, Feasibility of interstellar travel: A review, Acta Astronautica 14 (1986) 243–252.

[11] W. Robbins, An historical perspective of the nerva nuclear rocket engine technology program, in: Conference on Advanced SEI Technologies, 1991, p. 3451.

[12] M. S. El-Genk, Space nuclear reactor power system concepts with static and dynamic energy conversion, Energy Conversion and Management 49 (3) (2008) 402–411.

[13] B. Martin, Nuclear and particle physics, Wiley Online Library, 2006.

[14] R. G. Kennedy, The interstellar fusion fuel resource base of our solar system, Journal of the British Interplanetary Society 71 (2018) 298–305.

[15] L. Wittenberg, J. Santarius, G. Kulcinski, Lunar source of ^{3}He for commercial fusion power, Fusion technology 10 (2) (1986) 167–178.

[16] J. Lawson, Some criteria for a useful thermonuclear reactor, Publication. Culham, United Kingdom: Atomic Energy Research Establishment (1955).

[17] D. Petkow, R. Gabrielli, G. Herdrich, R. Laufer, H.-P. Röser, Generalized Lawson criterion for magnetic fusion applications in space, Fusion Engineering and Design 87 (1) (2012) 30–38.

[18] F. Romanelli, C. Bruno, G. Regnoli, Assessment of open magnetic fusion for space propulsion, ESA-ESTEC Final Report, ESA-ARIADNA Contract 18853 (05) (2005).

[19] J. Lilley, Nuclear physics: principles and applications, John Wiley & Sons, 2013.

[20] T. R. Jarboe, Review of spheromak research, Plasma Physics and Controlled Fusion 36 (6) (1994) 945.

[21] R. Chapman, G. Miley, W. Kernbichler, M. Heindler, Fusion space propulsion with a field reversed configuration, Fusion Technology 15 (2P2B) (1989) 1154–1159.

[22] Electric Propulsion and Plasma Dynamics Laboratory, Magnetic nozzle (2019). URL `https://alfven.princeton.edu/research/past/MagneticNozzle`

[23] I. R. Jones, A review of rotating magnetic field current drive and the operation of the rotamak as a field-reversed configuration (Rotamak-FRC) and a spherical tokamak (Rotamak-ST), Physics of plasmas 6 (5) (1999) 1950–1957.

[24] S. A. Cohen, A. H. Glasser, Ion heating in the field-reversed configuration by rotating magnetic fields near the ion-cyclotron resonance, Physical review letters 85 (24) (2000) 5114.

[25] S. A. Cohen, R. Milroy, Maintaining the closed magnetic-field-line topology of a field-reversed configuration with the addition of static transverse magnetic fields, Physics of Plasmas 7 (6) (2000) 2539–2545.

[26] H. Guo, A. Hoffman, L. Steinhauer, Observations of improved confinement in field reversed configurations sustained by antisymmetric rotating magnetic fields, Physics of plasmas 12 (6) (2005) 062507.

[27] S. J. Thomas, M. Paluszek, S. A. Cohen, Fusion-enabled Pluto orbiter and lander, NIAC Phase I Internal Report, Tech. rep., Princeton Satellite Systems, Inc. (2017).

[28] Y. S. Razin, G. Pajer, M. Breton, E. Ham, J. Mueller, M. Paluszek, A. H. Glasser, S. A. Cohen, A direct fusion drive for rocket propulsion, Acta Astronautica 105 (1) (2014) 145–155.

[29] S. Cohen, C. Swanson, N. McGreivy, A. Raja, E. Evans, P. Jandovitz, M. Khodak, G. Pajer, T. Roglien, S. Thomas, et al., Direct fusion drive for interstellar exploration, Published on JBIS (2019).

[30] N. McGreivy, SULI Report: UEDGE simulations of a direct fusion drive FRC rocket, Tech. rep., Princeton Plasma Physics Laboratory (2016).

[31] C. Swanson, Princeton Plasma Physics Laboratory and Princeton Satellite Systems, Private communication (2019).

[32] G. D. Porter, S. Allen, M. Brown, M. Fenstermacher, D. Hill, R. Jong, A. Leonard, D. Nilson, M. Rensink, T. Rognlien, et al., Simulation of experimentally achieved diii-d detached plasmas using the uedge code, Physics of Plasmas 3 (5) (1996) 1967–1975.

[33] F. Wising, D. Knoll, S. Krasheninnikov, T. Rognlien, D. Sigmar, Simulation of detachment in iter-geometry using the uedge code and a fluid neutral model, Contributions to Plasma Physics 36 (2-3) (1996) 309–313.

[34] M. Rensink, D. Knoll, G. Porter, T. Rognlien, G. Smith, F. Wising, Models and applications of the uedge code (1996).

[35] S. J. Thomas, M. Paluszek, S. Cohen, N. McGreivy, E. Evans, Fusion-enabled Pluto orbiter and lander, in: AIAA SPACE and Astronautics Forum and Exposition, 2017, p. 5276.

[36] S. J. Thomas, M. Paluszek, S. A. Cohen, A. Glasser, Nuclear and future flight propulsion-modeling the thrust of the direct fusion drive, in: 2018 Joint Propulsion Conference, 2018, p. 4769.

[37] Princeton Plasma Physics Laboratory and Princeton Satellite Systems, Private communication (2019).

[38] M. Paluszek, G. Pajer, Y. Razin, J. Slonaker, S. Cohen, R. Feder, K. Griffin, M. Walsh, Direct fusion drive for a human mars orbital mission (PPPL-5064) (2014).

[39] J. W. Cornelisse, H. Schoyer, K. F. Wakker, Rocket propulsion and spaceflight dynamics, London: Pitman, 1979 (1979).

[40] R. R. Bate, D. D. Mueller, J. E. White, W. W. Saylor, Fundamentals of astrodynamics, Dover publications, 2019.

[41] R. Fitzpatrick, Derivation of Gauss planetary equations (2016).
URL `https://farside.ph.utexas.edu/teaching/celestial/Celestial/node164.html`

[42] G. Monegato, Fondamenti di calcolo numerico, Clut, 1998.

[43] D. M. Young, R. T. Gregory, A survey of numerical mathematics, Vol. 1, Courier Corporation, 1988.

[44] NASA, Kuiper belt (2019).
URL https://solarsystem.nasa.gov/solar-system/kuiper-belt/overview/

[45] A. Delsanti, D. Jewitt, The solar system beyond the planets (2006) 267–293.

[46] D. Nesvornỳ, D. Vokrouhlickỳ, F. Roig, The orbital distribution of trans-Neptunian objects beyond 50 au, The Astrophysical Journal Letters 827 (2) (2016) L35.

[47] H. Hussmann, F. Sohl, T. Spohn, Subsurface oceans and deep interiors of medium-sized outer planet satellites and large trans-neptunian objects, Icarus 185 (1) (2006) 258–273.

[48] R. McGranaghan, B. Sagan, G. Dove, A. Tullos, J. Lyne, J. P. Emery, A Survey of Mission Opportunities to Trans-Neptunian Objects, Journal of the British Interplanetary Society 64 (9) (2011) 296.

[49] A. Gleaves, R. Allen, A. Tupis, J. Quigley, A. Moon, E. Roe, D. Spencer, N. Youst, J. Lyne, A survey of mission opportunities to Trans-Neptunian Objects-Part II, orbital capture, in: AIAA/AAS Astrodynamics Specialist Conference, 2012, p. 5066.

[50] J. Kreitzman, C. W. Stewart, E. Cansler, J. Brisby, M. Green, J. Lyne, Mission opportunities to Trans-Neptunian Objects—Part III, orbital capture, low-thrust trajectories and vehicle radiation environment during jovian flyby, Advances in the Astronautical Sciences 150 (2013) 1487–1506.

[51] G. Baskaran, A. S. Bonthalapati, J. D. Lewis, K. J. Malone, H. M. Ved, J. E. Lyne, A survey of mission opportunities to trans-neptunian objects-part iv, in: AIAA-AAS Astrodynamics Specialist Conference, 2014, p. 4353.

[52] J. Dankanich, Electric propulsion for small body missions (2010) 6614.

[53] NASA, Eris (2019).
URL https://solarsystem.nasa.gov/planets/dwarf-planets/eris/in-depth/

[54] NASA, Haumea (2019).
URL https://solarsystem.nasa.gov/planets/dwarf-planets/haumea/in-depth/

[55] NASA, Makemake (2019).
URL https://solarsystem.nasa.gov/planets/dwarf-planets/makemake/in-depth/

[56] Wikipedia, Trans-neptunian objects (2019).
URL https://en.wikipedia.org/wiki/Trans-Neptunian_object

[57] Wikipedia, Provisional designation in astronomy (2019).
URL https://en.wikipedia.org/wiki/Provisional_designation_in_astronomy

[58] D. L. Rabinowitz, K. Barkume, M. E. Brown, H. Roe, M. Schwartz, S. Tourtellotte, C. Trujillo, Photometric observations constraining the size, shape, and albedo of 2003 el61, a rapidly rotating, pluto-sized object in the kuiper belt, The Astrophysical Journal 639 (2) (2006) 1238.

[59] J. Ortiz, B. Sicardy, F. Braga-Ribas, A. Alvarez-Candal, E. Lellouch, R. Duffard, N. Pinilla-Alonso, V. Ivanov, S. Littlefair, J. Camargo, et al., Albedo and atmospheric constraints of dwarf planet makemake from a stellar occultation, Nature 491 (7425) (2012) 566–569.

[60] M. E. Brown, C. Trujillo, D. Rabinowitz, Discovery of a planetary-sized object in the scattered kuiper belt, The Astrophysical Journal Letters 635 (1) (2005) L97.

[61] D. P. Cox, R. J. Reynolds, The local interstellar medium, Annual Review of Astronomy and Astrophysics 25 (1) (1987) 303–344.

[62] P. C. Frisch, Characteristics of nearby interstellar matter, Space Science Reviews 72 (3-4) (1995) 499–592.

[63] D. McComas, F. Allegrini, P. Bochsler, M. Bzowski, M. Collier, H. Fahr, H. Fichtner, P. Frisch, H. Funsten, S. Fuselier, et al., IBEX—interstellar boundary explorer, Space science reviews 146 (1-4) (2009) 11–33.

[64] S. Stern, H. Weaver, J. Spencer, H. Elliott, et al., The new horizons kuiper belt extended mission, Space Science Reviews 214 (4) (2018) 77.

[65] Wikipedia, The heliosphere (2020).
URL https://en.wikipedia.org/wiki/Heliosphere

[66] D. McComas, J. Rankin, N. Schwadron, P. Swaczyna, Termination shock measured by voyagers and ibex, The Astrophysical Journal 884 (2) (2019) 145.

[67] B. Steigerwald, Voyager enters solar system's final frontier (2005).
URL https://www.nasa.gov/vision/universe/solarsystem/voyager-agu.html

[68] B. Steigerwald, Voyager 2 proves solar system is squashed (2007).
URL http://voyager.jpl.nasa.gov/news/voyager-squashed.html

[69] J.-R. C. Cook, D. Brown, NASA spacecraft embarks on historic journey into interstellar space (2013).
URL https://www.nasa.gov/mission_pages/voyager/voyager20130912.html

[70] D. Shiga, Voyager 2 probe reaches solar system boundary (2007).
URL https://www.newscientist.com/article/dn13029-voyager-2-probe-reaches-solar-system-boundary/

[71] T. Phillips, NASAś Goddard Space Flight Center, A Big Surprise from the Edge of the Solar System (2011).
URL https://www.nasa.gov/mission_pages/voyager/heliosphere-surprise.html

[72] D. Brown, J.-R. Cook, NASA probes suggest magnetic bubbles reside at solar system edge (2011).
URL https://www.nasa.gov/home/hqnews/2011/jun/HQ_11-174_Voyager_Update.html

[73] L. Burlaga, N. Ness, J. Richardson, Heliosheath magnetic field and plasma observed by voyager 2 during 2015 near solar maximum, The Astrophysical Journal 861 (1) (2018) 9.

[74] J. Richardson, J. W. Belcher, P. Garcia-Galindo, L. Burlaga, Voyager 2 plasma observations of the heliopause and interstellar medium, Nature Astronomy 3 (11) (2019) 1019–1023.

[75] L. Burlaga, N. Ness, D. Berdichevsky, J. Park, L. Jian, A. Szabo, E. Stone, J. Richardson, Magnetic field and particle measurements made by voyager 2 at and near the heliopause, Nature Astronomy 3 (11) (2019) 1007–1012.

[76] M. Gruntman, R. L. McNutt Jr, R. E. Gold, S. M. Krimigis, E. C. Roelof, J. C. Leary, G. Gloeckler, P. L. Koehn, W. S. Kurth, S. R. Oleson, et al., Innovative explorer mission to interstellar space, Journal of the British Interplanetary Society 59 (2) (2006) 71–75.

[77] K. Nock, Tau-a mission to a thousand astronomical units, in: 19th International Electric Propulsion Conference, 1987, p. 1049.

[78] P. Liewer, R. Mewaldt, J. Ayon, R. Wallace, Nasa's interstellar probe mission, in: AIP Conference Proceedings, Vol. 504, AIP, 2000, pp. 911–916.

[79] R. L. McNutt Jr, R. I. E. Team, G. Andrews, R. Gold, A. Santo, R. Bokulic, B. Boone, D. Haley, J. McAdams, M. Fraeman, et al., A realistic interstellar explorer, in: AIP Conference Proceedings, Vol. 679, AIP, 2003, pp. 830–833.

[80] R. L. McNutt Jr, R. E. Gold, T. Krimigis, E. C. Roelof, M. Gruntman, G. Gloeckler, P. Koehn, W. S. Kurth, S. R. Oleson, D. I. Fiehler, et al., Innovative interstellar explorer, in: AIP Conference Proceedings, Vol. 858, AIP, 2006, pp. 341–347.

[81] R. McNutt, J. Leary, R. Gold, S. Krimigis, E. Roelof, M. Gruntman, G. Gloeckler, P. Koehn, W. Kurth, S. Oleson, et al., Innovative interstellar explorer: radioisotope propulsion to the interstellar medium, in: 41st AIAA/ASME/SAE/ASEE Joint Propulsion Conference & Exhibit, 2005, p. 4272.

[82] A. Lyngvi, P. Falkner, A. Peacock, The interstellar heliopause probe, in: Tools and Technologies for Future Planetary Exploration, Vol. 543, 2004, pp. 11–16.

[83] H. Fichtner, B. Heber, M. Leipold, The science with the interstellar heliopause probe (2006).

[84] R. A. Wallace, J. A. Ayon, G. A. Sprague, Interstellar probe mission/system concept, in: 2000 IEEE Aerospace Conference. Proceedings (Cat. No. 00TH8484), Vol. 7, IEEE, 2000, pp. 385–396.

[85] F. W. Boltz, Orbital motion under continuous tangential thrust, Journal of Guidance, Control, and Dynamics 15 (6) (1992) 1503–1507.

[86] NASA-JPL Solar System Dynamics, JPL HORIZONS on-line solar system data and ephemeris computation service (2019).
URL `https://ssd.jpl.nasa.gov/?horizons`

[87] J. Kelley, C. Yen, Planetary mission opportunities with nuclear electric propulsion, in: Space Programs and Technologies Conference, 1992, p. 1560.

[88] S. Bourdarie, M. Xapsos, The near-earth space radiation environment, IEEE transactions on nuclear science 55 (4) (2008) 1810–1832.

[89] G. Genta, R. Ya. Kezerashvili, Achieving the required mobility in the solar system through direct fusion drive, Published abstract for 8th CSA-IAA Conference on Advanced Space Technology, Shangai, China (2019).

Ringraziamenti

Questa tesi non sarebbe stata possibile senza il supporto e il sostegno della mia famiglia, quindi il mio primo e più importante ringraziamento va a loro, a Mamma, a Papà, a Silvia e ai nonni.

Grazie a Martina, il mio piccolo punto di riferimento, ed a tutte le persone che mi hanno accompagnato in questi cinque anni e mi hanno aiutato ad arrivare fino a qui, crescendo con me.

Un ringraziamento speciale va a tutti gli amici che ho ritrovato e quelli che ho perso negli anni, e a quella seconda famiglia che il mondo del lavoro mi porterà ad abbandonare, AESA: vi auguro di avere almeno la metà di quello che ho avuto io.

Un pensiero va a Roman Kezerashvili, che ha accolto me e Marco, accompagnandoci durante questo duro lavoro di tesi. Ringrazio profondamente entrambi. Un ultimo ringraziamento va al Prof. Genta per avermi dato questa possibilità e alla Prof.ssa Corpino per aver accettato di farmi da relatrice.